Constraining the relationship between mantle circulation and supercontinent cycles.

Abigail Plimmer

School of Earth and Ocean Sciences

Cardiff University

Submitted in partial fulfilment of the requirements for the degree of

Doctor of Philosophy

February 2025

Abstract

Supercontinent cycles reflect countless processes acting within the Earth's interior. Whilst their assembly and dispersal are predominantly tectonic processes, the mechanisms which drive plate motion may originate deeper in the Earth.

The primary aim of this thesis has been to better constrain the relationship between mantle circulation and supercontinent cycles by exploring the interactions between mantle structures in a 'mantle circulation cycle'. This cycle comprises slabs sinking, the interactions between slabs and basal mantle structures, and the origins of upwellings. Each phase has been investigated using 3D mantle circulation models, driven by plate velocities at the surface. I explored the relative contribution of plate and mantle properties in controlling the dynamics of slabs as they sink through the mantle, and investigated the coupling between slabs, deep mantle structures and upwellings. These dynamics are investigated across the supercontinent cycle, to assess the degree to which plate tectonics and deep Earth dynamics are interconnected.

Downwellings are a fundamental driver of the mantle circulation cycle; slabs sink from the surface at a rate which is largely dependent on the interplay between mantle viscosity and plate properties which effect the surface velocity. They sweep warm material into piles at the base of the mantle, and form plumes where the flow converges. Basal mantle structures are therefore mobile

in response to changing subduction girdles at the Earth's surface. During supercontinent assembly, circum-continental subduction zones sweep material beneath the continent and antipodal ocean. Rapid reorganisation of the plates, tied to the formation of new subduction zones, leads to increasing complexity in the large-scale mantle flow pattern, disrupting these antipodal piles. Subduction zones are often long-lived features at the Earth's surface, such that the flow pattern in the mantle eventually restabilises, and deep mantle structures return to a predominantly degree 2 configuration.

The proximity of slabs and plumes can change the magnitude of upwellings, where the thermal anomaly is either dampened out by the downwelling, or plumes are swept laterally about the core-mantle boundary, entraining more warm material. When plumes are larger and hotter, their contribution to the forces driving plate tectonics is greater. The supercontinent cycle therefore comprises a fundamental component of the mantle circulation cycle (which describes the interaction of plates, downwellings, upwellings, and deep mantle structures), being both a driving force, and driven by mantle processes.

Acknowledgements

Theses are strange things, they are challenging and often frustrating, but writing this one has been a real passion project, and I am grateful for the opportunity to geek out about supercontinents for nearly 200 pages. Whilst my name may be on the cover page, this thesis reflects the amazing group of people who have supported me. There are far too few opportunities in life to acknowledge all of these remarkable people, so I'm going to take full advantage here, and it is going to be long.

My PhD has been funded by the NERC GW4+ DTP (Grant NE/S007504/1) and undertaken alongside the work of the NERC large grant "Mantle Circulation Constrained (MC2): A multidisciplinary 4D Earth framework for understanding mantle upwellings" (Grant NE/T012633/1). Thank you to everyone involved in securing this funding and for the invaluable support and training I've received. I would also like to thank the School of Earth and Environmental Sciences at Cardiff University, for providing a supportive environment, and thank John, especially, for letting me work in a room with a kettle that has been consistently turned on for 3.5 years. The supercomputing resources provided by Supercomputing Wales, ARCCA, and the UK's national supercomputer, ARCHER2 were vital to this work, and I am grateful for their commitment to updating and maintaining these complex systems.

Of course, I have to say a huge thank you to Huw Davies, I could not have asked for a better supervisor. Thank you for your patience when I've gone off on a tangent, your enthusiasm for science, and for your constant encouragement. You've become a true friend, and I am very grateful to have had such a positive PhD experience. I'd also like to thank my other supervisors, James Wookey for your enthusiasm and insights, and James Panton for your support, friendship, and for being the TERRA oracle. Working within such an incredible geodynamics group has been a privilege and I thank Huw, James, Nico, Gwynfor, and Duo for all of your insightful discussions, and genuine friendship. Being able to complete my research alongside the MC2 project has been an incredible opportunity. I'm especially grateful for the MC2 early careers researchers with whom I have had the pleasure of discussing everything from serious academic debates to Love Island.

My academic journey did not begin in Cardiff, and I would never have been able to get to this stage without the encouragement of those along the way. Stash, thank you for letting me ramble on about volcanoes for years and for first introducing me to Pangaea. Your support throughout the years has always been appreciated, and I'm very glad that you set this whole ball rolling. From my time at the University of Liverpool, I am especially grateful to Chris Stevenson who, despite his sedimentological preferences, has always been an great support. Thanks also to Moh Gouiza and Tim Craig at the University of Leeds, who first introduced me to geodynamic modelling (and supported me through a lot of the COVID chaos).

Of course, the last four years would not have been half as fulfilling without family and friends. A huge thanks to the Roath Park Runners (especially the Sunday crew: Mike, Simon, Dan, Pauliina, and Duncan), you have kept me sane. Ffion, thank you for being there with a wine whenever either of us needed a rant. Rhiannon, thank you for being so bonkers, you never fail to make a rubbish situation seem a bit better. To my friends in the department, Lisa, Jono, James, Paul, Anton, Joaquin, Giovanni, Fiona, Luca, Gwynfor, Laura, Tyrone, Alex, Emily, Sarah, Julia, and Mike; thank you for your support and humour, through endless pub quiz defeats and surreal lunchtime conversations. To Sara, thank you for always making me laugh with your Schitts Creek impressions, and for being the best person to discuss MAFS Australia with. Roberto, you have been the best friend to me these last few years, and I am so grateful for you, Charis, and Lorena. The board game nights, beach days, and carveries are some of my fondest memories of Cardiff. Nico, thank you for being there through it all, for not laughing at my rubbish French, and for your continued patience when I get stressy.

Away from Cardiff, I need to thank Cam Wedge, for the Crown quizzes, Essen trips, and enduring friendship. Lucy, I have always been grateful for your sense of humour and Mamma Mia obsession in the face of all the drama, thanks for being a fab friend. To the Geol Squad (Alice, Megan, Ellie, Harrie, Lily, Rob, Robbie, Harry, and Ed), your support and friendship through it all means the world to me, and I can't wait to see you all on the Center Parcs rapids ASAP. Anthony and Robbie, thank you for being great honorary Dynamos, and to the Dynamos themselves, you have shown me unconditional support through the years and have always been there with a bottle of wine when things got rough. You really are my rocks.

Finally, I thank my family. Glynn, your perseverance and passion has always inspired me. Bianca, your independence and positive outlook is phenomenal. I am grateful every day that you both became part of our family. Andrew, thank you for everything you've done over the last few years, and for keeping me humble by reminding me that my work is just a load of waffle. Vicky, thank you for being a phenomenal support and for your mad sense of humour which has always been the perfect therapy for whatever else is going on in the world. Mum, thank you for raising me to know my own mind and work hard at whatever I've set my mind to, even if it makes me stubborn. I know that you are always cheering me on. Dad, I appreciate your attempts to be interested in my work, despite not remembering what I said five minutes ago. I am thankful that you have always celebrated my quirks, and for reminding me that there is no problem that a cup of earl grey and a nap can't solve. Chris, thank you for always making me laugh, and for growing up from an annoying little brother to a best friend. Annabel, words cannot express my gratitude for everything that you've taught me; you have always been my role model and have shown me that no challenge is too big to manage. Barba, thank you for being my go-to person when I need a chat. You have always told me that if you could have your time again, you'd have studied more, whether that be ballet, medieval history, or plate tectonics. Your drive to continue learning inspires me every day and, as one of very few people who will ever read this thesis cover to cover, I hope that it makes you proud. Thank you all for everything that you do.

Table of contents

List of figures

List of tables

For Barba.

Chapter 1

Introduction

1.1 Earth Structure

The Earth formed 4.6 billion years ago from the accretion of dust and gas left over from the formation of the Sun. As these accumulations became more massive, their gravitational fields strengthened such that larger bodies collided and coalesced. These collisions induced huge volumes of melting which, alongside radioactive decay, resulted in a very hot Earth. Since this time, the Earth has been cooling and chemically segregating such that 3 distinct layers are now defined (figure 1.1); the crust, the mantle, and the core.

Mantle dynamics, which are the focus of this thesis, are driven largely by the hot and cold thermal boundary layers at the core-mantle boundary (CMB) and the surface, respectively. The mantle facilitates the transfer of both energy and physical structures from one boundary layer to the other, such that constraining mantle dynamics requires a knowledge of the three layers, which I briefly introduce in turn here.

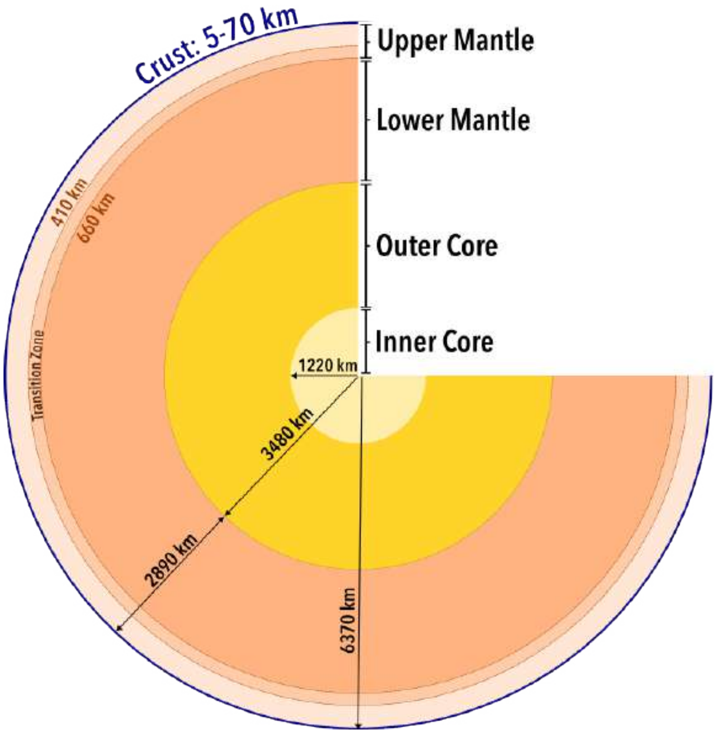

Figure 1.1 Structure of the Earth's interior, not to scale. Dashed lines represent seismic discontinuities, at 410 and 660 km depth.

1.1.1 The Crust

The Earth's crust forms as the final product of mantle differentiation, through the solidification of buoyant melts which rise to the surface. As such, this layer describes the uppermost 5-70 km of the planet (figure 1.1). As the only layer available for direct sampling and observation, it is by far the most thoroughly researched and well-understood, despite constituting less than 1% of the total Earth mass.

The thickness, composition, and density of the crust is largely bimodal, forming ocean basins and continents. Oceanic crust is the most areally extensive (65% of the global surface) and is produced at rifted margins, where two tectonic plates diverge. It is recycled back into the mantle at subduction zones and subsequently, this type of crust is thin (around 7 km) and relatively short-lived. Average ages of oceanic crust range from 60-70 Myrs, and rarely exceed 200 Myrs, often being produced and subducted within one supercontinent cycle (Spencer et al., 2017).

Continental crust is significantly older and thicker than the oceanic crust, with typical ages of around 2 Gyr and thickness of 30-70 km. Continents are often heterogeneous with cratonic centres dating back to the Archean, surrounded by highly deformed Proterozoic orogenic belts and Phanerozoic sedimentary basins (Artemieva, 2011, and references therein). Continental crust is currently produced at convergent plate boundaries, where a subducting slab dehydrates and the free water induces partial melting in the mantle wedge. As the resultant partial melts migrate through the crust, they mix and undergo fractional crystallisation such that more silicic rocks are erupted and emplaced near the surface, evolving into continental crust.

1.1.2 The Mantle

The mantle is the dynamic layer between the crust and the core, linking these domains by the transfer of both energy and physical structures. High mantle viscosities cause material to move very slowly relative to human timescales, through viscous creep processes. However, over geological time, the mantle is convecting vigorously with a Rayleigh number (a non-dimensional measure of convective vigour in a fluid) of $\sim 10^{8-9}$ (Wolstencroft et al., 2009; Bunge et al., 1997) and results in flow speeds of a few cm yr^{-1}. It is this convection which mixes the mantle and facilitates the movement of heat and different compositions and chemistries, primarily through downwellings slabs and upwelling plumes (figure 1.2).

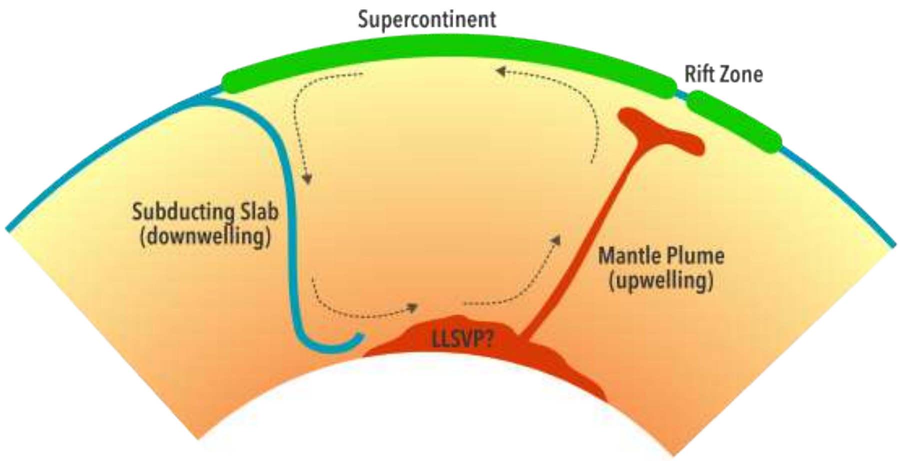

Figure 1.2 Simplified schematic slice through the Earth depicting the major features which link the crust and the mantle domains and a representative 'circulation cycle'.

Given its location, the mantle cannot be directly observed and therefore our understanding relies on seismological, geodetic, geochemical, and mineral physics data, alongside numerical models of the deep Earth, to understand its properties and behaviour.

The mantle is by far the largest layer of the Earth, at 84% of the total volume and 68% of the mass, and is itself comprised of mineralogically and mechanically stratified layers (figure 1.1) which may alter the nature and behaviour of structures which pass through them. The uppermost mantle is the coolest and most solid and, like the crust, deforms elastically on geological timescales. The two layers move mechanically coherently with plate motions (Artemieva, 2011) and are therefore grouped together and called the lithosphere. The behaviour of the lithosphere is crucial to this body of work, such that I highlight the distinction between crust and lithosphere, and predominantly refer to the latter hereafter. Beneath, the upper mantle extends to a depth of 660 km with the region between 410 km and 660 km being referred to as the transition zone. This transition zone is defined by seismic discontinuities, attributed to mineralogical phase changes (Ringwood, 1968). These phase changes have been sampled by triplications in body wave travel times (e.g. Stähler et al., 2012; Tajima and Grand, 1995; Tajima et al., 2009) and have some topography that is sensitive to changes in temperature or composition (Helffrich, 2000). Lateral temperature variations can be attributed to cold downwellings or hot upwellings within the mantle and may have implications for the velocity and behaviour of mantle structures which link the core and the crust.

The lower mantle is 1-2 of magnitude more viscous than the upper mantle and contains two large low shear-velocity provinces (LLSVPs), which have been identified beneath Africa and the Pacific Ocean (Garnero and McNamara, 2008; Garnero et al., 2016). The degree to which LLSVPs are thermal (Davies et al., 2012; Davies et al., 2015; Ritsema et al., 2007; Schuberth et al., 2009), or thermo-chemical (Tackley, 2012; Bower et al., 2013; Bull et al., 2009; Lassak et al., 2007; Panton et al., 2023) in origin is contested within the Earth Science community. It is, however, understood that there is likely some feedback between these structures, upwellings, and downwellings within the mantle, which is explored in this thesis.

1.1.3 The Core

The core occupies the centre of the Earth and can be further segregated into two distinct layers. The liquid outer core is defined by seismic shear wave velocities (Vs) of 0 m/s and is predominantly composed of a nickel-iron alloy whereas the inner core is solid and mostly iron. There is significant variation between the viscosities and densities of the core and mantle, such that the core-mantle boundary (CMB) is one of the most marked boundaries within the Earth. Conductive heat transfer across the CMB causes the largest hot thermal boundary layer within the Earth and it is this, coupled with the cold thermal boundary layer at the surface that ultimately drives mantle convection.

1.2 Plate Tectonics

Plate tectonic theory is based on the understanding that the lithosphere is split into a number of plates which move around the surface of the Earth. Wegener (1966) noticed the similarity between the South American and African coastlines, and suggested a historic supercontinent, Pangaea. In this theory, continents drifted passively, with little understood about the driving mechanism to facilitate this. It is therefore important to highlight the distinction between this theory of continental drift and the modern theory of plate tectonics. Plate tectonics builds upon Wegener's theory by suggesting that lithospheric plates are driven by a mantle mechanism. Despite increasing research (figure 1.3) since this time, many of the complex processes which facilitate the assembly and dispersal of supercontinents, and the degree to which these processes are related, remain unresolved.

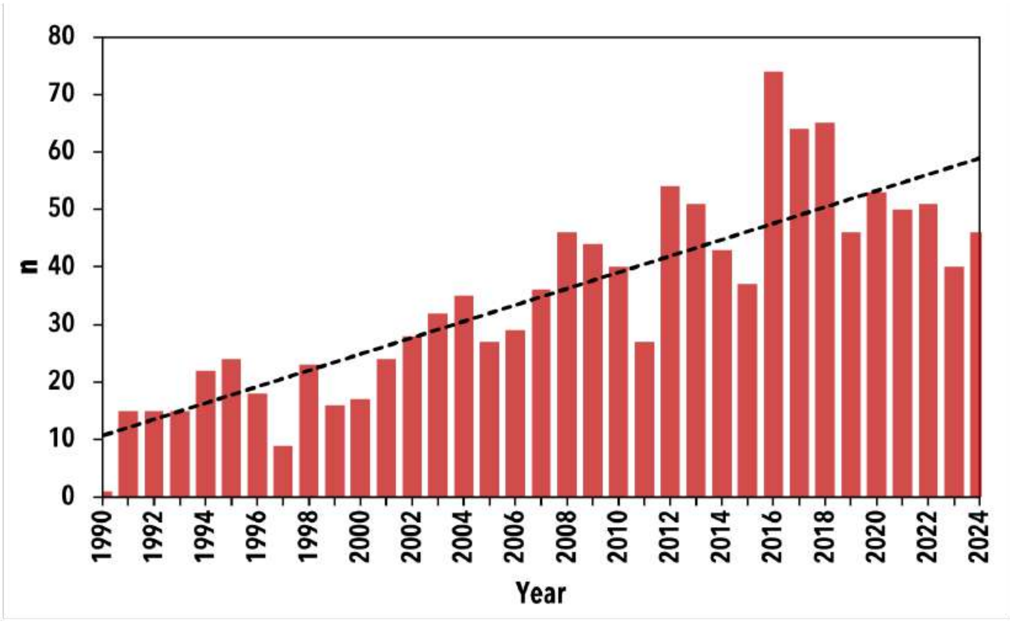

Figure 1.3 Number (n) of Web of Science results for search "Mantle Convection; Plate Tectonics" by year since 1990.

1.2.1 Earth's Tectonic Regimes

The Earth has evolved from a much hotter state following planetary accretion and collisional events, and therefore has experienced many different phases of tectonics which feed into the mechanisms which we observe today. The tectonics of the early Earth are unclear, and the range of potential tectonic regimes are highlighted in the contrasting models of continental crust growth (figure 1.4).

Armstrong (1981) based their study on near steady-state crustal growth and recycling within the first 1 Gyr of Earth history, prior to cratonisation and therefore suggests negligible crustal growth since 2.9 Ga. Variations in subduction rates and setting overprint this early phase of continental evolution, but ultimately, very little continental crust is produced (Dhuime et al., 2012; Vezinet et al., 2025). True steady-state dynamics cannot be achieved because

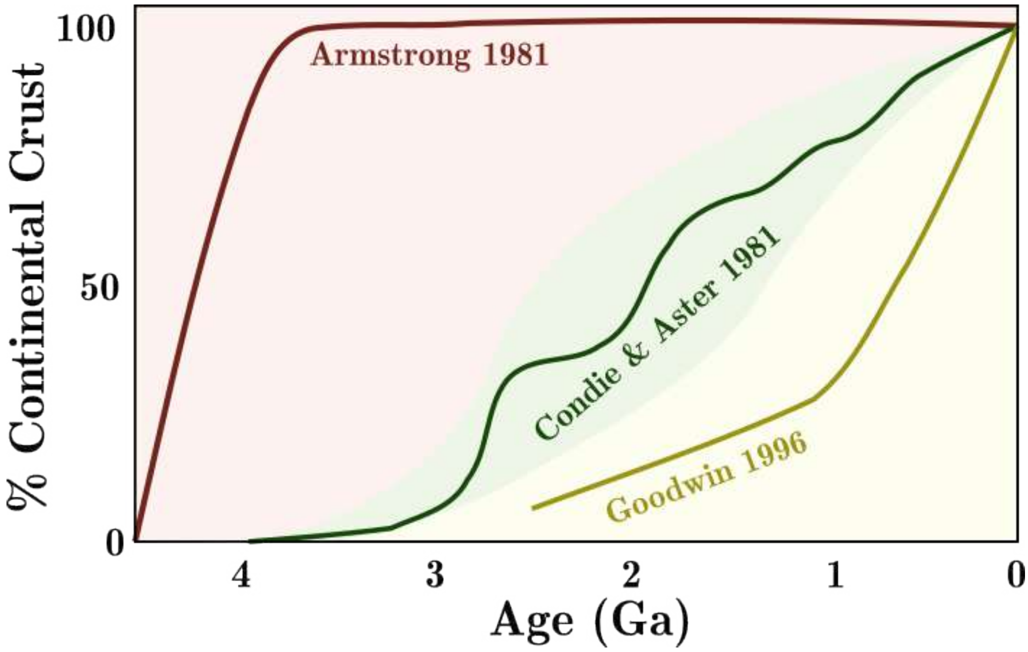

Figure 1.4 Contrasting models of continental crustal growth. Yellow space represents studies based on the distribution of rocks currently preserved at the Earth's surface; green space represents studies based on the assumption that the present distribution of rocks reflect relative volumes of crust present at different times throughout Earth's history; pink space represents studies which reflect rocks that may no longer be present at the Earth surface. Specific studies, which are referred to in the text, are highlighted. Adapted from Hawkesworth et al. (2019).

the driving energy of the Earth is assumed to decline with time, and therefore these two distinct phases of crustal growth may reflect very different tectonic regimes. Condie and Aster (2010) predict that 1/3 of the continental crust was formed during the Archean, marking one phase of tectonics during this time. Later, they compare the distribution of U-Pb zircon ages with the peaks of supercontinent assembly, suggesting that continental crust production rates increase when collisional events are more frequent. This suggests a close relationship between modern, supercontinent cycle-style tectonics and the present day distribution of continental crust, since 2.7 Ga (Pujol et al., 2013). Goodwin (1996) suggests that the majority of crustal growth has occurred during the last 1 Ga. This end member model is generally considered to be an oversimplification of Earth's history, and that the present day continental crust have been produced and recycled by this time (Hawkesworth et al., 2019; Dhuime et al., 2017), however it may indicate a change in tectonic regime over the last 1 Gyr. These selected studies reflect an extensive and ongoing body of work surrounding continental crust growth, which provide some insights into the potential tectonic evolution of the Earth. I briefly present a synthesis of suggested tectonic regimes across Earth history.

1.2.1.1 Hadean Tectonics

There is little direct evidence for the evolution of the Earth during the Hadean (Artemieva, 2011), which makes constraining the tectonic regime of this time difficult. Early Earth history was marked by heavy meteorite bombardment (Bottke and Norman, 2017; Wetherill, 1975), which increased the thermal budget (Ernst, 2017), introduced geochemical complexity but ultimately destroyed any geological record of this time. Many studies (e.g. Tonks and Melosh, 1993; Stern, 2004; Matsui and Abe, 1986) proposed that these high temperatures and associated low viscosities may indicate a global magma ocean. Whilst the planetary accretion of Earth and early bombardments were likely hot enough to develop this initial magma ocean (Valley et al., 2014; Tonks and Melosh, 1993; Nakajima and Stevenson, 2014), the cold thermal boundary layer at the Earth surface (Van Hunen et al., 2008; Lebrun et al., 2013) or vigorous mantle overturns (Ernst, 2017) would lead to rapid freezing of those oceans (e.g. Elkins-Tanton, 2008; Hamano et al., 2013; Maurice et al., 2017; Solomatov, 2007).

Ephemeral, ductile platelets may have been generated during the solidification of a magma ocean (Kröner, 1981; Ernst, 2017; Ernst, 2009) as the surface temperatures dropped below the peridotite and basalt solidi. As the mantle overturned rapidly, poorly organised mantle convection cells may have driven segments of a surficial lithosphere against and beneath one another and, ultimately, to be destroyed. Ernst (2017) suggests that this rapid convection may be why we do not observe the parental magma ocean in the rock record. Moore and Webb (2013) proposed an alternative mechanism for the dynamics of the early Earth, where a cold, thick lithosphere may begin to develop from successive volcanic eruptions attributable to a 'heat-pipe' mode of cooling. While heat pipes are active, Kankanamge and Moore (2016) suggest that the lithosphere gets progressively thicker and lithospheric isotherms are kept flat by the solidus, suppressing plate tectonics.

1.2.1.2 Archean Tectonics

By the onset of the Archean, mantle temperatures were 100-300 °C hotter than the present day (Van Hunen et al., 2008), suggesting higher volumes of melting and a less viscous mantle and lithosphere. At this stage, it is unlikely that the lithospheric strength was sufficient to sustain subduction. Successive overturn events would diminish large thermal heterogeneities, until the Earth's surface could sustain small, slightly negatively buoyant platelets (Stern, 2018; Ernst, 2009). Small plates may be associated with a plutonic-squishy lid regime (Lourenço et al., 2020), characterised by high intrusion efficiency. An abundance of deep-seated ascending plumes may have generated a thick basalt crust which was prone to decoupling from the mantle lithosphere; sub-crustal subduction may have allowed the mantle lithosphere to be recycled whilst the thick crust remained at the surface (Van Hunen et al., 2008). It is this shallow return flow and partial fusion of the surficial basalts that may have produced the first granite-greenstone belts and tonalite-trondhjemite-granitoid (TTG) complexes, suturing together into distinct lithotectonic entities (Stern, 2018; Sizova et al., 2015).

The Archean may be characterised by crustal growth, firstly with platelets then eventually stitching together into larger plate-like structures. However, unlike modern plate tectonics, the dynamics of these plates are likely more independent of underlying mantle processes. Much of the crust may have remained near the surface whilst the mantle overturned in 300-500 Myr intervals (Bédard, 2018), where a thick mafic crust is supported by extremely high decompression melting fluxes, in accord with many craton genesis models (e.g., Campbell and Hill, 1988; Sizova et al., 2015).

1.2.1.3 Proterozoic Tectonics

The continued crustal growth through the Archean towards the Proterozoic likely led towards a stagnant lid mode of tectonics, characterised by anomalously high mantle melt fluxes and temperatures (Bédard, 2018; Moresi and Solomatov, 1995). This regime is typified by the development of broad continental platforms, emergence of crustal freeboard, coeval sedimentary differentiation, and intra-continental suture belts (Ernst, 2017; McLennan and Taylor, 1983; Schubert and Reymer, 1985). These intervals may correspond to periods of layered mantle convection (evidenced by lithophile and rare gas element abundances; Stein and Hofmann, 1994; O'nions and Tolstikhin, 1996), where efficient cooling is restricted to the upper mantle, perturbing the Earth's heat generation/loss balance, eventually triggering mantle overturns (Bédard, 2018). Over time, the mantle overturns under a stagnant-lid are less efficient than plate tectonics at transporting internal heat towards the surface (Ernst, 2017). Compared to the Archean, residence times at the surface may have been longer such that progressively cooler, thicker, oceanic plates became increasingly negatively buoyant until subduction becomes a more fundamental process by around 1 Ga. Thermal blanketing by a broad lithospheric lid causes a convective build-up of energy beneath the plate, with conductive heating of the upper mantle, thinning, lithospheric extension and eventually, rifting. This period may reflect the transition from the vigorous overturning of the Archean to present-day plate tectonics or a stagnant phase in an episodic lid regime (Roberts, 2013; Sobolev and Brown, 2019).

1.2.1.4 Modern Tectonics

Modern day tectonics, or Wilson-cycle tectonics (Wilson, 1966), describes the cyclical opening and closing of ocean basins by the subduction and rifting of tectonic plates. The cycle comprises six key stages: (1) the rifting of a continent; (2) seafloor spreading and the initiation of a new ocean; (3) the formation of large oceanic basins; (4) new subduction initiation; (5) ocean basin closure through subduction of oceanic lithosphere; (6) continent-continent collision and complete closure of the basin (Wilson, 1966; Wilson et al., 2019).Sobolev and Brown (2019) propose that this period of tectonics is facilitated by subduction lubrication events, in which sediments accumulate at the continental edges and in trenches. This modern phase of tectonics is the best understood given that we can observe and understand mantle structures using seismology and geochemical investigations, and can also observe some processes in motion during earthquakes and eruptions.

In this case, there is a complex feedback between lithospheric plates and the mantle, where subduction is both a driving force, and driven by mantle convection (see section 1.3 for further discussion of these processes). It is important to this body of work to highlight the distinction between the Wilson Cycle and the Supercontinent Cycle, as the two are often used interchangeably.

Whilst both refer to tectonic plates colliding and rifting, the spatio-temporal scales are different. Wilson Cycles describe the cyclical opening and closing of individual oceans (thus acting on a regional scale), whilst the formation of a supercontinent may constitute more than one life-cycle of at least one ocean (Heron, 2019), and the large-scale movement and aggregation of tectonic plates. Broadly, the Wilson Cycle relates to the tectonic regime of the Earth, and this in turn results in the larger scale Supercontinent Cycle. The four main phases of tectonic evolution discussed throughout this section are summarised in figure 1.5.

1.2.2 Supercontinent Cycles

The supercontinent cycle has implications for vast ecosystems, including the evolution of the geosphere, hydrosphere, atmosphere, and biosphere (Nance et al., 2014), with supercontinent amalgamation, especially, being linked with an acceleration of biological diversification and climatic variation. As such, understanding supercontinents may have significant implications for all fields within Earth and biological sciences.

Before the opening of the Atlantic Ocean, the continents were assembled into one tight landmass, Pangaea ($\sim$ 335-200 Ma). The subsequent breakup of this continent means that similar geological structures and fossils are now found across the globe; separated by huge oceans which cannot have existed earlier in Earth's history. Whilst Pangaea is the best understood and most ubiquitously known supercontinent, it is not a unique feature. Many supercontinents have come and gone since the onset of tectonics, around 3 billion years ago, with each breaking up and reassembling over hundreds of millions of years. This repeating process of breakup and amalgamation constitutes the supercontinent cycle.

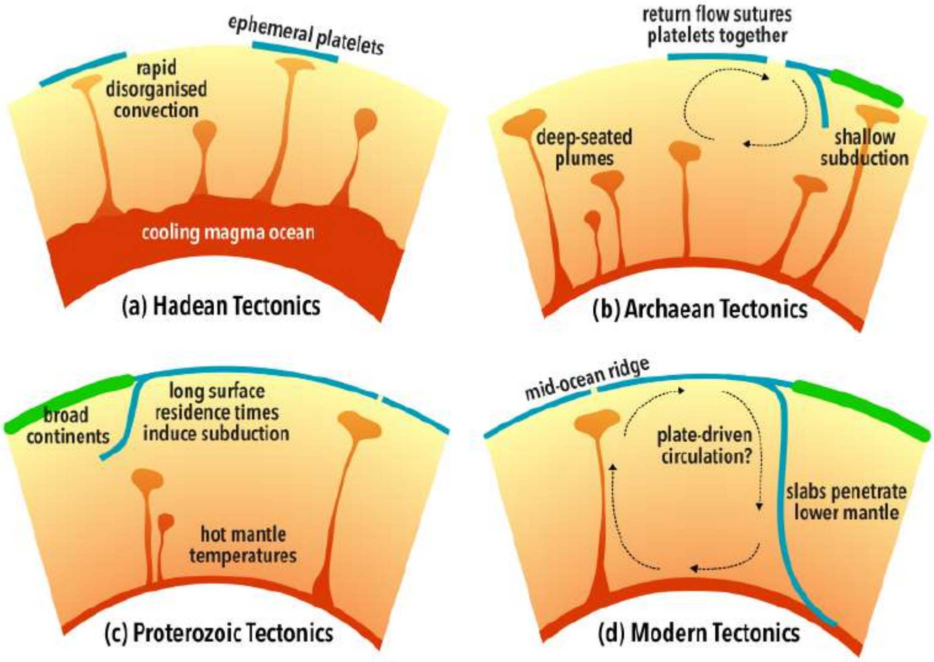

Figure 1.5 Schematic diagram showing the stages of Earth's tectonic evolution. Oceanic crust = blue; continental crust = green. (a) Cooling magma-ocean following the culmination of planetary accretion; (b) earliest evolution of 'plate' tectonics, related to alternating phases of mantle overturn and stable platelets; (c) phase of convection typified by the amalgamation of larger crustal bodies and the transition from stagnant-lid to plate tectonics; (d) modern Wilson-cycle tectonics (modified from Ernst, 2017).

Zhong et al. (2007) suggested that the supercontinent cycle is characterised by an alteration between spherical harmonics degree 1 and 2, in which sub-supercontinental upwellings are driven by the return flow of circum-continental subduction. The geoid high associated with upwellings changes the moment of inertia of the Earth (Evans, 2003), forcing supercontinents towards the equator where they split up (Phillips et al., 2009). As the thermal anomalies re-equilibrate with the ambient mantle, the Earth tends back towards a degree

1 structure, inducing rapid true polar wander (TPW) as a new supercontinent assembles (Phillips et al., 2009; Zhong et al., 2007).

Condie (2002) proposed that the degree of fragmentation of a supercontinent is controlled by the location relative to subduction arrays. At the point of breakup, supercontinents are likely encircled by inwardly dipping subduction zones at the boundary between oceanic and continental domains (Murphy and Nance, 2013). There is debate surrounding the role of active and passive processes in supercontinent breakup (e.g. White and McKenzie, 1989; Storey, 1995; Sengör and Burke, 1978), though Wolstencroft and Davies (2017) propose that this a false dichotomy and that both end members are crucial. They propose that if plumes are considered to rise actively through the mantle, then the passive return flow must generate extensional forces at the surface. The geometry of breakup may follow zones of pre-existing weakness (Dang et al., 2020), as is observed on all scales of structural geology, where on the largest lithospheric scales, rift geometry is inherited from previous orogens (Fossen et al., 2017; Buiter and Torsvik, 2014; Peron-Pinvidic et al., 2022).

The mechanisms which control the assembly of supercontinents are somewhat ambiguous, with a complex interplay between introversion, extroversion, or the combination of both (Yoshida and Santosh, 2011). In classic Wilson Cycle models, oceanic crust is formed during supercontinent breakup and destroyed during supercontinent assembly, so that the supercontinent turns inside in (introversion; Murphy and Nance, 2003). When supercontinents disperse, the outside edge of each continental fragment may collide, effectively turning outside in (extroversion).

Orogenic granitoids and detrital zircons have episodic appearance in the rock record, correlated with supercontinents since the Precambrian (Bradley, 2011). Peaks in detrital zircon records seem to reflect peaks of supercontinent assembly (figure 1.6), and therefore suggest that multiple supercontinents have existed throughout Earth history. Whilst the size and definitions of these supercontinents may differ, I briefly describe each of the most well-constrained supercontinents that have likely existed (for more detailed descriptions of previous supercontinents, see Nance et al., 2014, and references therein)

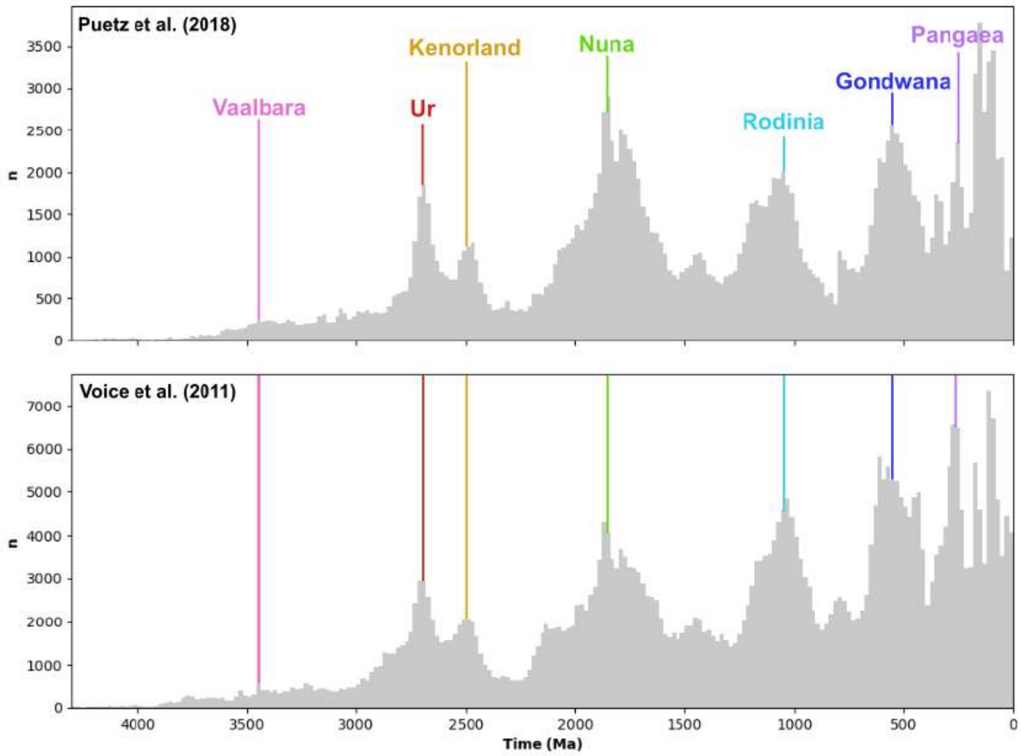

Figure 1.6 Age distribution of zircons from global U-Pb databases compiled by Puetz et al. (2018) and Voice et al. (2011). Histograms are binned into 20 Myr intervals and are correlated with the peaks of supercontinent assembly.

1.2.2.1 Vaalbara (3.6-2.8 Ga)

Vaalbara was an early supercontinent, which may have existed from 3.6-2.8 Ga. It's definition as a supercontinent is contentious, given that the landmass was likely much smaller than all present-day continents (Evans and Muxworthy, 2019). More accurately, Vaalbara can be described as a supercraton, formed from the Kaapvaal, Pilbara and potentially Singhbhum cratons (Kumar et al., 2017). Given the age of this supercraton, it is difficult to reconcile all the data across the regions. The evidence for this supercraton lies within the geological similarities across the cratons, palaeomagnetic data, and the zircon isotope data. However, the TTG rocks across the cratons highlight differences in geochemistry and age profiles (Evans, 2013; Gardiner et al., 2021). Following the aggregation of this supercraton, additional cratons, which had become stable by around 3 Ga, were all located within a small region (Rogers and Santosh, 2003), perhaps indicating subsequent, larger supercratons, Ur (2.8-2.4 Ga) and Kenorland (2.7-2.1 Ga). The increasing volume of continental crust after this time allows for the differentiation between supercontinents and supercratons (where supercontinents evolve through the assembly of now evolved continental lithosphere rather than as sutured cratons). Therefore, the proposed supercratons Arctica and Atlantica (Bradley, 2011) are not discussed here.

1.2.2.2 Nuna (1.8-1.35 Ga)

Nuna is regarded as the first true supercontinent and was formed by proto-subduction processes (Zhao et al., 2004), in what may be regarded at the Earth's first supercontinent cycle (Elming et al., 2021). Nuna amassed its great size through the collision of Laurentia, Baltica, Siberia, proto-Australia, North China, and India, (Elming et al., 2021) plus the formation of accretionary magmatic belts and the associated growth of the supercontinents at the continental margins (Zhao et al., 2004). Whilst the initial assembly of Nuna occurred via collision of small blocks (Evans and Mitchell, 2011), the breakup of the Nuna's core started around 1.5 Ga, and took the form of widely spaced rifts that separated sub-continent sized fragments, indicating the transition towards Wilson-cycle tectonics.

1.2.2.3 Rodinia (1.1-0.7 Ga) and Gondwana (550-180 Ma)

The assembly of Rodinia epitomises the supercontinent cycle, comprising many of the same large continental blocks as Nuna but in a different configuration. Whilst Laurentia, Siberia, and much of present-day China were assembled by 1.1 Ga, Li et al. (2008) suggests that supercontinent assembly did not peak until 900 Ma. Widespread rift-related volcaniclastic successions and intra-continental mafic-ultramafic intrusions are interpreted as the presence of a superplume, which may have been a driving force for continental rifting (Li et al., 2008). This breakup may have occurred through the fragmentation of continental blocks around Laurentia, which then collided on the other side of the Earth (Hoffman, 1991). Gondwana remained distinct from Laurentia through this time, therefore Gondwana is not always regarded as a true supercontinent, but can instead be considered similarly to the present day Eurasian-African continental landmass.

1.2.2.4 Pangaea (335 - 175 Ma)

Pangaea is the best known and most recent supercontinent to have existed on Earth, formed by the Variscan Orogeny. Mitchell et al. (2021) describes Pangaea as 'the keystone that upholds the concept of what a supercontinent is and the detailed understanding of it provides the central principles on which the understanding of older supercontinents depends'. Laurentia collided with

Baltica and Avalonia to form Laurasia, which then joined with Gondwana at the peak of supercontinent assembly. Sm-Nd isotope evidence suggests that Pangaea accreted through introversion, following the extroversion which formed Gondwana (Murphy and Nance, 2003). Given that Pangaea is the most recent supercontinent, it was the first recognised by geologists (Wegener, 1966), though the specific geodynamics and kinematics have been discussed for a century. Pangaea has been associated with large low shear-velocity provinces (LLSVPs) which reside at the base of the mantle, linked by mantle plumes which erupt at the surface as large igneous provinces (LIPs), highlighting the coupling between supercontinents and mantle processes. The relationship between these two domains can be explored through mantle circulation models, where plate motion reconstructions are implemented as a surface boundary condition. I implement this methodology throughout this body of work to better understand the feedback between surface and mantle dynamics.

1.3 Mantle and Lithosphere Dynamics

Research surrounding mantle convection and supercontinents has accelerated since the influential Anderson (1982) paper which noted a correlation between the Atlantic-African geoid high with the predicted position of Pangaea. This work suggested that continents promote the growth of broad thermal anomalies in the Earth through thermal blanketing, and by shielding the underlying mantle from the cooling effects of subducting slabs. These thermal anomalies were proposed to induce geoid highs, force polar wander and ultimately, cause rifting. The coupling between rift and subduction processes, and the subsequent effects of subduction and upwellings on mantle convection, necessitates research which considers great spatial and temporal scales (Li and Zhong, 2009). I briefly describe some of the fundamental concepts relating the lithosphere and mantle, which then form the foundation for each research chapter in this thesis.

1.3.1 Mantle Downwellings

Studies of differing approaches have yielded opposing models for the driving forces of plate motion. End-member processes include surface tectonic forces (from geochemical studies; e.g. Iwamori and Nakamura, 2015), mantle drag forces acting on the base of the lithosphere (Alvarez, 1982), and a 'slab pull' mechanism, based on geodynamic studies (e.g. Forsyth and Uyeda, 1975, Conrad and Lithgow-Bertelloni, 2002). Many studies suggest that slab pull dominates plate motion processes; predictions of Cenozoic plate motions requires the total contribution of slab pull to plate driving forces to be $> 90\%$ (Collins, 2003), with the majority of this force being focussed in the lower mantle. Cold, strong slabs in the upper mantle transmit stress directly to subducting plates at the surface, whilst a detached slab descending through the mantle is proposed to exert a 'slab suction' force by invigorating mantle flow and increasing traction at the base of the plates at the surface (Conrad and Lithgow-Bertelloni, 2004). This suction would rapidly draw plates towards the subduction zone and promote back-arc extension.

The relative contributions of slab suction and slab pull to downwelling dynamics are estimated at 40 and 60 %, respectively (Conrad and Lithgow-Bertelloni, 2004), which suggests that understanding the character and behaviour of slabs in the deep mantle is crucial to understand surface deformation and subduction dynamics throughout the supercontinent cycle. Furthermore, Kameyama and Harada (2017) suggest that our ability to understand the entire supercontinent cycle is reliant on understanding the dynamic behaviour of slabs; they propose, as have others (e.g. Cao et al., 2021a; Yoshida and Santosh, 2011; Heron et al.,

2015) numerical models in which dense materials at the base of the mantle flow horizontally toward the region beneath a newly-formed supercontinent in response to cold downwellings. These dense zones may then initiate upwelling which ultimately induces breakup within their models. The dynamics of subducting slabs within the mantle are, however, the subject of much discussion. As such, I highlight the necessity to better constrain the link between the surface and slabs within the mantle at a fundamental level; a subject which this work will address.

The trajectory of slabs may determine the convective wavelength within the mantle; shallow slabs induce counter flows which localise diverging tractions at the base of the lithosphere which may induce back-arc rifting, and form marginal basins within 10 Myr whilst deep mantle slabs reorganise counter flow into long wavelength cells (Dal Zilio et al., 2018). In the latter case, sub-continental tractions are higher and more sustained over longer periods and distances, which may result in the opening of a distal basin. It is therefore important to recognise that subduction has been proposed as a possible mechanism for both supercontinent assembly and dispersal, such that it is undoubtedly a critical process which must be further explored within this study.

1.3.2 Deep Mantle Structures

At present, there are two LLSVPs in the deep mantle which cover between 20-50% of the CMB (Burke et al., 2008b; Garnero and McNamara, 2008; Garnero et al., 2016). Currently, they sit beneath Africa and the Pacific ocean, roughly antipodal to one another. The importance of these structures lies in the proposed relationships between LLSVPs, hotspots, large igneous provinces (LIPs), long-wavelength geoid highs, and former subduction zones (Davies et al., 2015). Multiple models exist for the origins of LLSVPs, especially the extent to which these features are purely thermal, or thermochemical (e.g. Davies et al., 2012; Davies et al., 2015; Ritsema et al., 2007; Schuberth et al., 2009; Bower et al., 2013; Bull et al., 2009; Lassak et al., 2007). The anti-correlation of bulk-sound and shear-wave velocity anomalies has been used to suggest a distinct composition between LLSVPs and the ambient mantle (Ballmer et al., 2014), though a consensus regarding the origin of such material is lacking. The most widely supported sources for compositional heterogeneity are a primordial layer formed early during Earth's history (e.g. Lee et al., 2010), or a dense eclogite component of subducted slabs (e.g. Niu, 2018).

For LLSVPs to remain stable over long periods of time, any thermal buoyancy must be counterbalanced by some negative chemical buoyancy to maintain an equilibrium. Numerical models have shown that large-scale compositionally anomalous structures can be formed by mechanical stirring where thermally induced positive buoyancy is balanced by a fraction of some dense material at the CMB (Mulyukova et al., 2015). If LLSVPs are predominantly thermal structures, then Davies et al. (2015) suggests that they are less stable than previously suggested, and instead their location is related to subduction zones and the trajectory of slabs through the mantle.

Palaeomagnetic data suggests that plumes form at the edges of LLSVPs (Torsvik et al., 2010; Ganerød et al., 2010; Ganerød et al., 2011; Heron, 2019; McNamara, 2019; O'Connor et al., 2018); LIP eruption sites over the past 300 Myr lie above the 1% slow shear-velocity contours around the African and Pacific LLSVPs, subsequently termed Plume Generation Zones (PGZs; Burke et al., 2008b). PGZs projected towards the surface approximately match positive geoid anomalies, suggesting that LLSVPs are the dominant control on long-wavelength geoid contours (Burke et al., 2008b) which may determine the location of supercontinents. Maruyama et al. (2007) and Senshu et al. (2009)

propose a direct relationship between LLSVPs and the supercontinent cycle, proposing superplumes rise from LLSVPs and break apart a supercontinent. There are many questions surrounding the origin, nature, and stability of LLSVPs that remain unanswered within the geodynamic community. Given that LLSVPs have been associated with downwelling and upwelling dynamics, this thesis will address the long term stability and behaviour of LLSVPs within this cyclical context.

1.3.3 Mantle Upwellings

Plumes may form as the result of thermal or chemical instabilities at the CMB (Condie et al., 2015a), from the edges of deep mantle structures (Davies et al., 2015) or, more controversially, through thermal insulation and blanketing of the mantle by a supercontinent (Anderson, 1982; Condie, 1998). Within the context of the supercontinent cycle, mantle upwellings may be critical to supercontinent breakup. Previous studies have suggested that plateauing of mantle plumes against the base of the lithosphere is sufficient to induce breakup (Condie, 1998), whilst Collins (2003) proposed that pre-established rifting and mantle decompression acts to localise the magmatic output of plumes at hotspots. The latter also suggests that such hotspots at the surface accelerate mid-ocean ridge (MOR) development through thermal softening of the extending lithosphere, highlighting the closely coupled nature of mantle upwellings and rifting events.

Condie et al. (2015b) noted a correlation between LIP events and zircon age peaks, indicating an association between LIPs and supercontinent breakup. Additionally, Condie et al. (2015a) proposed two processes whereby plumes impact supercontinent assembly and breakup; (a) upwellings located beneath supercontinents may act to initiate breakup, and (b) plume ascent may increase the frequency of craton collisions and the rate of crustal growth by accelerating subduction.

Whilst subduction forces are considered the dominant mechanism of plate motion, the spatial contribution of subduction vs. plume push may be variable across a supercontinent. Numerical simulations have suggested that at the centre of a supercontinent, plume push forces are three times greater than that of subduction retreat, which are limited to a 600 km wide zone at the supercontinent boundary (Zhang et al., 2018). Additionally, Zhang et al. (2018) proposes that a hot anomaly of 50 K beneath the supercontinent is sufficient to produce a push force capable of inducing supercontinent breakup. The mechanisms which break up a supercontinent and those which sustain plate motion of smaller fragments may be different. It is reasonable that a supercontinent may begin to disassemble under the effects of a plume push force but may only attain total lithospheric breakup under the pervasive force of slab pull. Therefore this work aims to address two questions regarding upwellings; firstly I aim to explore the origin of plumes in the deep mantle, and to investigate mantle parameters which may affect the capacity for plumes to significantly thin and weaken the lithosphere.

1.4 Thesis Outline

In this thesis, I aim to build upon previous work to synthesise the role of the lithosphere in the supercontinent cycle and how plate tectonics both drives, and is driven by, mantle circulation. This will be achieved using 3D mantle circulation models, driven by plate motion at the simulated surface.

I consider the aforementioned hypothetical mantle circulation cycle (figure 1.2) in terms of three chapters; (i) a top-down approach to subduction and slab sinking, (ii) exploring the coupling between slabs, LLSVP stability and plume generation, and (iii) a whole mantle investigation into the sensitivity of circulation to lithosphere properties. The first will include changing the surface properties of the lithosphere and analysing the morphologies and velocities of slabs in the mantle where subduction processes are isolated from distal mantle structures. Next, I will consider the stability of LLSVP-like structures in the deep mantle in response to plate motion history, and explore plume development within this class of models. Finally, I will analyse the degree to which upwellings, downwellings, and deep mantle structures are interconnected, and how these feedback through supercontinent assembly to breakup in response to a heterogeneous lithosphere. Ultimately, I aim to consider the role of the lithosphere in the breakup and assembly of the supercontinent by exploring the degree to which upwellings, downwellings, and deep mantle structures are intrinsically linked to plate tectonics.

Chapter 2

Methods

2.1 Introduction

This work centres around 3D mantle circulation models, a type of convection model which implements plate velocities at the surface. This approach allows us to simulate a mantle which is more spatially consistent with the Earth than models which implement a free-slip surface boundary condition, and therefore can be constrained by comparing our models to geological and geophysical data.

This chapter will comprise; (i) a brief introduction to TERRA, the mantle convection code, and its governing mathematical equations, (ii) an introduction to mantle circulation models, and (iii) the plate motion reconstructions used as velocity boundary conditions within this thesis.

It is intended that this chapter forms a relatively concise introduction to the fundamental aspects of the methodology, which are shared across each subsequent chapter in this thesis, with chapter-specific methodologies in each respective section.

2.2 TERRA

2.2.1 Background

TERRA (Baumgardner, 1985; Bunge and Baumgardner, 1995; Davies et al., 2013; Yang and Baumgardner, 2000) is a 3D spherical mantle convection code which has been in use since the 1980s. The collaborative approach to its development has meant that this code is computationally efficient, with an efficient multigrid solver, and can represent the whole mantle at high convective vigour.

Over the last four decades, TERRA has been developed to run in parallel (Bunge and Baumgardner, 1995) so that computationally expensive calculations can be run across multiple processors and ultimately provide higher resolution results faster. For this thesis, the code is ran in parallel via The National Supercomputer, ARCHER2, and on the local supercomputing cluster as Cardiff University, HAWK (supported by ARCCA, Supercomputing Wales).

TERRA can incorporate plate motion reconstructions from GPlates (Bunge et al., 1998; Müller et al., 2018) as a surface boundary condition by assigning velocities at each point on the TERRA grid, which is fundamental to this body of work. With this comes the ability to constrain the spatial distribution of downwellings and therefore produce more Earth-like simulations, and the last time step (which reflects the present day) can be ratified against seismic tomography. Additional improvements to TERRA are continuously developed, from temperature-dependent viscosities (Yang, 1997) to the the implementation of particles to investigate complex chemical processes (Stegman et al., 2002). This dedication to optimisation and development have made TERRA into a scientifically robust code which is capable of answering many geodynamic questions. In this case, those geodynamic questions relate to the degree of coupling between the surface and the mantle across the supercontinent cycle.

2.2.2 The TERRA Grid

The TERRA grid is a scalable regular icosahedron comprising 20 equilateral triangles, projected onto a sphere (Baumgardner and Frederickson, 1985), combined into 10 diamonds each of which has a vertex at either the north or south pole (figure 2.1).

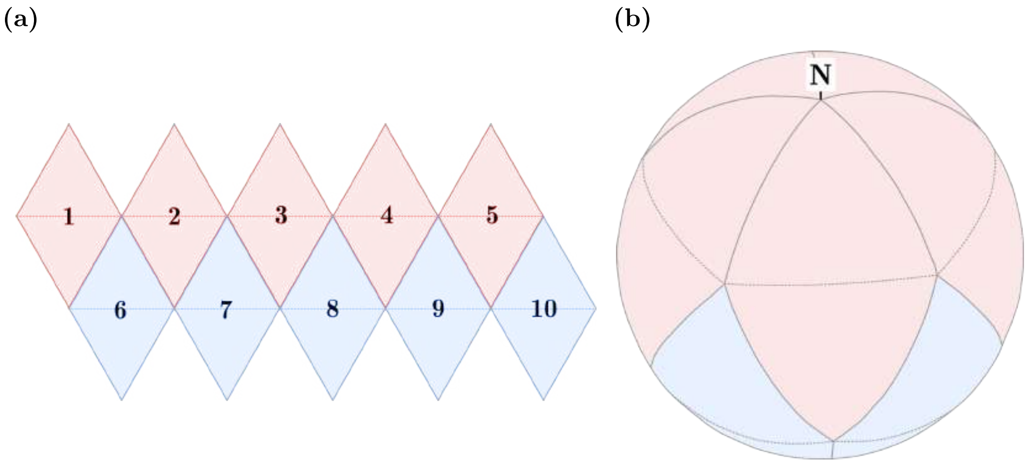

Figure 2.1 (a) Flat plan of the TERRA grid, comprising 10 diamonds; (b) diamonds (made of two triangles) forming an icosahedron, projected onto a sphere, where pink diamonds have a vertex at the north pole, and blue diamonds at the south pole.

Grid refinement is achieved by subdividing each equilateral triangle into smaller equal-sized triangles. Initially, the midpoints of each side of the triangle are connected, so that 4 smaller triangles are created. At each stage of refinement, this splitting at the midpoints results in a factor of 4 increase in the number of triangles and nodes. This increase in resolution is controlled by defining the *mt* value, that is the number of smaller triangles that each original triangle edge is divided into (figure 2.2).

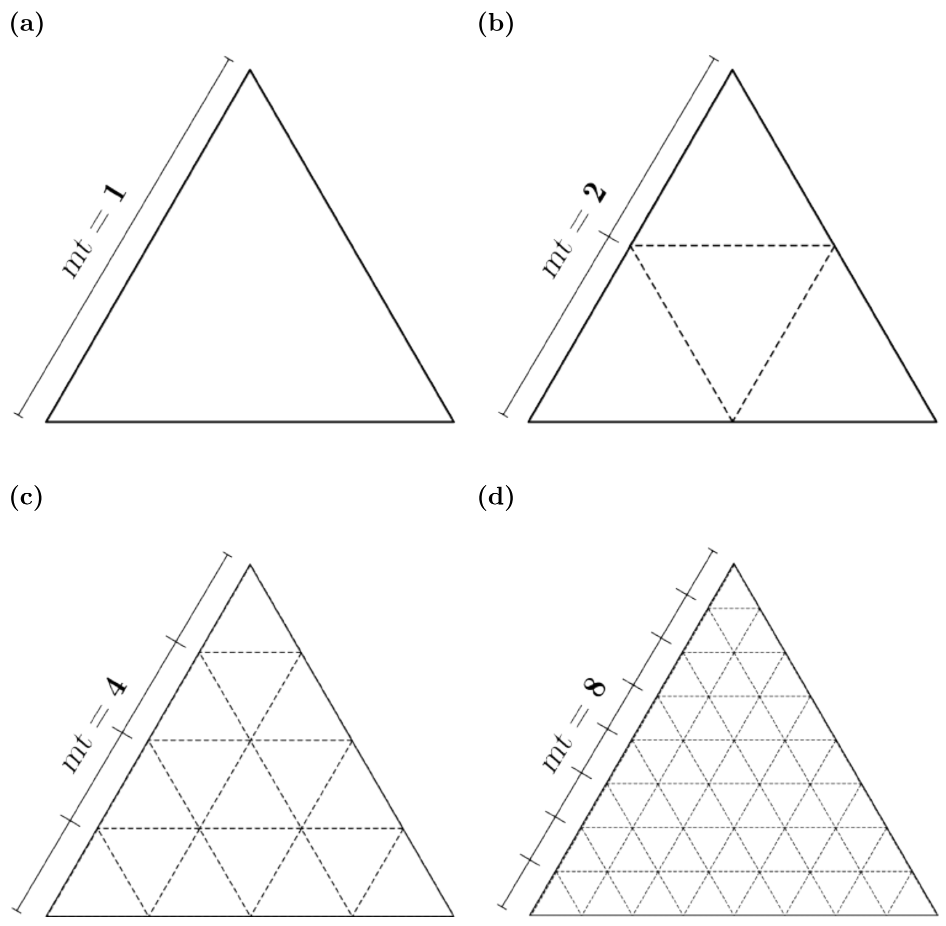

Figure 2.2 (a) Representative triangle which make up the diamonds of the icosahedral TERRA grid; (b-d) Recursive refinement of each triangle in the grid.

To model the Earth's interior, the shell must be repeated at radii ranging from the radius of the surface to the radius of the CMB. Connecting the grid points of these nested shells forms radial layers, where each cell is a triangular prism with a spherical end formed between the nodes of adjacent shells. Therefore, the number of radial layers (nr) within each model is equal to the number of radial shells minus one.

Subsequently, the nr value will define the radial resolution of each simulation. Yang (1997) found that stability is optimised when finite element cells have an aspect ratio approaching 1 and so for our models, which maintain the ratio of CMB to surface radii (~ 0.55), it was found that the optimum value of $nr = mt/2$.

With $nr + 1$ spherical shells within the model volume, where each shell contains $10mt^2 + 2$ nodes, the total number of nodes can be calculated. Table 2.1 indicates the relationship between mt and the radial and lateral resolution of each simulation.

Table 2.1 Resolution of TERRA grid at different values of *mt*.

mt	no.global nodes	Average lateral spacing (km)		Radial spacing (km)
		Surface	CMB	
32	174,114	239.8	131	180.6
64	1,351,746	119.9	65.6	90.3
128	10,649,730	59.9	32.8	45.2
256	84,541,698	30	16.4	22.6
512	673,710,594	15	8.2	11.3

As the resolution of the model increases, so too does the computational requirement. This is a major consideration within our models, where sufficient resolution of the lithosphere is critical to our analyses (minimum $mt = 128$). The number of processes required for a calculation is given by equation 2.1:

$$n_{proc} = \left(\frac{mt}{nt}\right)^2 \frac{10}{nd} \tag{2.1}$$

where nt is the number of the grid intervals along the edge of a local subdomain (figure 2.3) and nd defines how many diamonds (5 or 10) are mapped to a local process.

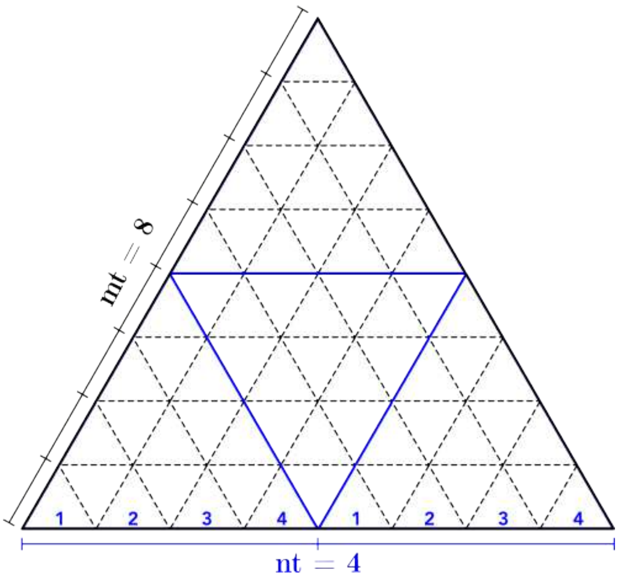

Figure 2.3 Representative triangle comprising the TERRA grid at $mt = 8$, showing the relationship between mt and nt.

2.2.3 Governing Equations

TERRA is formulated based on the three governing equations of fluid dynamics, which concern the conservation of mass (2.2), energy (2.3), and linear momentum (2.4):

$$\frac{\partial \rho}{\partial t} = -\nabla.(\rho u) \tag{2.2}$$

$$\frac{\partial T}{\partial t} = -\nabla.\left(Tu\right) - \left(\gamma - 1\right)T\nabla.u + \frac{\tau : \nabla u + \nabla\left(k\nabla T\right) + H}{\rho c_p} \tag{2.3}$$

$$\nabla.\tau - \nabla P + \rho g\hat{r} = 0 \tag{2.4}$$

The variables in equations 2.2, 2.3, 2.4 are summarised in table 2.2

Table 2.2 Variables and parameters within the 3 governing equations of TERRA.

Symbol	Parameter
ρ	density
t	time
u	fluid velocity
T	temperature
γ	Grüneisen parameter
τ	deviatoric stress field
κ	thermal diffusivity
H	radiogenic heat production
C_p	specific heat at constant pressure
P	dynamic pressure field
g	gravitational acceleration
$\hat{r}$	unit vector in radial direction

A compromise must be made within the calculations, such that the computational requirement is reduced yet the results are still justifiably Earth-like. As such, several assumptions are made. Firstly, the mantle rheology is modelled as a highly viscous, Newtonian fluid where the Prandtl Number (Pr, the ratio of viscous to inertial forces) tends towards infinity. As a result, the inertial forces can be neglected. We remove lithostatic pressure from the momentum equation (2.3) by subtracting a reference density and pressure gradient, so that simulations can be calculated based on density differences rather than absolute densities. Most of our simulations (chapter 3, chapter 5) are run assuming incompressibility (McKenzie et al., 1974), applying a Boussinesq approximation, which takes ρ as constant in all terms excluding our buoyancy term, such that $\Delta\rho$ is expressed as:

$$\Delta\rho = \rho\alpha(T_{rad} - T) \tag{2.5}$$

where α is the thermal expansivity and T_{rad} is the reference temperature for a radial layer.

By assuming incompressibility of the mantle, we can reduce the divergence of velocity to 0, and implement the constitutive law of linear momentum to produce simplified equations for conversation of mass (2.6), energy (2.7), and momentum (2.8),

$$\nabla.u = 0 \tag{2.6}$$

$$\frac{\partial T}{\partial t} + \boldsymbol{u} \cdot \nabla T - \kappa \nabla^2 T - \frac{H}{C_p} = 0 \tag{2.7}$$

$$\nabla \cdot (\mu\{\nabla \boldsymbol{u} + (\nabla \boldsymbol{u})^T\}) - \nabla P + \alpha\rho(T_{av} - T)g = 0 \tag{2.8}$$

where μ is dynamic viscosity. Chapter 4 presents a suite of compressible simulations, which are explored in more detailed within that chapter.

The mantle is a vigorously convecting system, as denoted by the dimensionless Rayleigh number for internal heating,

$$Ra = \frac{\rho^2 g \alpha H h^3}{k \kappa \mu} \tag{2.9}$$

where h is the distance between the surface and CMB radial shells, and κ is thermal diffusivity. This equation assumes a constant viscosity, which is applicable to some of the models in this thesis, but many have varying viscosity throughout the mantle volume. Most models implement a radially varying viscosity profile, such that Ra will vary between each radial layer and, where viscosity is dependent on temperature, across each respective layer also.

2.3 Mantle Circulation Models

Mantle circulation models differ from convection models by applying plate velocities as the surface boundary condition. This class of models is used consistently across this thesis to ensure that results develop in a way that is spatially consistent with plate motion reconstructions (and therefore is sensitive to supercontinent cycles). However, it is necessary to highlight that the dynamics of these models differs from the Earth in that plates are driven into the mantle by the prescribed plate velocities, rather than sinking as a result of their negative buoyancy. Previous works have sought to produce models with self-consistent plate like behaviour at the model surface using a sequential data assimilation approach, integrating surface kinematics and seafloor distribution with mantle convection models (Bocher et al., 2016; Coltice and Shephard, 2018). Coltice and Shephard (2018) proposed simulations which develop with self-consistent plate-like behaviour between 30-0 Ma. This approach used plate motion reconstructions as a surface boundary condition before extracting the mantle temperature field and computing free convection flow. Whilst this approach may better reflect the dynamics of the Earth during this window from 30-0 Ma, since slabs will sink passively rather than being driven into the mantle, this approach is not yet constrained enough to produce self-consistent plate-like behaviour over the course of multiple supercontinent cycles, which is critical to this thesis. Often, my models are pre-conditioned such that they have evolved from an initial condition (chapter 4 and chapter 5 of this thesis), and mantle structures are spatially consistent with initial plate stage of the circulation run to be analysed. For this pre-conditioning phase, models are first run as mantle convection models, initiated by instabilities caused by perturbations to the temperature field. I implement an initial temperature field derived from small scale random perturbations which break down as the models progress from their numerical initiation towards a more mixed mantle. These convection models have a free-slip boundary at the surface and CMB, and a two-layer viscosity structure, with an increase in viscosity across the 660 km transition zone (typically the lower mantle is 30 times more viscous than the upper mantle at the beginning of our simulations), but with no difference between the upper mantle and the lithosphere (Van Keken and Ballentine, 1998). A single plate stage is then fixed as a surface velocity boundary condition for sufficient time to allow the spatial distribution of the mantle to be consistent with the first plate stage included in analysis (the timing of this phase varies across different studies, given the variation in other initial conditions; details can be found in each subsequent chapter). At this time, the viscosity structure becomes three-layered, where the topmost radial layers are typically two orders of magnitude more viscous than the upper mantle, representing the lithosphere.

Circulation models are additionally complex as the imposed surface velocities are set independently of the convective vigour of the simulated mantle. When

Rayleigh numbers are lower than are Earth-like ($< 10^{8-9}$), convection is sluggish compared to the Earth, and applying published plate velocities can induced surface shearing. The solution to this is to slow plate velocities to match the natural velocity of the convection solution (attained during the first preconditioning phase). A scaling factor (S_v) is applied to the models according to the root mean square (RMS) velocity of the Earth surface at the present day and those calculated in convection simulations (equation 2.10).

$$S_v = \frac{v_{EARTH}}{v_{MODEL}} \tag{2.10}$$

The present day surface RMS velocity is chosen as a representative value as the Rayleigh number of our simulations do not vary significantly, such that a constant scaling factor is preferred and the present day velocity is the best constrained. This scaling factor is then applied to every time step. Surface velocities are multiplied by the reciprocal of S_v, ensuring that the relative plate motions are consistent with the plate motion history, just slowed to match the convective vigour of the simulations. As such, the duration of the simulation must be increased by the same factor to compensate for the reduced velocities and reflect Earth-like subduction and upwelling fluxes. Subsequently, there is an important distinction between model time (simply the assigned duration of each simulation) and Earth time (the geological time represented by the simulation). Model time is, in most cases, a factor of S_v greater than the Earth time it represents. For simplicity, any time presented within this thesis refers to the Earth time that the simulations represent, unless stated otherwise. Whilst the use of a velocity scaling factor S_v enables plate motions to be reconciled with the convective vigour of models operating at sub-Earth Rayleigh numbers, it is important to recognise the limits of this approach. The scaling law assumes that the relationship between surface velocities and internal convection is consistent across the models. Since the mantle viscosity in some models is fixed rather than self-consistently evolving, the rescaled velocities may not fully capture feedbacks between slab dynamics and mantle flow, and the effects of processes such as thermal diffusion would be exaggerated when plate motion is slowed down. Therefore, S_v should be considered as a pragmatic tool for ensuring geologically reasonable slab fluxes, rather than a physically rigorous transformation.

2.4 Plate motion reconstructions

The behaviour of convecting material at the boundaries of the models is constrained by the boundary conditions. The initial pre-conditioning stage of our models imposes free-slip boundary conditions at the CMB and surface of the simulations, where tangential stress is zero and the boundaries are impermeable. Conversely, for circulation modes, the upper boundary is defined by the imposed plate velocities. Since this study aims to understand the spatial and temporal relationship between the surface and the mantle, it is important to implement and compare various models of plate motion histories. Each chapter in this thesis implements the following plate motion reconstructions:

- Chapter 3 - Müller et al. (2022), Merdith et al. (2021)
- Chapter 4 - Müller et al. (2022), Merdith et al. (2021), Cao et al. (2021b)
- Chapter 5 - Müller et al. (2022)

It is useful to compare the fundamentals of each of these models, to better understand the similarities and differences between them, therefore I present the key details of each one in turn here (see each respective article for full descriptions of each reconstruction). Each plate motion history is similar for the present day, but diverge significantly further back in Earth's history.

2.4.1 Merdith et al., (2021)

This plate motion history is presented first in this thesis since it is closely related to, and is built upon for the Müller et al. (2022) reconstruction. Plate motion models are characterised by the reconstruction framework which is used to describe the motion of rigid objects on a sphere using Euler's rotation theorem (Merdith et al., 2021). Along with the angular rotation vector for each object, the theorem requires each rotation vector to be defined relative to another object producing a relative plate motion. The Merdith et al. (2021) model defines these rotations relative to a palaeomagnetic framework. The model considers the relative movement of plates based on a hierarchy of geological precedence, where terranes move relative to blocks, blocks relative to cratons, and cratons relative to supercontinents. As such, crust with more preserved data, providing the greatest constraints on the models, are placed above crust with less preserved data within the hierarchy. This geological data is used simultaneously with the palaeomagnetic data to iterate towards a solution (Merdith et al., 2021). Initially, palaeomagnetic data is used to build a continental drift framework, then geologically constrained plate boundaries are applied, with structural and metamorphic data used to determine the polarity of subduction, timing of collision, and the orientation of rifting. There is a significant body of deep Earth research which implements this plate motion reconstruction as a constraint (e.g. Flament et al., 2022; Wolf and Evans, 2022; Young et al., 2022). As such, using this model within our research provides an opportunity to consider the implications of our results directly within the context of the wider deep Earth community.

2.4.2 Müller et al., (2022)

The Müller et al. (2022) plate motion model comprises a global set of topological plate polygons with associated plate boundaries and velocities. These features span from 1 Ga to the present day in 1 Myr intervals, with the greatest constraints since the assembly of Pangaea ($\sim$ 335 Ma). Briefly, this model is based on a 'mantle reference frame' where plate positions are estimated relative to the mantle through time as opposed to the spin axis. The convecting mantle is not a stable reference frame, therefore this method aims to isolate the motion of the plates relative to the turbulence of the mantle. True polar wander (TPW) is excluded such that the method automatically provides both palaeo-latitudes and palaeo-longitudes relative the mantle, and therefore the reference frame is expressed as rotations of plates relative to a stationary axis. This model combines the plate motion model of Merdith et al. (2021), and the tectonic-rules-based approach to mantle reference frames proposed by Tetley et al. (2019).

Many absolute mantle reference frames are considered in this approach, and fit metrics are calculated by evaluating (i) net lithospheric rotation rate (NR), (ii) trench migration rate (TM), (iii) the fit of present-day hotspots to the major age-progressive hotspot tracks between 80-0 Ma (HS), and (iv) median global continental absolute plate velocity (PV). These metrics are applied with the assumption that NR rates should be minimised but greater than 0, TM is minimised to favour trench retreat, the misfit between model and present-day hotspots are minimised through space and time, and median continental plate velocities remain $<$60 mm yr^{-1}. This study builds upon the work of Merdith et al. (2021), integrates many fit metrics, and has been widely used across geodynamic studies since 2022 (e.g. Li et al., 2023; Timmerman et al., 2023;

Wang et al., 2024; Nance et al., 2022) making it the preferred plate motion reconstruction across this thesis.

2.4.3 Cao et al., (2021)

Cao et al. (2021b) proposed a global model of relative plate motions, comprising continuously closing polygons and three contrasting absolute reference frames; no-net rotation (NNR), stable supercontinent location (SSL), and orthoversion (OV). The plate motions build upon the plate reconstruction from 250-0 Ma by Young et al. (2019), and extends back to 1 Ga in 1 Myr increments.

SSL considers three supercontinents across the last 1 Gyr, all of which occur in the same location as Pangaea (Cao et al., 2021b). The OV frame is similar to the SSL frame in that they are both based on the reference frame from Young et al. (2019), which itself is a hybrid of a hotspot track reference frame between 70-0 Ma, and a palaeomagnetic reference frame between 250-100 Ma. Both reference frames minimise net lithospheric rotations whilst the NNR reference frame evaluates the net rotation of the lithosphere with respect to the mantle and removes this value from the SSL reconstruction. The OV model differs from SSL in that the initial supercontinent (which they call SC1; Cao et al., 2021b) is 90° East of Pangaea.

Chapter 3

TOP DOWN DYNAMICS:

Evaluating the relative importance of plate geometry and velocity vs. mantle viscosity on slab transit times through the mantle.

Abstract

Subduction and slab sinking through the mantle are some of the most fundamental processes on Earth, linking the surface to the deep interior and transferring energy and material across the entire mantle. Despite this, our understanding of the controls on slab dynamics is not comprehensive. Subduction (a surface process) and slab sinking (a mantle process) reflect different stages in the life cycle of the oceanic lithosphere, yet the degree to which the dynamics of slab sinking are driven by the surface is unclear. This study aims to explore the relative importance of plate velocity and trench length on slab transit times through the mantle by considering the applicability of Stokes' Law which describes objects sinking through a viscous medium.

Stokes' Law (which includes a viscosity term but not plate parameters in it's initial derivation) can predict the sinking velocity of slabs in mantle circulation models with some success, but adapting this equation to include plate velocity and trench length yields better results. While Stokes' Law is used as a conceptual framework by which to explore the interplay between plate and mantle properties, it is crucial to highlight that plates are driven into the mantle from the surface in these models, rather than passively sinking. I provide an empirical equation which consistently predicts slab sinking times within circulation simulations, with an average error of $< 5\%$. This can be used by geodynamic modellers to improve the efficiency of the modelling process, and contribute to our understanding of the controls on slab dynamics. Whilst mantle viscosity is likely the primary control on slab sinking, the force balance between surface and mantle processes varies with depth. In the upper mantle, it is the interplay between these three parameters, relative to a natural sinking velocity for a plate through a given mantle viscosity, that controls the morphology and radial velocity of a slab.

3.1 Introduction

The degree to which slab sinking is driven by the plate velocity and trench length during subduction or is controlled by the viscosity of the mantle is uncertain, but is crucial to better understand the Earth's deep interior. Slab sinking can be considered as a constituent process of a mantle circulation cycle, where slabs sweep deep mantle material and promote mantle upwellings. Since slab pull and plume push are the dominant mechanisms proposed for supercontinent breakup, the transit of slabs from the surface to the deep Earth may be considered one of the most important processes to understand the Earth's geodynamic evolution on the largest spatial and temporal scales.

Van der Meer et al. (2018) provides an atlas of 94 subducted slabs imaged by seismic tomography and suggests an average whole mantle sinking rate of 1.2 ± 0.25 cm yr^{-1}, corresponding to slab sinking times of 199-304 Myrs. Conversely, Peng and Liu (2022) use global mantle convection models to reproduce present day slab geometries and suggest significantly faster slabs, sinking at an average rate of 2.1 cm yr^{-1}, corresponding to a 134 Myrs slab sinking (transit) time. Additionally, geomagnetism studies have proposed a relationship between geomagnetic reversals and slab sinking times of 120 Myrs (Hounslow et al., 2018), corresponding to radial velocities of 2.4 cm yr^{-1}. This lack of consensus highlights the discourse surrounding slab dynamics and the necessity to better understand the properties controlling the rate of slab sinking through the mantle.

This study uses Stokes' Law, which describes the drag force exerted on spherical objects in a viscous fluid as a conceptual framework to predict slab transit times. In these simulations, it is important to highlight that plates do not sink passively but are instead driven from the surface. Different derivations of Stokes' formula make the law applicable to non-spherical objects, specifically cylinders and prisms in this study. The drag force is proportional to velocity in low-speed flows, so Stokes' formula should be applicable to sinking times of each slab in 3D mantle circulation models (when the slabs are approximated as spheres, cylinders, and prisms). I aim to test the success of Stokes' Law (which includes a viscosity term but not plate velocity or trench length) at different mantle viscosities, to evaluate the degree to which viscosity controls slab transit times. I derive empirical formulae which include terms to represent the dynamics of the plate at the surface (in terms of trench length and plate velocity), and their affect on slab sinking. Initially, the relative importance of mantle viscosity versus plate parameters are tested on simple, single plate-driven simulations and our empirical equations are then applied to circulation models driven by global plate motion reconstructions.

This study considers the interplay between model parameters to better understand the factors controlling slab dynamics as they sink through the mantle and propose that whilst mantle viscosity is the primary control on the radial velocities of slabs, plate velocity and trench length are also important to predict the dynamics in our mantle circulation models, highlighting the coupling between the surface and deep Earth.

3.2 Methods

3.2.1 Modelling method

Each simulation utilises the 3D mantle convection code, TERRA, (Baumgardner and Frederickson, 1985; Bunge and Baumgardner, 1995; Bunge et al., 1997; Davies et al., 2013; Yang and Baumgardner, 2000) driven at the surface by prescribed plate velocities and with a free slip condition at the core-mantle boundary (CMB). Calculations are based on the governing equations outlined in section 2.2.3, for conservation of mass (equation 2.6), energy (equation 2.7), and linear momentum (equation 2.8), where incompressibility is assumed (McKenzie et al., 1974) and the Boussinesq approximation is applied.

Calculations are performed on an icosahedral mesh with over 10 million grid points and an average radial spacing of 45 km, extending from the model Earth's surface to the core-mantle boundary (CMB) across 65 radial layers (lateral spacing of 32.7 km at the CMB increasing to 59.9 km at the surface). These models are initially simple, where only a single plate drives the surface and sinks through an isoviscous mantle. Models are analysed as they evolve from the initial condition, as opposed to with a pre-conditioning phases as is typical for other mantle circulation models (section 2.3), to mitigate the degree to which the simulations are affected by mantle structures which may develop away from the focus slab.

The relevant model parameters for the reference simulation are listed in table 3.1.

3.2.2 Stokes' Law

Stokes' Law (Stokes, 1851) describes the drag force exerted on spherical objects in a viscous fluid, defined by:

$$F_D = 6\pi r_s \mu v \tag{3.1}$$

where $\mathrm{F_D}$ is the drag force, r_s is the radius of the sphere (m), μ is the fluid viscosity ($Pa\,s$), and v is the velocity of the sphere (ms^{-1}). Landau and Lifshits (1987) suggested that Stokes' formula does not accurately describe flow around non-spherical objects, even when the Reynolds number of the convecting fluid

Table 3.1 Reference model parameters

Parameter	**Symbol**	**Value**	**Units**
Reference density	ρ	4500	kg m^{-3}
Gravitational acceleration	g	10	m s^{-2}
Thermal expansivity	α	2.5 x 10^{-12}	K^{-1}
Thermal diffusivity	k	9 x 10^{-6}	m^{2}s^{-1}
Specific heat capacity	C_p	1000	J K^{-1} kg^{-1}
Radiogenic heat production rate	H	4.0 x 10^{-12}	W kg^{-1}
Surface temperature	T_s	300	K
CMB temperature	T_{CMB}	3000	K
Reference viscosity	μ	2.0 x 10^{23}	Pa s
Rayleigh number	Ra	$\approx 10^7$	-

is small and instead provide a refined Stokes' formula which is applicable to flow past a cylinder to give the drag force per unit length:

$$F_D = \frac{4\pi\mu v}{0.5 - C - log(vr_c/4\nu)} \tag{3.2}$$

where C is Euler's constant, r_c = radius of the cylinder, $\nu = \mu/\rho$. Leith (1987) provided a general form of Stokes' Law which is applicable to non-spherical objects by characterising a dynamic shape factor (K_n) such that:

$$F_D = 3\pi\mu v d_n K_n \tag{3.3}$$

where d_n is the diameter of a sphere whose projected area is the same as the area of the slab projected normal to its direction of motion. Many empirical formulae exist for characterising the shape factor (explored in section 3.3.5), based on spheres with equivalent surface area, volume and projected surface area to the slab.

From Stokes' Law for a sphere (equation 3.1), the settling velocity of a particle is expressed by:

$$v = \frac{2R^2 \rho g}{9\mu} \tag{3.4}$$

where ρ = density, g = acceleration due to gravity, and R = the radius of the sphere, or a representative sphere when the slab is approximated as a cylinder or prism. Substituting equations 3.2 and 3.3 into equation 3.4 we present the representative radii for each approximation as:

$$R_{sphere} = r_s \tag{3.5}$$

$$R_{cylinder} = \frac{l}{1.5(0.5 - C - log(v_s r_c/4\nu))} \tag{3.6}$$

$$R_{prism} = 0.5 d_n K_n \tag{3.7}$$

where l = length of the slab in metres (average slab depth in the mantle), and v_s is the surface velocity of the slab in ms^{-1}.

To more easily quantify the radii and shape factor of the slabs, when approximating as spheres, cylinders, and prisms, the geometry of slabs is simplified to a cuboid (figure 3.1) with principal axes that vary in length across each simulation. The x-axis reflects the length of the subduction trench, and the y-axis represents the thickness of the slab as it subducts which varies with the age of the plate (and therefore relates to the distance from the trench to the spreading ridge and the surface velocity). For our initial suite of simple models, y is measured across each timestep, and the average is taken for each simulation. Our z-axis is calculated as the average slab depth in the mantle. For this study, z has a constant value of z of 1345 km, representing the average depth between the surface and 2690 km (200 km above the CMB, since some slabs may never sink all the way to the boundary layer).

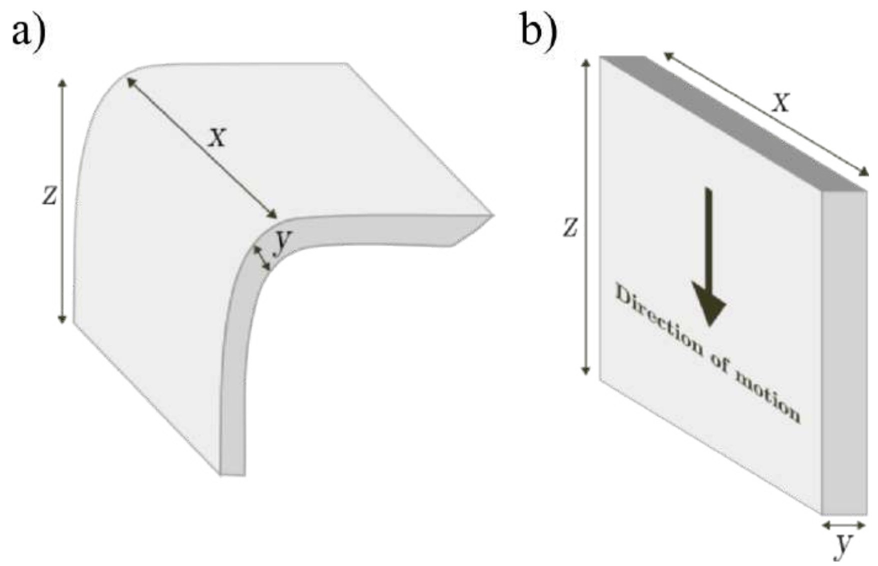

Figure 3.1 a) Schematic representation of subducting plate, where x is the length of the subduction trench, y is the thickness of the slab and z is the depth of the slab in the mantle; b) Simplified slab geometry used to quantify radii and shape factor to use in Stokes' Law equations, where we assume that slabs descend vertically, parallel to the z-axis.

3.3 Single Plate Simulations

3.3.1 Single-plate Parameter Space

Our first suite of models are driven by a single moving plate at the surface. To understand the applicability of Stokes' Law to slab sinking, we vary viscosity, plate geometry, and surface velocity. Initially, I implement an isoviscous profile throughout the mantle which varies between $1\text{x}10^{22}$ to $2\text{x}10^{24}$ Pa s across the simulations. For these models, I produce 11 plate motion histories with a single moving plate using the GPlates software (Müller et al., 2018), in which the subducting trench length and the length from the trench to the spreading ridge are systematically varied to define the geometry of a subducting plate. Therefore, each plate is bound by a subduction zone and a spreading ridge, which are linked by two transform faults. The dimensions of the moving plate are defined by latitude and longitude values which are symmetrical across the equator and prime meridian and vary between $\pm$ 80°to $\pm$ 5°across the suite of simulations. Particles are generated (Stegman et al., 2002) within these defined limits and store the temperature, radial velocity, and strain rate fields. These particles can therefore be used to isolate the slab from the surrounding mantle and track the structures through time and space. Surface velocities of this plate vary between 0.2 cm yr^{-1} to 4 cm yr^{-1}, where 4 cm yr^{-1} is close to the average plate velocity on Earth at present. Most of these models have slower surface velocities than is considered Earth-like given the numerical limitations of the simulations, where I aim to limit instabilities developing at the boundaries between the stationary surface and single moving plate. Whilst implementing this surface condition, where plates are pushed into the mantle rather than sinking passively and pulling the plates as in nature, is not Earth-like, it provides a framework by which to isolate the dynamics of a single slab from global circulation.

Each simulation evolves from the initial conditions outlined in Table 3.1, though the value for viscosity varies across simulations 001-004. Viscosity, trench length, trench-ridge length, and surface velocity are varied according to Table 3.2. Each model can be compared to the reference simulation (003R), with an isoviscous structure of 2×10^{23} Pa s, a trench length of 7784 km (corresponding to latitudes of ± 35°), an average plate thickness (thickness of the thermal lithosphere) of 195 km, and a surface velocity of 0.8 cm yr^{-1}.

Table 3.2 Parameter space for the suite of simulations driven by a single moving plate at the surface.

Case	Trench Length, x (km)	Plate Thickness, y (km)	Viscosity, μ (Pa s)	Surface Velocity, v_s (cm yr^{-1})
001	7784	150	1E+22	0.8
002	7784	150	2E+22	0.8
003R	**7784**	195	**2E+23**	**0.8**
004	7784	160	2E+24	0.8
005	7784	250	2E+23	0.8
006	7784	235	2E+23	0.8
007	7884	230	2E+23	0.8
008	7784	185	2E+23	0.8
009	7784	165	2E+23	0.8
010	17791	210	2E+23	0.8
011	14455	190	2E+23	0.8
012	11119	215	2E+23	0.8
013	4448	200	2E+23	0.8
014	1112	205	2E+23	0.8
015	7784	195	2E+23	4.0
016	7784	215	2E+23	0.4
017	7784	300	2E+23	0.2

3.3.2 Slab behaviours in single plate models

Understanding the effect of viscosity, surface velocity, and slab geometry on slab sinking is observed in the range of dynamic behaviours across the simulations.

At low viscosities, the plate velocity has little effect on the sinking of slab material, as material drips rapidly from beneath the moving plate (model 001; figure 3.2). Radial velocities and strain rates increase with depth indicating an acceleration of material throughout the mantle. As viscosity increases, the slab becomes increasingly coherent, and radial velocities (which are expressed by negative values given their downwards trajectory) decrease by almost two orders of magnitude (figure 3.2). Model 004, which has the greatest viscosity, exhibits slab thickening as it descends and slab dips shallow in the uppermost mantle relative to the less viscous cases.

Figure 3.3 shows the geometry of the slabs associated with varying trench-ridge distances. The radial velocities across each of these models (003, 005-009) are similar, with a peak in velocity in the upper mantle and remaining high until the slab approaches the CMB. The effect of the trench-ridge distance (and the plate thickness) is therefore relatively minor at a global scale. Greater variations in radial velocity and strain rate are seen in the models in which the length of the trench is varied (figure 3.4). For wide trenches, the centre of the slabs descend faster than the edges, where the deepest parts of the slab are narrower than the trench at the surface. Comparing models 010-012 to models 003,013-014 (figure 3.4) I suggest there is a maximum slab width (where slab width is the profile expression of the trench length within the mantle) that facilitates slab sinking at a consistent velocity across the profile plane, where our longest trench lengths have very slow velocities at the slab peripheries compared to narrow slabs. This may be an artefact of the surface boundary condition, where the velocities of the moving plate are defined by angular rotations, therefore when the trench length is very long, the angular rotation at higher latitudes corresponds to lower absolute velocities than near the equator. Subsequently, the centre of the plate is moving faster than the edges, and this

Figure 3.2 3D visualisation of the descending slab in simulations 001-004 as they reach 200 km above the CMB, showing radial velocities and strain rate across the slab.

translates to the radial velocities in the upper mantle for very large plates. For our case with the smallest plate, case 014 (figure 3.4), our slab rapidly develops a cylindrical geometry, rather than the planar geometry observed across the other simulations, and spreads laterally near the CMB, much like an inverted plume.

At faster plate velocities, the centre of the slabs descends slower than the edges and corresponds to lower strain rates, whereas at slow plate velocities of 0.8 cm yr^{-1} (figure 3.5; model 003), the greatest radial velocities are in the centre of the slab. The morphology of the slabs with different plate velocities and viscosity (figure 3.2 and 3.5), suggest an interplay between the two parameters. Where surface velocities are too slow for a given mantle viscosity, material begins to drip from the the lithosphere without being forced downwards from the surface whereas when the velocities are as fast, or faster than the natural sinking velocity for a given viscosity, the slab descends as a more uniform sheet (though may thicken if the plate velocities at the surface are faster than the natural sinking velocity).

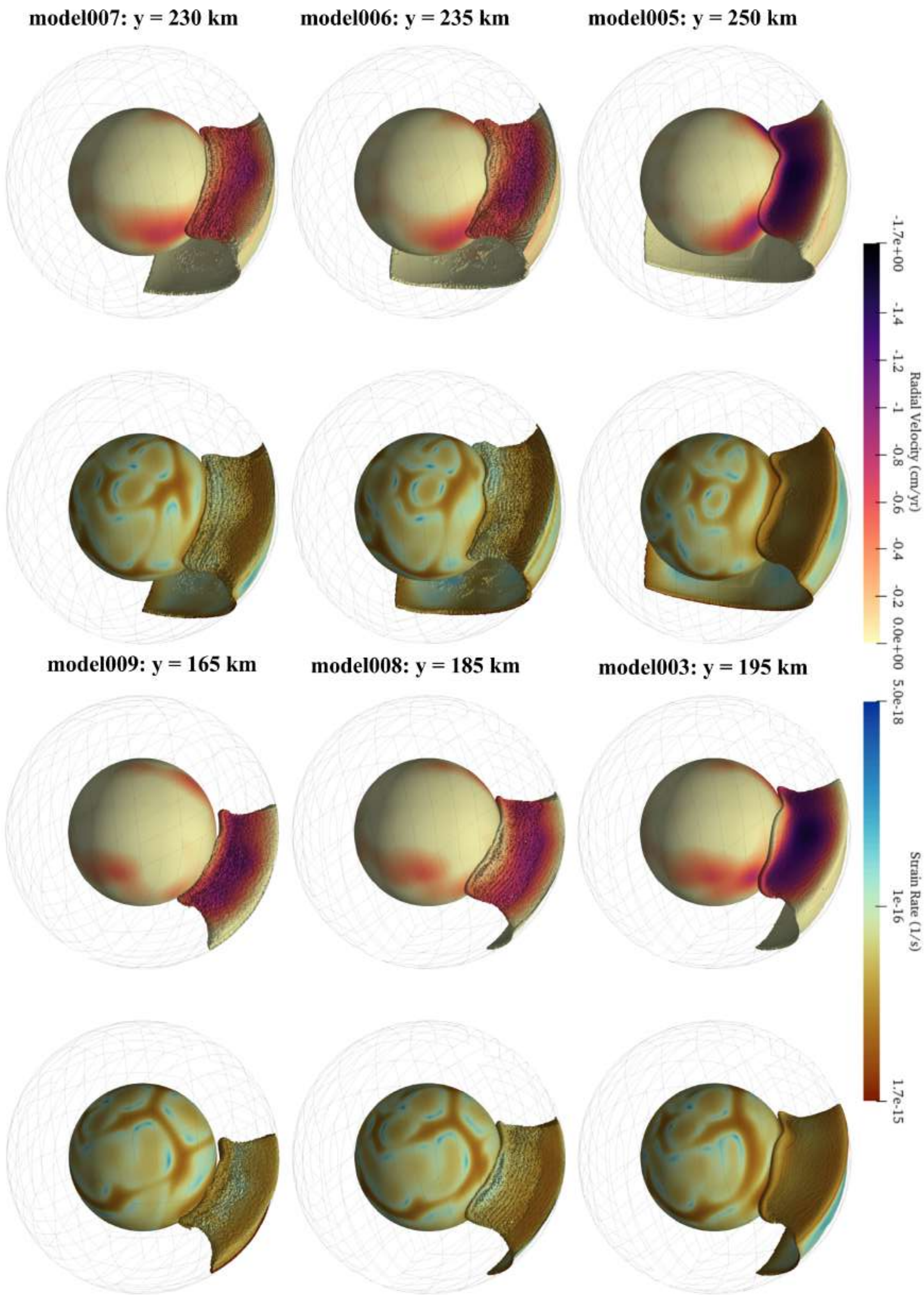
model007: y = 230 km
model006: y = 235 km
model005: y = 250 km
model009: y = 165 km
model008: y = 185 km
model003: y = 195 km
Radial Velocity (cm/yr)
-1.7e+00
-1.4
-1.2
-1
-0.8
-0.6
-0.4
-0.2
0.0e+00
Strain Rate (1/s)
5.0e-18
1e-16
1.7e-15

Figure 3.3 (Previous page.) 3D visualisations of the slab in simulations 003, 005-009 with varying plate thickness at the trench (y; related to varying trench-ridge distance) as they approach the base of the mantle.

3.3.3 Applying Stokes' Law to slabs approximated as spheres

I calculate the velocity of slabs based on 3 spherical approximations for slab geometry, based on (a) a sphere with the same surface area as the slab, (b) a sphere with the same volume as the slab, and (c) a sphere with the same projected surface area of the slab, normal to the direction of motion. Velocities are calculated according to equation 3.4 and are compared to the measured radial velocities across the simulations (figure 3.6).

Spheres with equivalent normal projected areas and volumes overestimate the measured radial velocities of the slab by a factor of $\sim 3-4.5$, which I attribute to the difference in surface area between the spheres and cuboids with different projected areas and volumes, significantly affecting the drag forces acting on the slab. Using a sphere with equivalent surface area is more successful at predicting the true velocities, and I consider that this equation may define the natural sinking velocity for the slab without being driven at the surface. This

Figure 3.4 (Next page.)3D visualisations of the descending slab in simulations 003, 010-014 for varying values of x, which represents the length of the subducting trench.

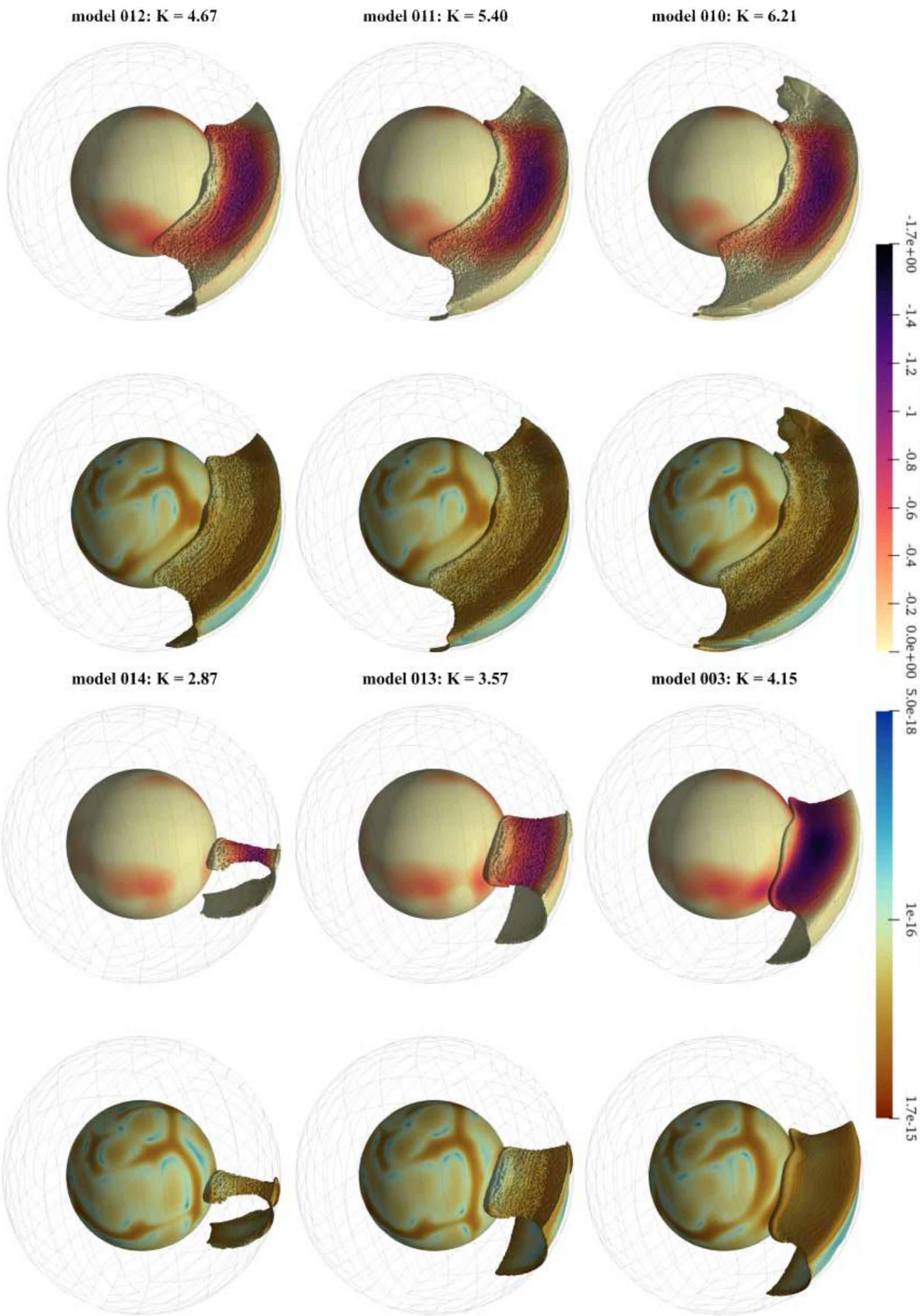
model 012: K = 4.67
model 011: K = 5.40
model 010: K = 6.21
model 014: K = 2.87
model 013: K = 3.57
model 003: K = 4.15
Radial Velocity (cm/yr)
-1.7e+00
-1.4
-1.2
-1
-0.8
-0.6
-0.4
-0.2
0.0e+00
Strain Rate (1/s)
5.0e-18
1e-16
1.7e-15

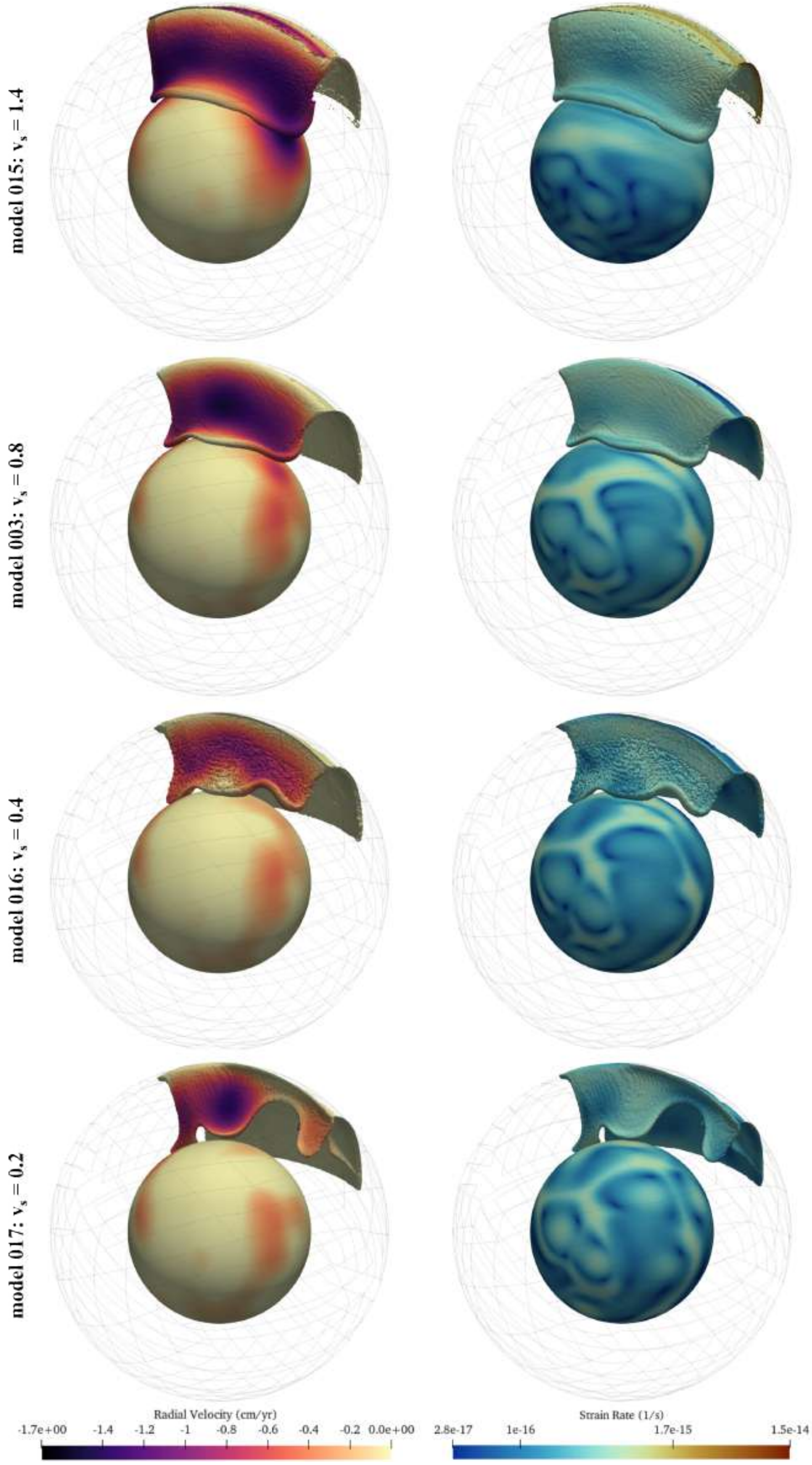

Figure 3.5 3D visualisations of the descending slab in simulations 003, 015-017 as they reach 200 km above the CMB showing the radial velocities and strain rate for simulations with varying plate velocities at the surface.

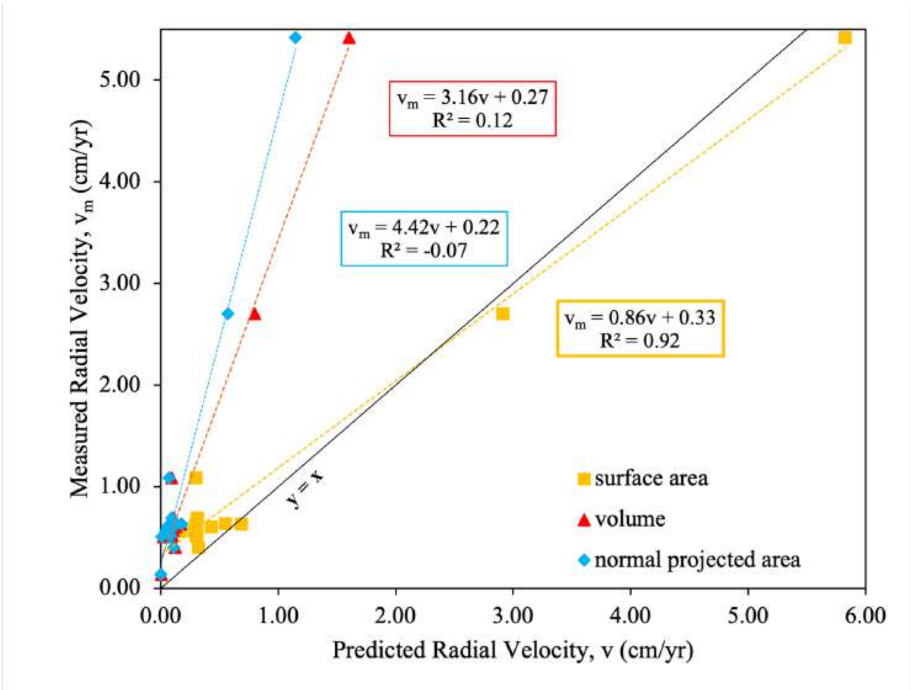

Figure 3.6 Graphical comparison of predicted and measured radial velocities calculated based on spheres with equivalent surface area, volume, and normal projected area to the imposed slab. R^2 is calculated relative to the 1:1 line.

equation does overestimate the velocities at lower viscosities such that I seek to refine this approach.

Stokes' Law better predicts the sinking velocities in the lower mantle than the upper mantle, with upper mantle velocities often under-predicted by this model. Despite this, there is a significant scatter in the data from the lower mantle, attributable to varying trench length and surface velocity, suggesting that the role of these surface parameters are significant on the dynamics of slabs throughout the entire mantle volume. Since the lower mantle is not defined by a change in viscosity in these simple isoviscous models, I consider that our equations better predict the lower mantle velocities given the greater distance from the surface, where the slab sinks at a rate close to the natural sinking rate for that viscosity.

Based on the graphical solutions (figure 3.7), I propose a refined empirical solution to predict the slab radial velocity:

$$v = \frac{0.193R^2\rho g}{\mu} + (-3.04\text{e}{-08}x + 0.6)v_s^{0.62} \tag{3.8}$$

This equation yields an R^2 value of 0.997, and a gradient of $m = 0.996$ indicating the strong correlation between our predicted and measured radial velocities. Across the suite of models I calculate an absolute relative error in our calculated radial velocities of 12.7% , and an average absolute relative error of 9.5% for slab sinking times. These figures are skewed by the calculated velocity for case004, which has the greatest viscosity, and in turn the lowest radial velocity of any of our simulations. Here, I predict a radial velocity of 0.34 cm yr^{-1} compared to the measured value of 0.14 cm yr^{-1}, inducing significant percentage error despite only being a 2 mm yr^{-1} deviation in radial velocities. Since these velocities are below what is generally considered realistic for an Earth-like

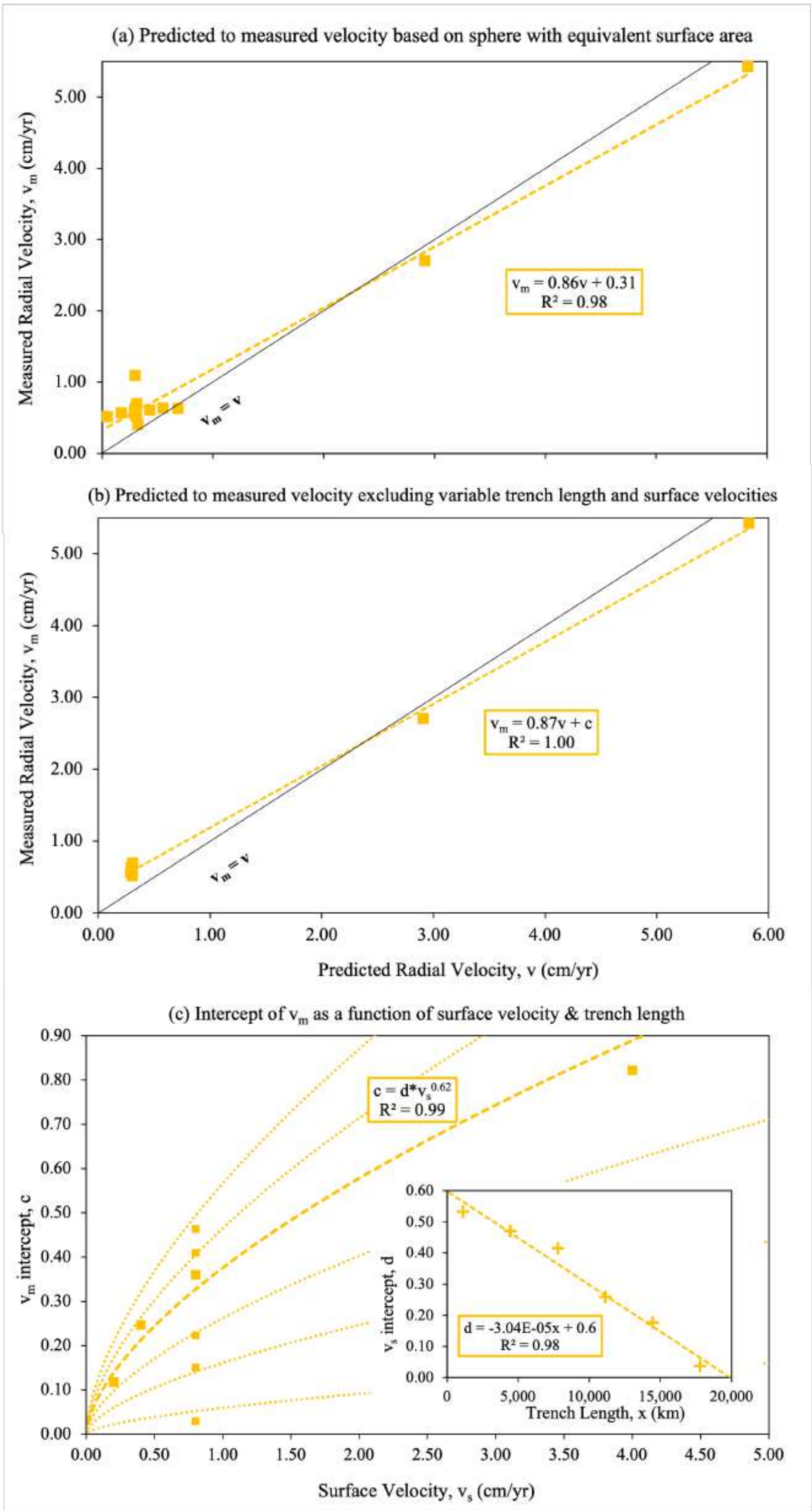

Figure 3.7 (a) Comparison of predicted and measured radial velocities calculated based on spheres with equivalent surface area to the slab, showing the lateral scatter attributable to varying trench length, and vertical scatter attributed to varying surface velocity; (b) Comparison of predicted and measured radial velocities excluding simulations with varying trench length and surface velocity; (c) calculated intercept between predicted and measured radial velocities as a function of surface velocity, which can also be expressed as a function of trench length (inset).

slab (Van der Meer et al., 2018; Peng and Liu, 2022; Hounslow et al., 2018), I remove this data point from the averages. Doing so yields an average error of the absolute values of 4.9% for the velocities, and 5.7% for the sinking times (table 3.3) and allows further refinement of equation 3.8 for Earth-like radial velocities (equation 3.9):

$$v = \frac{0.191R^2\rho g}{\mu} + (-3.04\text{e}{-}08x + 0.6)v_s^{0.62} \tag{3.9}$$

$$\text{where } R_{sphere} = \sqrt{(2(xy + yl + xl)/4\pi)} \tag{3.10}$$

which marginally improves the coefficient of determination to $R^2 = 0.998$ and the gradient, $m = 1.003$. I propose that the original Stokes' Law term in equation 3.9 predicts the natural sinking velocity of the slab. If the trench length and surface velocity term is positive, then the subducting slab is driven into the mantle faster than the natural sinking velocity and thickens. If the term is negative, it may indicate that the natural sinking velocity is faster than the slab can enter the mantle, and therefore the slab becomes less coherent.

Individual simulations have relative errors between measured and predicted velocities of between 0.25% to 14.7% indicating that this equation is more successful at predicting the radial velocities of a suite of models rather than any one individual slab. Overall, the refined equation for slab sinking times based on a slab approximated as a sphere is successful, when surface velocity and trench length are considered, indicating the importance of these factors in slab sinking dynamics. There is a conceptual difference between Stokes' Law (free sinking of a sphere) and these constrained plate subduction models. Therefore, these findings can be considered with respect to the ways in which plate-mantle coupling, rather than passive sinking, shapes slab transit behaviour. This difference is crucial to the results across this chapter, and is highlighted throughout.

Table 3.3 Predicted and measured radial velocities based on slabs approximated as spheres

Case	v_m (cm yr^{-1})	v (cm yr^{-1})	Error %	Measured Time (Myr)	Predicted Time (Myr)	Error %
001	5.42	5.33	(-)1.7	50	50	0.0
002	2.70	2.82	4.5	100	95	(-)5.0
003	0.62	0.58	(-)7.5	414	467	12.8
005	0.69	0.59	(-)14.7	390	459	17.7
006	0.57	0.58	2.7	470	461	(-)1.9
007	0.51	0.58	14.0	535	462	(-)13.6
008	0.60	0.57	(-)4.4	450	469	4.2
009	0.56	0.57	2.1	489	472	(-)3.5
010	0.63	0.64	2.6	437	418	(-)4.4
011	0.63	0.61	(-)2.6	433	438	1.2
012	0.60	0.60	0.2	450	447	(-)0.7
013	0.56	0.56	(-)1.1	574	484	2.1
014	0.51	0.54	5.9	528	503	(-)4.7
015	1.08	1.12	3.1	250	241	(-)3.6
016	0.51	0.47	(-)8.5	522	574	10.0
017	0.40	0.41	3.4	696	653	(-)6.2
		Average	4.9		**Average**	5.7

3.3.4 Slabs approximated as cylinders

Cylindrical approximations differ from spherical approximations in that the equation for the radius (equation 3.6) includes a velocity term. Since the measured radial velocity is an output of our simulations, I implement surface velocity into these equations. Whilst this is somewhat arbitrary, I find that substituting surface velocity more successfully predicts the radial velocities (figure 3.8a) than the more circular subsitution of calculated radial velocity (figure 3.8b).

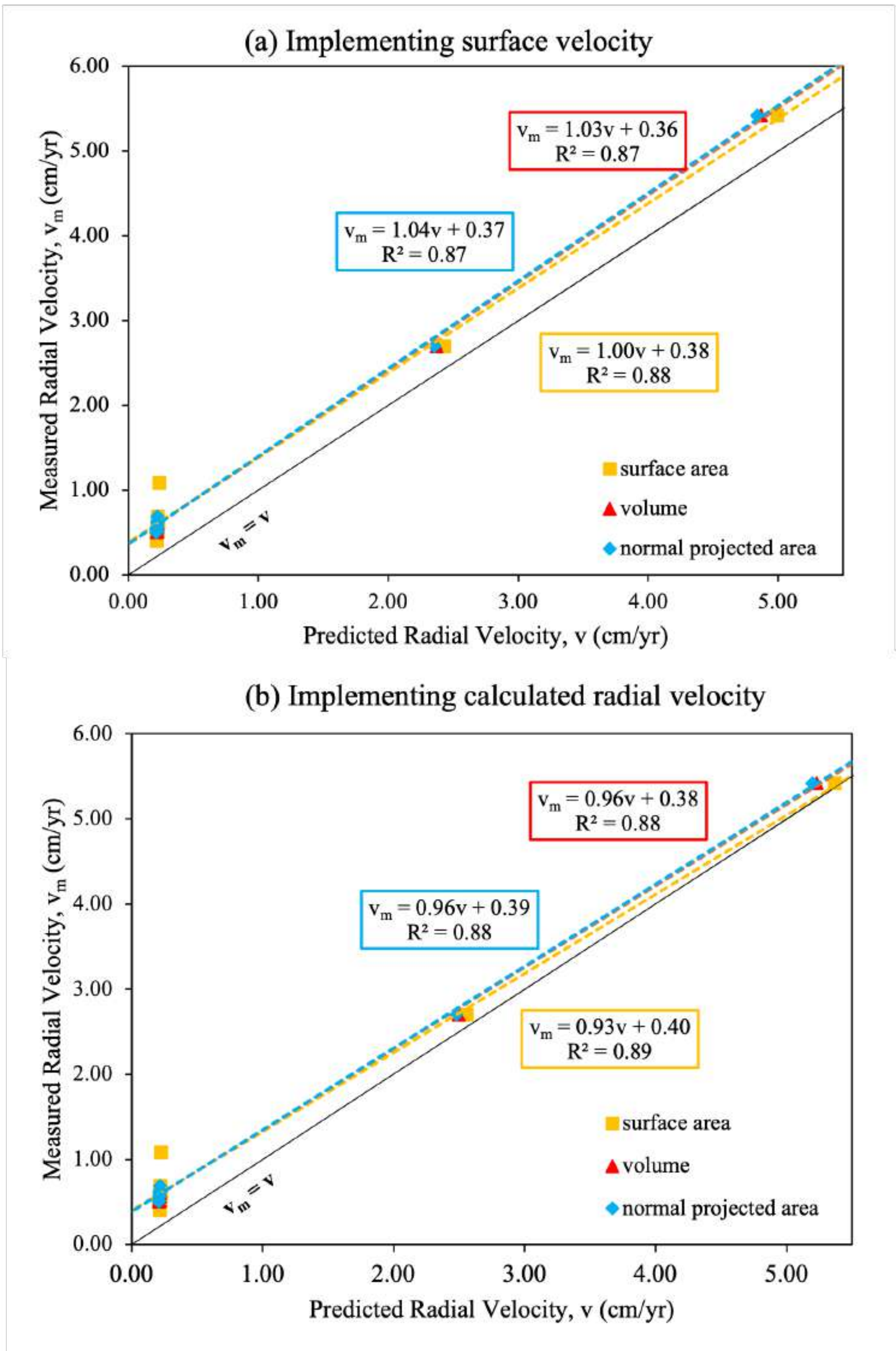

Figure 3.8 Comparison of predicted and measured radial velocities calculated based on cylinders with equivalent surface area, volume, and normal projected area to the imposed slab, where the velocity term is (a) the plate velocity, and (b) the calculated radial velocity from our simple empirical equation (3.11). R^2 is calculated relative to the 1:1 line.

Approximating the sinking particle to a cylinder with equivalent volume and normal projected area as the slab can reduce the scatter associated with surface velocity (figure 3.8a) but consistently under-predicts the velocity at lower viscosities. Conversely, there is a better correlation between predicted and measured velocities for cylinders with equivalent surface areas as the slab, though consistently under-predicts measured velocities (figure 3.8a). Following the approach outlined when approximating the slab as a sphere, to correct for surface velocity for cylinders with equivalent surface area, the discrepancy between measured and predicted velocities can be expressed as a function of surface velocity, to give the equation:

$$v = \frac{2R^2\rho g}{9\mu} + 0.428v_s^{0.503} \tag{3.11}$$

$$\text{where } R_{cylinder} = \frac{l}{1.5(0.5 - 0.577 - log(v_s r_c/4\nu))} \tag{3.12}$$

$$\text{and } r_c = \frac{-2\pi l + \sqrt{4\pi^2 l^2 + 16\pi(xy + yl + xl)}}{4\pi} \tag{3.13}$$

These equations yield radial velocities and sinking times summarised in table 3.4. Our predictions here are comparable to our spherical approximations (table 3.3).

The relationship between measured and predicted velocities are expressed as a gradient of $m = 1.002$ and a R^2 value of 0.998, indicating the success of our predictive equation across the suite of simulations. Despite this, the average errors across this suite of models is 5.9% for the slab radial velocity and for the sinking times, slightly higher than those calculated based on the refined spherical equation (equation 3.9; table 3.3). Whilst a cylindrical approximation is better at representing the geometry of the slabs, it is less successful at predicting slab velocities than our refined spherical equation, which includes

Table 3.4 Predicted and measured radial velocities based on slabs approximated as cylinders

Case	v_m (cm yr^{-1})	v (cm yr^{-1})	Error %	Measured Time (Myr)	Predicted Time (Myr)	Error %
001	5.42	5.37	(-)0.9	50	50	0.0
002	2.70	2.81	4.4	100	96	(-)4.0
003	0.62	0.61	(-)2.7	414	444	7.3
005	0.69	0.61	(-)11.9	390	444	13.9
006	0.57	0.61	6.6	470	444	(-)5.5
007	0.51	0.61	18.6	535	444	(-)17.0
008	0.60	0.61	0.9	450	444	(-)1.3
009	0.56	0.61	8.5	489	444	(-)9.2
010	0.63	0.61	(-)2.7	437	441	0.9
011	0.63	0.61	(-)3.5	433	442	2.1
012	0.60	0.61	1.2	450	443	(-)1.6
013	0.56	0.60	7.2	574	446	(-)5.9
014	0.51	0.59	17.7	528	452	(-)14.7
015	1.08	1.10	1.1	250	245	(-)2.0
016	0.51	0.49	(-)4.9	522	552	5.8
017	0.40	0.40	1.1	696	668	(-)4.0
		Average	5.9		**Average**	5.9

an additional term to consider the relationship between surface velocity and slab geometry.

3.3.5 Slabs approximated as prisms

Leith (1987) synthesises many previous studies to provide the following equation to characterise a dynamic shape factor for non-spherical objects:

$$K_n = \frac{1}{3} + \frac{2d_s}{3d_n}. \tag{3.14}$$

where d_n is the diameter of a sphere with the same projected area as the object, normal to the direction of motion, and d_s is the diameter of a sphere with the same effective surface area as the object. In terms of the dimensions of the slab, these values are:

$$d_n = 2 \cdot \sqrt{\frac{xy}{\pi}} \tag{3.15}$$

$$d_s = 2 \cdot \sqrt{\frac{xy + 2(yl + xl)}{4\pi}} \tag{3.16}$$

Substituting each value of K_n into equation 3.7, and following the approach for refinement outlined in section 3.3.3, I derive the following equation for sinking velocity:

$$v = \frac{0.3R^2\rho g}{\mu} + (-3.23\text{e}{-08}x + 0.61)v_s^{0.68} \tag{3.17}$$

Equation 3.17 successfully predicts the slab sinking times within < 15% error for all except case006 (table 3.5). Despite this, I find our most successful equation to be equation 3.9, given the number of accurately predicted slab sinking times, and the lower relative error across the entire suite of simulations.

Table 3.5 Predicted and measured radial velocities based on slabs approximated as prisms, based on our equation 3.17.

Case	v_m (cm yr^{-1})	v (cm yr^{-1})	Error %	Measured Time (Myr)	Predicted Time (Myr)	Error %
001	5.42	5.36	(-)1.2	50	50	0.0
002	2.70	2.83	4.9	100	95	(-)5.0
003	0.62	0.58	(-)7.1	414	465	12.3
005	0.69	0.60	(-)12.9	390	449	15.1
006	0.57	0.59	4.4	470	454	(-)3.4
007	0.51	0.59	15.8	535	455	(-)14.9
008	0.60	0.57	(-)4.3	450	468	4.00
009	0.56	0.57	1.6	489	475	(-)2.9
010	0.63	0.65	4.4	437	411	(-)5.6
011	0.63	0.62	(-)2.2	433	436	0.7
012	0.60	0.61	1.7	450	441	(-)2.0
013	0.56	0.56	(-)0.6	574	482	1.7
014	0.51	0.54	6.2	528	501	(-)5.1
015	1.08	1.19	9.8	250	226	(-)9.6
016	0.51	0.47	(-)8.3	522	572	9.6
017	0.40	0.43	6.8	696	632	(-)9.2
		Average	5.7		**Average**	6.3

3.4 Global mantle circulation models

3.4.1 Circulation model methods

This study aims to assess the relative importance of plate velocity, trench length, and mantle viscosity on slab transit times by deriving empirical equations based on Stokes' Law. Following on from the simple simulations, I determine the success of the equations by applying them to global mantle circulation models which are driven by full plate motion reconstructions at the model surface. I focus on the Phoenix Plate and Farallon Plate for this study, as defined in both the Merdith et al. (2021) and Müller et al. (2022) plate motion histories. These global plate motion reconstructions both comprise a set of topological plate polygons with associated plate boundaries and velocities at 1 Myr intervals; for this investigation I utilise the interval from 500-0 Ma. These models differ in their reference frame, where Merdith et al. (2021) uses a palaeomagnetic reference frame, whilst Müller et al. (2022) uses a mantle reference frame, combining the plate motion model of Merdith et al. (2021), and the tectonic-rules-based approach to mantle reference frames proposed by Tetley et al. (2019) (further information surrounding these reference frames can be found in each of the respective articles and in section 2.3). We implement both plate motion histories as they share similar topologies, and the Müller et al. (2022) model builds upon the Merdith et al. (2021) model, whilst the different reference frames result in plate geometries and velocities which differ across the two models, introducing a wider parameter space to this investigation (table 3.6). The Farallon and Phoenix plates are chosen to test the equations as these plates persist at the surface for 100's Myrs, ensuring that these models will capture the time taken for a slab to reach 200 km above the CMB before the plate is entirely subducted at the surface.

Table 3.6 Input parameters for global circulation simulations

Case	Plate motion model	Plate	μ profile	ref μ (Pa s)	v_s (cm yr^{-1})
m01p	Merdith et al., 2021	Phoenix	radvar1	1E+22	9.42
m01f	Merdith et al., 2021	Farallon	radvar1	1E+22	4.29
tviscp	Merdith et al., 2021	Phoenix	radvar2	4E+21	9.42
tviscf	Merdith et al., 2021	Farallon	radvar2	4E+21	4.29
mup	Müller et al., 2022	Phoenix	radvar3	4E+21	7.93
muf	Müller et al., 2022	Farallon	radvar3	4E+21	5.85

Global circulation models are more numerically stable than our single-plate simulations, such that they can sustain more complex viscosity structures, referred to as radvar1, radvar2, and radvar3 in table 3.6. Each viscosity profile is shown in figure 3.9, where radvar2 is dependent on temperature and depth, according to:

$$\mu(T, d) = \mu(r) \cdot exp(V_a z' - E_a T') \tag{3.18}$$

where $\mu(T, d)$ is the temperature and depth dependent viscosity and $\mu(r)$ is the reference radial viscosity. $V_a = 1$ and $E_a = 1.5$ are the non-dimensional constants that control the sensitivity to depth and temperature, z' and T', which are non-dimensionalised by mantle depth and $\Delta T = T_{CMB} - T_{surf}$, respectively.

3.4.2 Predicting slab velocity in complex mantle circulation models

Whilst the equations in section 3.3.3 describe the relationship between plate velocity, trench length, and mantle viscosity in single-plate models, this has limited applicability to understanding the real Earth. To better determine the success of these equations, I test their applicability to mantle circulation models constrained by global plate motion histories at the surface. X is the average great circle length of the subduction zone as defined by the plate motion

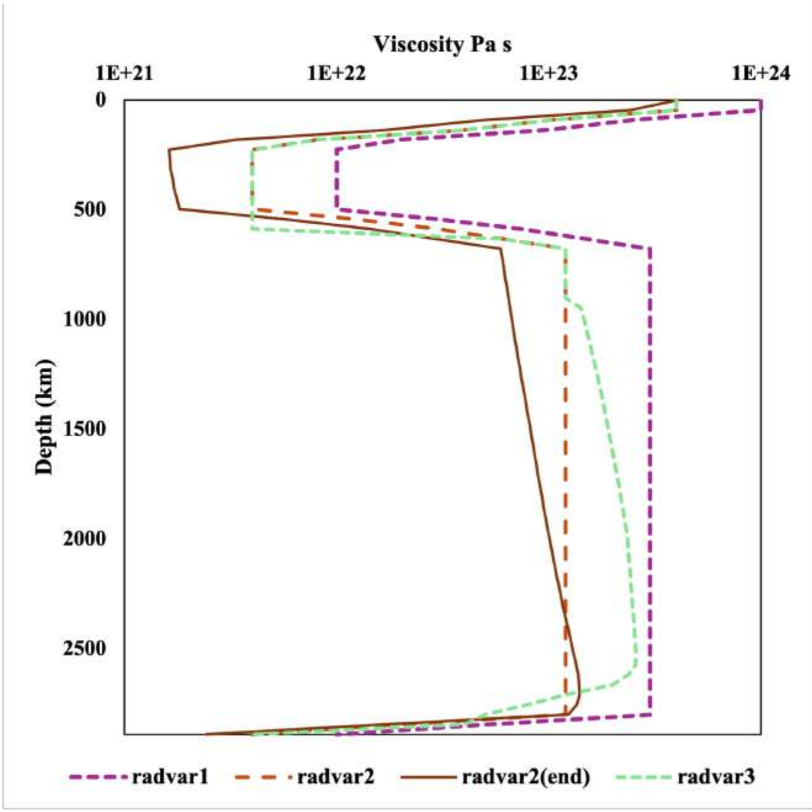

Figure 3.9 Viscosity profiles for radvar1-3, where radvar2 is dependent on temperature and depth. Radvar2 is shown at the beginning and at the end of the simulation, as the temperature dependence has an increasing effect on the viscosity profile through time.

histories rounded to the nearest 100 km during the period between 500-0 Ma. Z is constant, at 1345 km (half of 2690 km mantle depth over which I measure slab transit times) and y = 170 km (since I have shown that the plate thickness has little effect on the radial velocity in these simulations). Our equations use a single value of viscosity, which up to now has simply been the consistent value of viscosity across our isoviscous models. For these more complex models which implement a radially varying viscosity profile, I calculate the harmonic mean across the radial layers to a depth of 2690 km. Similarly, I calculate the harmonic average of the surface velocity from the plate motion histories, output at 5 Myr intervals. These values give the following predicted slab sinking times:

Table 3.7 Predicted values for slab sinking times for each model slab in the suite of global mantle circulation models and their relevant input parameters.

Case	**x (km)**	**y (km)**	**z (km)**	μ **Pa s**	v_s **(cm yr^{-1})**	**Time (Myr)**
m01p	9000	162	1345	6.27E+22	9.42	**120**
m01f	15500	178	1345	6.27E+22	4.76	**139**
tviscp	9000	162	1345	2.51E+22	9.42	**74**
tviscf	15500	180	1345	2.51E+22	4.76	**62**
mup	5000	165	1345	2.27E+22	7.93	**88**
muf	9700	172	1345	2.27E+22	5.85	**77**

Table 3.8 shows the measured slab sinking times and the corresponding relative error between the measured and predicted values. Across the suite of models there is an average error across the absolute values of the individual simulations of 10%. Furthermore, the average measured slab sinking time is 96 Myr, compared to the 93 Myr average calculated from these equations. Between the measured and predicted slab sinking times, $R^2 = 0.93$, indicating the success of our equations. The relative errors are higher for temperature dependent viscosities, though still within the $< 15\%$ threshold which is deemed to be successful. Both of these models (tviscp & tviscf) predict shorter sinking times than measured. I attribute the slower measured velocities to the higher viscosities in the immediate vicinity of the cold slabs, which the predictive equations do not account for. Increasing the viscosity value used in the calculations by 10% yields predicted slab sinking times of 78 and 68 Myr, compared to measured values of 85 and 69 Myr for tviscp and tviscf, respectively,

therefore reducing the relative error for each model from 13.98% and 11.09% to 7.69% and 0.14%. I propose that our equations will consistently under-predict the slab sinking times for simulations with a temperature-dependant viscosity profile and, for these simulations, a correction of 10% in viscosity is sufficient to better predict the measured values though more work would be required to determine if this correction is applicable to a larger number of simulations.

Table 3.8 Comparison of predicted and measured slab sinking times across the suite of global mantle circulation models showing the relative error between the two values.

Case	**Predicted Time (Myr)**	**Measured Time (Myr)**	**Rel. Error (%)**
m01p	120	109	8.94
m01f	139	132	4.83
tviscp	74	84	(-)13.98
tviscf	62	69	(-)11.09
mup	88	100	(-)13.64
muf	73	80	(-)9.59
		Average	**10**
Average	**93**	**96**	**3.38**

These equations can be used to successfully predict slab sinking time across a suite of models, even when the trajectories and individual slab sinking histories may be variable (figure 3.10), due to the interplay between the three parameters tested within this study. The sinking profiles are most similar in models with the same viscosity profile (radvar 1,2, and 3; figure 3.9, table 3.6), supporting the idea that it is the mantle viscosity which is the primary control on slab transit times.

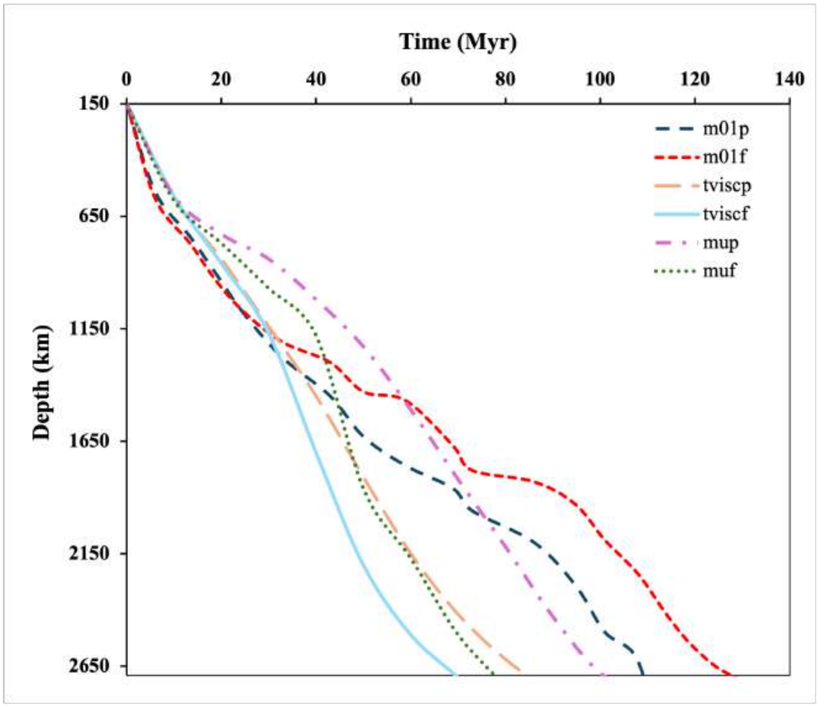

Figure 3.10 Slab sinking profiles of depth through time for each global circulation model (tables 3.7, 3.8) variable slab velocities through the mantle.

3.5 Application of equations to tune geodynamic models

Whilst this study primarily aims to better understand slab dynamics, it has an additional application for geodynamicists to refine their modelling approach. The empirical equation 3.9 can be used to tune geodynamic models to a target slab velocity which can then be directly compared to observations from other fields within the Earth sciences. Various geodynamic and seismic studies have discussed slab sinking rates of between 1 cm yr^{-1} to more than 2 cm yr^{-1} (Van der Meer et al., 2018; Peng and Liu, 2022; Hounslow et al., 2018). I demonstrate here the applicability of the equation to consider this range of velocities and tune our geodynamic models to 1.35 cm yr^{-1}, corresponding to a sinking time of 200 Myr to a depth of 2690 km, 200 km above the CMB.

4 test models are ran with a parameter space based on equation 3.9, summarised in table 3.9.

Table 3.9 Parameter space for our test models, in which we aim to tune simulations to a sinking time of $\sim$ 200 Myr (x = trench length, μ = viscosity, v_s = surface velocity, v = predicted radial velocity)

Case	x (m)	μ (Pa s)	v_s (cm yr^{-1})	v (cm yr^{-1})
t01	7.784E+06	1E+23	3.8	1.348
t02	7.784E+06	2E+23	5.9	1.345
t03	7.784E+06	2E+24	8.0	1.345
t04	7.784E+06	1.24E+23	4.0	1.344

Additionally, each of these simulations assume constant values of y = 170 km (based on the average thickness of the thermal lithosphere at the subducting trench across each of our previous simulations), and z = 1345 km (for the median depth of slap sinking across these models). Such values yield predicted slab sinking times of 199, 199, 200, and 201 Myr for cases t01, t02, t03, and t04, respectively (table 3.10).

When viscosities and surface velocities are higher, slabs sink more vertically at shallow depths, as the slab is pushed through the mantle by faster surface velocities. At greater depths, the viscosity becomes the dominant control on slab sinking, away from the forces of surface velocity, and the slab decelerates. Conversely, when viscosities and surface velocities are lower, then the slab sinks more slowly at shallow depths (given that less slab material is being pushed down into the mantle in a given time). As the slab sinks away from the surface, the lower viscosities facilitate slab acceleration.

Table 3.10 Comparison of predicted and measured slab sinking times for a goal sinking time of $\sim$ 200 Myr across 4 test models.

Case	**Predicted Time (Myr)**	**Measured Time (Myr)**	**Rel. Error (%)**
t01	199	177	12.4
t02	199	221	(-)9.9
t03	200	214	(-)6.5
t04	201	195	3.1
		Average	**8.00**
Average	**200**	**202**	**1.0**

I find a relative error between our predicted and measured slab sinking times of 12.4%, 9.9%, 6.5% and 3.1%, for simulations t01, t02, t03, and t04, respectively, all firmly within the goal of 15% (table 3.10). Viewing the suite of models holistically, I find an error between the average predicted time and average measured time across these cases is 1%, indicating the success of the equations.

3.6 Discussion

3.6.1 Towards understanding slab behaviour

Previous studies have shown that mantle viscosity is the primary control on slab sinking rates (e.g Van der Meer et al., 2018; Butterworth et al., 2014; Griffiths and Turner, 1988; Marquardt and Miyagi, 2015; Wang and Li, 2020; Conrad and Lithgow-Bertelloni, 2002), though the extent to which the surface velocity is also a primary control is contested (Peng and Liu, 2022; Fukao et al., 2001; Becker and O'Connell, 2001; Jadamec and Billen, 2010). Additionally, studies which have sought to understand the influence of plate velocities on subduction have seldom approached this from a whole-mantle perspective, with studies often focussed on the dynamics in the upper mantle (e.g Schellart and Moresi, 2013; Becker et al., 1999; Schellart et al., 2008). Building upon these studies and the results from my own models, I suggest rather than considering mantle viscosity and plate velocity individually, it is the relationship between them that determines the behaviour of slabs. I consider the natural sinking velocity to be the velocity at which a slab sinks through a given viscosity, with little contribution from the top down, and limiting slab thickening or instabilities. Given that this natural sinking velocity is primarily dependent on the mantle viscosity rather than the plate parameters, it may better reflect the dynamics of slabs in reality, where slabs pull plates rather than being driven into the mantle as in these models.

The morphology of the slab in these models is largely dictated by the deviation from this natural velocity in the upper mantle; where slabs are driven into the mantle by high plate velocities faster than they can naturally sink through the given mantle viscosity, they thicken and the dip shallows (figures 3.2, 3.5). For the slowest plate velocities, when the mismatch between the surface and the sinking velocity becomes too large, the slab develops its own instabilities and sinks as drips rather than as a homogeneous sheet, with higher strain rates across the fastest moving portions of the slab.

In the lower mantle, the effect of surface velocity is reduced, especially in the more complex simulations where the lower mantle is characterised by a viscosity transition (figure 3.10). In the lower mantle, viscosity is the dominant control on slab sinking rates such that I consider the velocities in this region to be most similar to the natural sinking velocity. Whilst the surface velocity may not be as fundamental to the slab dynamics in the lower mantle, understanding the mechanisms which underpin the behaviour in the upper mantle is crucial to better predict slab sinking times and dynamics across the entire mantle volume.

Trench-parallel slab length has often been invoked as a parameter controlling trench retreat and curvature (Schellart et al., 2007; Schellart, 2024; Royden and Husson, 2006; Stegman et al., 2006; Stegman et al., 2010). Schellart (2024) suggests that narrow slabs have strong local return flow patterns in the upper mantle close to the slab whilst wider slabs sink forwards through trenchward subducting plate motion. Our simulations indicate that faster slab sinking rates are associated with longer trenches, in keeping with the work of Schellart (2024) and suggesting that the balance between sinking and resistance forces can be considered, at least in part, as a function of slab trench length. This effect is secondary to the balance between viscosity and surface velocity, but is nonetheless relevant to accurately predict slab sinking times in this class of models where plates are pushed into the mantle from the surface.

The preferred equation derived in this study accurately predict slab sinking times to a depth of 2690 km, and is applicable to simple, single-plate simulations, and complex global mantle circulation models. Whilst a greater error was expected in these more complex models, as slabs were affected by further-field forces associated with other slabs and proximal upwellings, the opposite is observed. It may be that the equation is similarly applicable to each suite of models as the simple models may also develop other surface instabilities. These instabilities may evolve into cold downwellings, though it may not be appropriate to call them slabs given that they are not associated with any surface motion and are instead associated with the complexity of numerically solving for only a single moving plate at the surface. Alternatively, it may be that the slabs truly have little effect on one another within the mantle. As slabs generate a passive return flow, it may be that each slab develops a convective cell which effectively shields it from the forces of other slabs. Any influence from other mantle structures may be most marked when implementing a temperature-dependent viscosity, as the viscosity near the slab is most crucial for slab sinking dynamics. Since slabs are cold, they likely impart a greater effect on the proximal temperature dependent viscosity, and the far-field effects of any more distal mantle structures will be significantly reduced.

3.6.2 Limitations

This study would benefit from a greater number of simulations upon which to base our empirical equations. Increasing the number of simulations would continue to refine these equations, though this approach may result in overfitting the data. The current derived equations are still successful at predicting slab sinking times. When the initial simulations (cases000-017), test models (t01-04), and global circulation models (m01p, m01f, tviscp, tviscf, mup, muf) are considered as one suite of simulations, the equations have shown to be successful for a much wider parameter space and across a range of slab sinking times, beyond just those that are proposed as Earth-like.

Given the uncertainty surrounding mantle viscosities, I do not suggest that these empirical equations are applicable to predict slab sinking times on Earth at present. They do, however, give an indication as to the relationship between the mantle and surface controls on slab sinking, which is applicable beyond mantle circulation modelling.

Whilst I consider these equations successful, individual simulations still exhibit a significant relative error between predicted and measured slab transit times. It is likely that there are additional forces at play within the mantle which are complex and hard to reconcile within our relatively simple equations. Future work should seek to reconcile these parameters across a larger suite of models to further refine these empirical equations.

3.7 Conclusions

This study has shown that Stokes' Law is applicable to slab sinking when slabs are approximated as spheres, but requires an additional term to consider two fundamental surface conditions, the plate velocity and the trench length. This highlights the interplay between surface and mantle processes and the degree to which they are coupled, where mantle processes alone are not sufficient to accurately predict slab behaviour. Slabs have a natural sinking velocity which is determined by the mantle viscosity, but the relationship between this natural sinking velocity and the plate velocity is important for slab sinking. The effects of plate velocity and trench length are most marked in the upper mantle, especially when geodynamic models implement a viscosity discontinuity between the upper and lower mantle. In the lower mantle, the surface controls on slab sinking are reduced and slabs fall more in-keeping with their natural velocity, determined by the viscosity. These equations therefore resolve these two regions of the mantle to accurately predict slab transit times to a depth of 2690 km across a range of viscosity profiles, surface velocities, and plate geometries. I propose that these empirical equations can be used by geodynamic modellers to predict slab sinking times prior to running a simulation, improving the efficiency of the modelling process, whilst also providing insight into the interplay between mantle and surface properties on controlling slab behaviour.

Chapter 4

DEEP MANTLE DYNAMICS:

The stability of deep mantle structures and origins of mantle upwellings in response to subduction zone histories

Abstract

The coupling between the surface and deep Earth is fundamental to the dynamics of the planet, yet the nature of these interactions remain poorly understood through space and time. These processes are elusive, in part, because of a lack of constraint on the nature and evolution of two antipodal large low shear-velocity provinces (LLSVPs) near the core-mantle boundary (CMB), and the role they play in mantle circulation. The origins and long-term stability of these features are debated. This study aims to assess the relative stability of LLSVP-like structures in 3D mantle circulation models, through the coupling between these structures, upwellings and downwellings.

The ‘superpile cycle’, named after its close ties to the supercontinent cycle, depicts the evolution of the deep Earth in response to supercontinent dynamics. Supercontinents assemble with stable subduction girdles and antipodal basal mantle structures, then break apart. During dispersal, as new subduction zones form, slabs induce more complex mantle flow and disrupt the stable degree 2 structure in the lowermost mantle. As subduction zones stabilise, LLSVP-like structures tend back to two antipodal piles, and a new supercontinent may assemble. These findings highlights the cyclical and coupled nature of structures in the deep Earth and at the surface.

4.1 Introduction

The relationship between Earth's surface and deep interior is one of the most fundamental aspects of mantle dynamics. Many previous studies have shown that the two domains are intrinsically linked (e.g. Arnould et al., 2020; Burke, 2011; Davies, 1977; Jellinek and Manga, 2004; Silver et al., 1988; Yoshida and Santosh, 2011; Zhao, 2004), with slabs transferring energy and material from the surface towards the core-mantle boundary (CMB) and, in return, plumes may develop from near the CMB and rise towards the surface. Two large low shear-velocity provinces (LLSVPs) are observed at the base of the mantle, beneath Africa and the Pacific Ocean, using seismology Dziewonski et al., 1977; Garnero et al., 2016. These have been spatially correlated with hotspots at the Earth's surface. and the edges of LLSVPs have often been invoked as plume-generation zones (e.g. Burke et al., 2008b; Ganerød et al., 2010; Ganerød et al., 2011; Heron, 2019; McNamara, 2019; O'Connor et al., 2018). The relationship between downwelling slabs and LLSVPs is less clear, in part because the nature of the LLSVPs is enigmatic. Studies have suggested thermal Davies et al., 2012; Davies et al., 2015; Ritsema et al., 2007; Schuberth et al., 2009, or thermo-chemical Tackley, 2012; Bower et al., 2013; Bull et al., 2009; Lassak et al., 2007; Panton et al., 2023 origins for these structures, and recently, their intrinsic density has also been debated McNamara, 2019; Garnero et al., 2016; Yuan and Li, 2022; Panton et al., 2025. These models lead to different proposed morphologies, with thermal plume clusters Davies et al., 2012; Schuberth et al., 2009, thermochemical superplumes Le Bars and Davaille, 2004; Olson and Amit, 2015; Gamal El Dien et al., 2019 or dense piles McNamara and Zhong, 2005; Heyn et al., 2020; Lassak et al., 2007 described across the literature. This lack of consensus regarding the nature of LLSVPs has also raised questions regarding their dynamics, with some studies suggesting these antipodal structures have been stable for hundreds of millions to billions of years Torsvik et al., 2008; Conrad et al., 2013; Huang et al., 2015; Huang et al., 2020; Burke et al., 2008b; Mulyukova et al., 2015, whilst others indicate that they are mobile about the CMB Davaille and Romanowicz, 2020; MacLeod et al., 2023; Zhang et al., 2010; Zhong and Rudolph, 2015; Li and Zhong, 2009. This study investigates the relationship between LLSVP stability and plate tectonics using 3D spherical mantle circulation models, building upon an extensive body of work (e.g. Cao et al., 2021b; Cao et al., 2021a; Shi et al., 2024; Zhong et al., 2007; Doucet et al., 2020; Li and Zhong, 2009; Heron, 2019), to investigate the relationships between slabs, piles in the lower mantle, and plumes, synthesising these into a model referred to as 'The Superpile Cycle'.

4.2 Methods

4.2.1 Reference model

As in the previous chapter, each simulation uses the 3D mantle circulation code, TERRA (Baumgardner, 1985; Bunge and Baumgardner, 1995; Bunge et al., 1997; Davies et al., 2013; Yang and Baumgardner, 2000). Calculations are again performed on a structured regular mesh based on an icosahedron (Baumgardner and Frederickson, 1985), with over 10 million grid points, an average radial spacing of 45 km, and a lateral spacing of 59.9 km at the model surface which decreases to 32.7 km at the CMB. Gassmöller et al. (2020) suggested that the dynamics near to boundary layers, or features with dynamic density gradients may not be well modelled in incompressible simulations. Since these simulations are interested in basal mantle structures, which may be associated with such dynamic density gradients, these models are compressible, based on the Murnaghan equation of state, with isothermal boundary conditions at the surface (300 K) and CMB (4000 K) and an internal heating at a rate of 4.0×10^{-12} W kg^{-1}.

Simulations develop from a randomly perturbed temperature field, with a two-layer viscosity structure (where the lower mantle is 30x more viscous than the upper mantle; Hager et al., 1985; Van Keken and Ballentine, 1998) and free-slip boundaries at the surface and CMB to allow the initial field to evolve and develop upwellings and downwellings. After 500 Myrs of conditioning, surface velocities are applied according to 1 Gyr of plate motion history (Müller et al., 2022, section 2.4.2) .

As plate velocities are applied, a more complex temperature and depth-dependent viscosity structure is implemented, with an initial 3-layer radial structure (where the viscosity of the lithosphere is 100x greater than the upper mantle). Temperature-dependence is calculated according to the equation:

$$\mu = \mu_{ir} \cdot e^{(Va \cdot z' - Ea \cdot T')} \tag{4.1}$$

where μ_{ir} is the reference radial viscosity, Va is the non-dimensionalised constant for activation volume, z' is the non-dimensionalised depth (scaled by mantle depth), Ea is the non-dimensionalised constant for activation energy, and T' is the non-dimensionalised temperature (scaled by the temperature difference between the CMB and surface temperature). For the reference case $Va = 1$ and $Ea = 1.5$, representing a mild temperature dependence. Parameters for the reference model are summarised in Table 4.1.

4.2.2 Particles, composition, and seismic conversion

To define LLSVP-like structures in these simulations, seismic velocities are calculated based on temperature, pressure, and composition. Whilst the chem-

Table 4.1 Reference model initial conditions for simulation investigating the stability of basal mantle structures (BMSs).

Parameter	**Symbol**	**Value**	**Units**
Surface temperature	T_s	300	K
CMB temperature	T_{CMB}	4000	K
Internal heating rate	H	4.0 x 10^{-12}	W kg^{-1}
Reference density	ρ	4500	kg m^{-3}
Gravitational acceleration	g	10	m s^{-2}
Thermal expansivity	α	2.5 x 10^{-5}	K^{-1}
Thermal conductivity	κ	4	$Wm^{-1}K^{-1}$
Specific heat capacity	C_p	1000	$JK^{-1}kg^{-1}$
Reference viscosity	μ_0	4.0 x 10^{21}	Pa s
Lithosphere multiplication factor	$\Delta\mu_{li}$	100	-
Lower mantle multiplication factor	$\Delta\mu_{LM}$	30	-
Viscosity - depth dependence	Va	1	-
Viscosity - temperature dependence	Ea	1.5	-
Basally heated Rayleigh number	Ra_H	$\approx 3 \times 10^6$	-
Internally heated Rayleigh number	Ra_H	$\approx 5 \times 10^7$	-

ical evolution of mantle structures is not a focus of this study, the evolution of composition throughout the simulations are briefly described as it relates to calculating seismic velocities. Further details surrounding the chemical evolution of dynamic models can be found in references Panton et al., 2023; Price et al., 2019; Van Heck et al., 2016. Active particles are used to track chemical compositions throughout the simulations, where bulk composition (C) varies between 0 (depleted; representing harzburgite) and 1 (enriched; representing basalt), with an assumed average composition of $C = 0.2$ (representing lherzolite). Half of particles initialise with a composition of $C = 0.2$, $3/8$ with $C = 0.0$, and $1/8$ with $C = 1.0$. Melting is controlled by a linear solidus which is dependent on depth (z) and bulk composition (Price et al., 2019; Van Heck et al., 2016):

Table 4.2 Molar compositions of three particle lithologies (harzburgite, lherzolite, and basalt), from (Panton et al., 2023)

	Harzburgite	**Lherzolite**	**Basalt**
SiO_2	36.184	38.819	52.298
MgO	56.559	49.894	15.812
FeO	5.954	6.145	7.121
CaO	0.889	2.874	13.027
Al_2O_3	0.492	1.963	2.244

$$T_{solidus,dry}(z, C) = T_{meltsurf} + zT_{meltslope} + (1 - C)T_{meltcomp} \tag{4.2}$$

where $T_{meltsurf} = 1400$ K is the melting temperature of basalt material at the surface, $T_{meltslope} = 2.5$ K km^{-1} is the gradient of the solidus and $T_{meltcomp} = 500$ K is the difference in solidi temperature between harzburgite and basalt material. The temperature of each particle is linearly interpolated from the grid and if it exceeds the solidus, then it is considered that melting has occurred and the bulk composition is reduced until the particle plots on the solidus for the given temperature and pressure.

To convert particle compositions to seismic velocities, each of the three lithologies (harzburgite, lherzolite, and basalt) are assigned a constant six-oxide composition (Table 4.2) Baker and Beckett, 1999; Walter, 2003; White and Klein, 2014, after the methodology outlined in reference Panton et al., 2023.

The pressures, temperatures, and compositions on each particle are converted to seismic properties using lookup tables for each of the characteristic lithologies. The lookup tables use Gibbs free energy minimisation, as implemented in Perple_X (Connolly, 2009) and the associated thermodynamic mineralogical dataset of Stixrude and Lithgow-Bertelloni, 2021, to calculate values of density and perfectly elastic seismic velocities for each lithology. Attenuation is accounted for using model Q7g Goes et al., 2004; Maguire et al., 2016, in agreement with the data from reference Matas and Bukowinski, 2007. Seismic velocities are calculated as a post-processing step by taking the harmonic average of harzburgite, lherzolite, and basalt, weighted by the mass fractions of each bulk composition.

4.2.3 Parameter space

To explore the influence of downwelling dynamics on deep-mantle structures and the potential for these structures to be the sites of plume generation, surface and mantle properties are systematically varied across a suite of 24 models. The uncertainties regarding the role parameters(CMB temperature (Lay et al., 2008), mantle viscosity (e.g. Garnero et al., 2016; Murakami et al., 2024; King, 1995), and the nature of LLSVPs) play on the intrinsic stability of deep-mantle structures are considered across the parameter space. Therefore, in addition to changing the dynamics of the plate motion at the surface in these simulations, CMB temperature, viscosity structure, and the thickness and density of a basal primordial layer are explored. At the surface, plate velocities are varied by applying a scaling factor (S_v; equation 2.10, section 2.3), such that the global RMS velocity is reduced by a factor of S_v. In the reference model, this scaling factor is calculated based on the comparison between the average velocity of the plate motion reconstruction and the natural surface velocities of the pre-conditioning convection solutions. Given that the certainty of published plate motion histories decreases back in time, and there is debate as to the most appropriate reference frame by which to calculate the relative plate motion histories, 5 different plate motion reconstructions are implemented which use different reference frames to explore a wider parameter space of surface dynamics.

The fundamentals of the three plate motion reconstructions used in this study (Müller et al., 2022; Cao et al., 2021b; Merdith et al., 2021) are outlined in section 2.4. For ease, they are briefly described here also: Müller et al. (2022) comprises a set of topological plate polygons and associated plate boundaries and velocities in 1 Myr intervals. This model combines the plate motion model of Merdith et al. (2021) and the tectonic rules-based approach to mantle references frames of Tetley et al. (2019). Merdith et al. (2021) defines the rotation of each plate relative to a palaeomagnetic framework. The model considers the relative movement of plates based on a hierarchy of geological precedence, which is then used with the palaeomagnetic data to iterate towards a solution. Conversely, Cao et al. (2021b) proposes a global model of relative plate motions, comprising continuously closing polygons and 3 contrasting absolute reference frames; stable supercontinent location (SSL), orthoversion (OV), and no-net-rotation (NNR). SSL considers 3 supercontinents across the last 1 Gyr, all of which occur in the same location as Pangaea. OV is similar in that they are both based on the absolute reference frame from 250-0 Ma from Young et al. (2019), which is itself a hybrid of a hotspot track reference frame between 70-0 Ma, and a palaeomagnetic reference frame before 100 Ma. The OV model differs from SSL in that the initial supercontinent is 90° E of Pangaea. Both reference frames minimise net lithospheric rotation whilst the NNR reference frame evaluates the net rotation of the lithosphere with respect to the mantle and removes it from the SSL reconstruction.

The parameter space across this investigation is summarised in Table 4.3, and viscosity profiles at the beginning and end of each simulation (to show the evolution with temperature dependence) are shown in figure 4.1.

LLSVP-like material is defined in the simulations by being both +200 K hotter than average and a negative Vs anomaly of no more than -1.5% , extending

Table 4.3 Parameter space for suite of models where models 000-004 have varying CMB temperature, 005-007 have varying plate velocity at the surface, 008-013 have different viscosity structures, 014-016 have different thickness of a basal primordial layer, 017-019 changes the density of a 300 km thick primordial layer, and 020-023 implement different plate motion histories with different reference frames.

Model No	**CMB temp. (K)**	**Plate vel. (cm/yr)**	**Visc. profile**	**Primordial layer thickness**	**Density of primordial layer**	**Plate motion history**
Ref	4000	2.3	v1	-	-	Mu
001	4250	2.3	v1	-	-	Mu
002	4500	2.3	v1	-	-	Mu
003	3500	2.3	v1	-	-	Mu
004	3000	2.3	v1	-	-	Mu
005	4000	9.1	v1	-	-	Mu
006	4000	4.5	v1	-	-	Mu
007	4000	1.5	v1	-	-	Mu
008	4000	2.3	v2	-	-	Mu
009	4000	2.3	v3	-	-	Mu
010	4000	2.3	v4	-	-	Mu
011	4000	2.3	v5	-	-	Mu
012	4000	2.3	v6	-	-	Mu
013	4000	2.3	v7	-	-	Mu
014	4000	2.3	v1	150	3%	Mu
015	4000	2.3	v1	300	3%	Mu
016	4000	2.3	v1	75	3%	Mu
017	4000	2.3	v1	150	1%	Mu
018	4000	2.3	v1	150	5%	Mu
019	4000	2.3	v1	150	10%	Mu
020	4000	2.3	v1	-	-	Me
021	4000	2.3	v1	-	-	NNR
022	4000	2.3	v1	-	-	OV
023	4000	2.3	v1	-	-	SSL

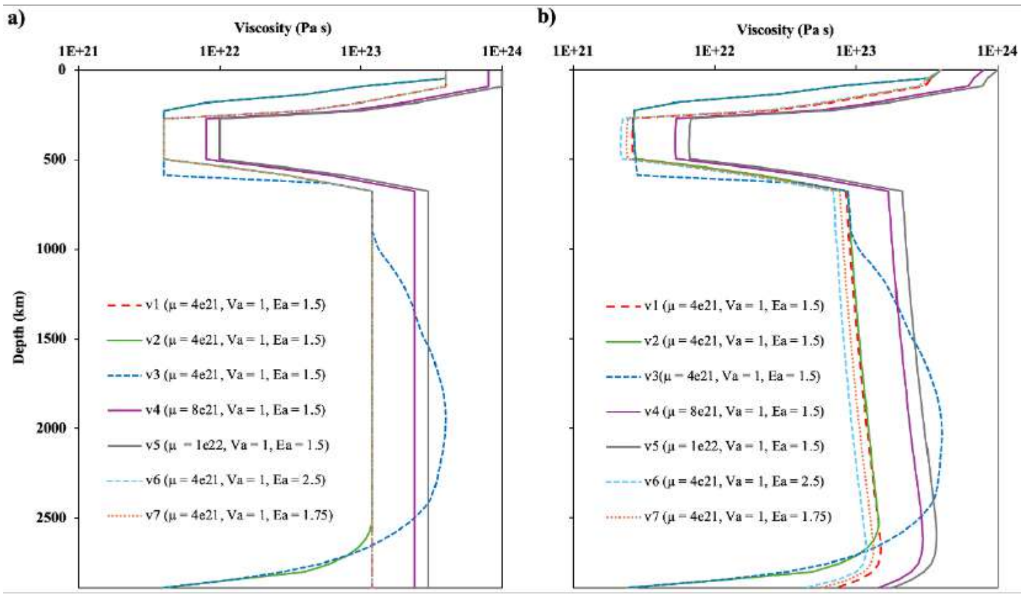

Figure 4.1 7 different viscosity profiles used throughout the parameter space of this study at (a) the beginning of the simulations and (b) at the end of the simulations, once the effect of temperature dependence is more developed.

up to 800 km above the CMB. In the simulations the Vs anomaly is largely dependent on the simulated temperature field, yet both the temperature and Vs thresholds are chosen to define the LLSVP-like material to better constrain the geometry of the structures (since this method excludes some hot material not connected to the CMB). This means that the material deemed to be LLSVP-like can change throughout the simulations and can be recycled through the mantle, as opposed to defining the material at the models initiation and tracking this original material. Plumes are identified using a combination of K-means and density-based clustering performed on the simulated temperature and radial velocity fields (Nowacki et al., 2024). The depth between 300-2500 km is chosen to reduce the effect of the cold surface boundary layer and primordial layers at the base of the mantle, where present.

4.3 Results

In each of mantle circulation models, the LLSVP-like basal mantle structures (BMSs) comprise a series of clustered linear features, with cylindrical upwellings developing at their confluences (figure 4.2). For models with a primordial layer, basal mantle structures are pile-like in morphology, though linear features still form areas of higher topography at the top of the structure. The linearity of BMSs has been observed in previous studies Bower et al., 2013; Cao et al., 2021a, and pile-like morphologies may be attributable to the limited resolution inherent in seismic tomography Schuberth et al., 2009; Ritsema et al., 2007; Bull et al., 2009. Superpiles, as referred to in this study, are so named for a number of reasons. Studies have used the term to familiarly refer to LLSVPs Davies, 2022 regardless of their proposed morphology and, when considered alongside supercontinent dynamics, the similarity in nomenclature is intended to highlight the close coupling between the two realms. Additionally, when the data is filtered to be consistent with the resolution of seismic tomography, or a basal layer is present, the morphologies of the structures are 'pile-like', though closely associated with clusters of upwellings. In this study, BMS stability is considered in terms of structure volume, change in shape, and the generation of plumes associated with BMSs.

4.3.1 Volume stability

For the models where I vary the CMB temperature, primordial layer thickness and primordial layer density, most models exhibit a similar evolution though time, though the absolute volumes increase with hotter CMB temperatures, or a thicker, denser primordial layer (shown by the near parallel lines representing each model in figure 4.3a, d, e). I attribute this to the increase in material

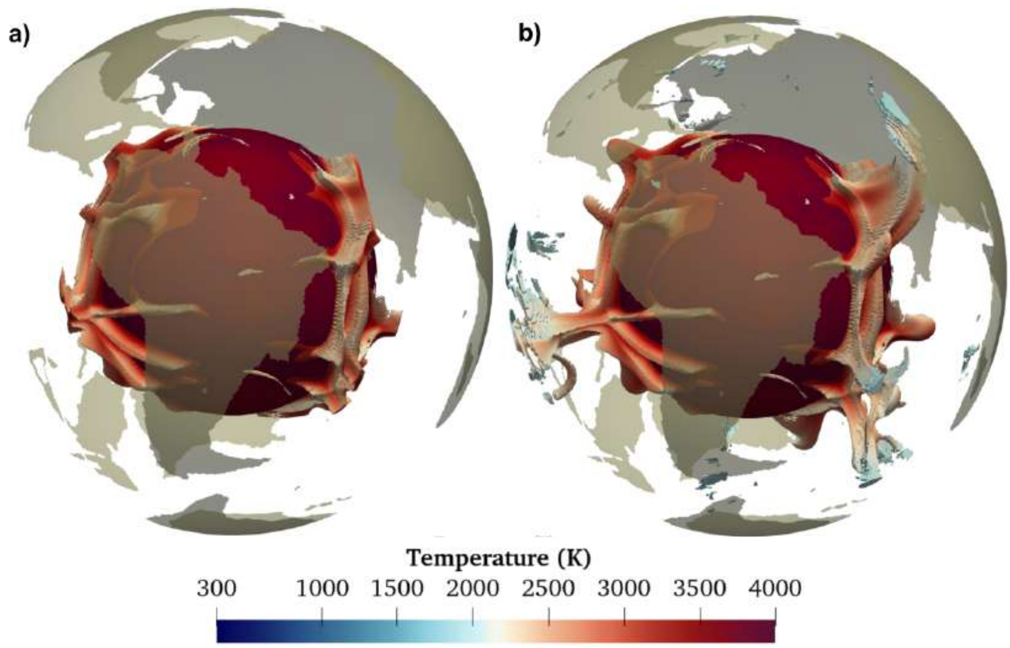

Figure 4.2 LLSVP-like basal mantle structures (BMS) as defined by a 200 K temperature anomaly and a -1.5% Vs anomaly, in (a) the bottom 800 km of the mantle, and (b) across the mantle volume for the reference model. Present-day configuration of plates show the location of the basal mantle structures at the end of the simulation.

which is determined to be LLSVP-like, given the higher temperatures and different compositions withing the primordial layer.

Whilst the absolute volumes of BMS material are similar across the simulations with different plate velocities (implemented by different scaling factors) and plate motion histories, their temporal evolutions differ significantly (figure 4.3b, f). Therefore, whilst parameters acting on the deep Earth (CMB temperature, primordial layer thickness and density) may impart the greatest control on the absolute volume of LLSVP-like material (figure 4.3a, d, e), the spatial distribution of slabs through time (which are controlled from the top down) may have a greater effect on the temporal evolution of BMSs (figure 4.3b, f).

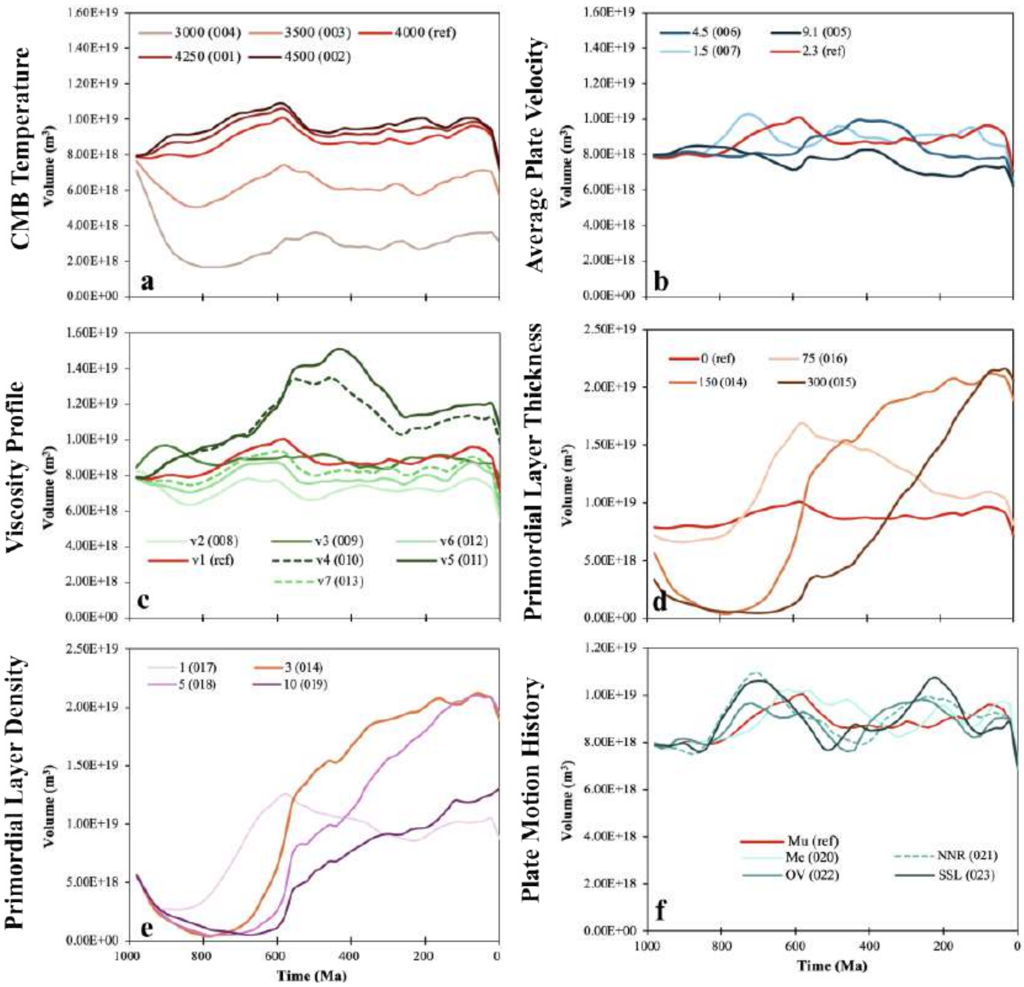

Figure 4.3 Volumes of material defined as LLSVP-like in the lowermost 800 km of the mantle across each simulation, grouped by the varying parameter (CMB temperature, average plate velocity, viscosity profile, primordial layer thickness, primordial layer density, and plate motion reconstruction).

The global length of subduction zones in the plate motion reconstruction Müller et al., 2022 show peaks during supercontinental assembly, and troughs during periods of supercontinent dispersal, (shown by the similar patterns between subduction zone length and detrital zircon records which reflect the degree of continental crust preservation, figure 4.4, inset). When global lengths of subduction zones are cross-correlated to the change in volumes across the models, most models show a correlation with the subduction zone lengths if they are shifted by an average of 160 Myrs (figure 4.4), representing the time for a slab to sink to a depth where it can affect the volume of the structures (figure 4.5).

There are cyclical alternations between positive and negative correlations, with an average cycle duration of 220 $\pm$ 60 Myrs across most models (calculated from the average time between significant peaks in cross-correlation algorithm (see figure 4.6 caption for more details), reflecting the average cyclicity of peaks in the global length of subduction zones . Models with thick or dense layers of primordial material (models 014, 015, 018, 019) do not exhibit this same cyclicity, which can be attributed to the rapid volume growth of these structures through time shown in figure 4.3.

During supercontinent assembly, the development of circum-continental subduction zones may result in the development of antipodal BMSs (figure 4.7a, b), where material is swept simultaneously beneath the supercontinent and beneath the superocean, localising into two piles. Therefore, the cyclicity of volume change may be considered a response to changes in subduction zone geometries or locations (where peaks in subduction zone length reflect higher degree of supercontinentality with longer, circum-continental trenches compared to periods of peak supercontinent dispersal) , and the 160 Myr time lag reflects the time required for slabs to reach a significant depth to affect the deep Earth (figure 4.5). The relationship between subduction zone lengths and changes in volume are much more cyclical and regular beneath the Pacific (figure 4.7c, d) whereas the relationship is not statistically significant beneath Africa (as denoted by a p-value of 0.43; figure 4.7c), which is attributed to the more chaotic flow beneath this region through time. Throughout the plate motion reconstruction, the area where Africa currently resides has exhibited more complex subduction patterns, as material is swept not just by circum-continental slabs but intra-continental

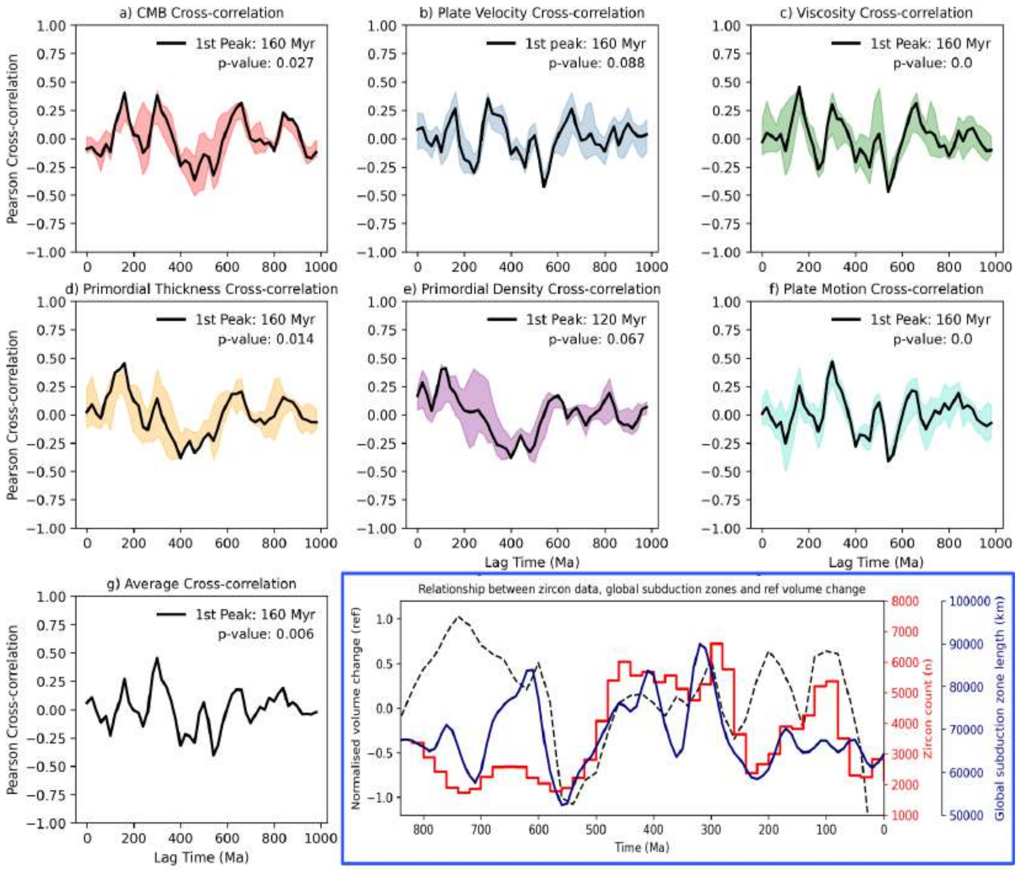

Figure 4.4 Results of cross-correlation algorithm showing the relationship between global length of subduction zones and the change in volumes across basal mantle structures through time (inset: global length of subduction zones (blue), detrital zircon records ((red); Puetz et al., 2021), normalised change in volume from reference model (black). Global subduction zone lengths are shifted forwards by 160 Myrs to show the relationship with normalised volume change. Detrital zircon records are also shifted by 160 Myrs to show the close relationship between subduction zone lengths and supercontinent configuration). (a-f) Black lines show the average cross-correlation for models with different CMB temperatures, plate velocities, viscosities, primordial layer thicknesses, primordial layer densities, and plate motion histories, respectively. Coloured space represents the range of values across each individual model. g) average across all of the models. P-values are calculated from a Monte-Carlo simulation with 1000 iterations, where subduction data is randomly shuffled and compared to the model data.

subduction as internal oceans have closed throughout different phases of the supercontinent cycle (figure 4.8) inducing a more complex flow pattern in the mantle.

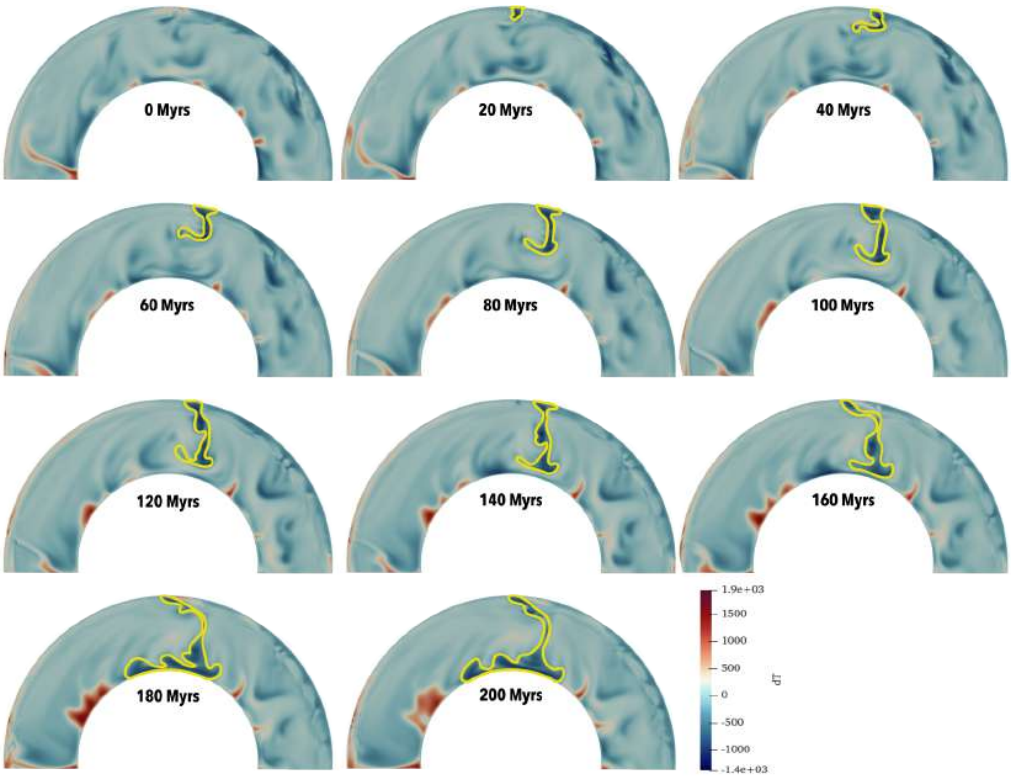

Figure 4.5 Example slab (defined in yellow by -300 K thermal anomaly) in reference model, showing the time taken to sink through the mantle. Additionally, hot material is shown to be mobile about the CMB and migrates away from slabs as they sink.

4.3.2 Variation in BMS morphology

Simulated seismic velocities near the CMB are smoothed up to a spherical harmonic degree four structure, in line with many global seismic tomography studies of the CMB (e.g. Creager and Jordan, 1986; Morelli and Dziewonski, 1987; Obayashi and Fukao, 1997; Boschi and Dziewonski, 2000; Sze and Hilst, 2003; Tanaka, 2010; Lassak et al., 2010; Koelemeijer et al., 2012), such that measured change in shape is most sensitive to long-wavelength variations in mantle flow. At this degree of smoothing, a contour value of -0.3 % Vs anomaly encompasses roughly the same structures as the -1.5 % Vs contour in the raw data (figure 4.9a).

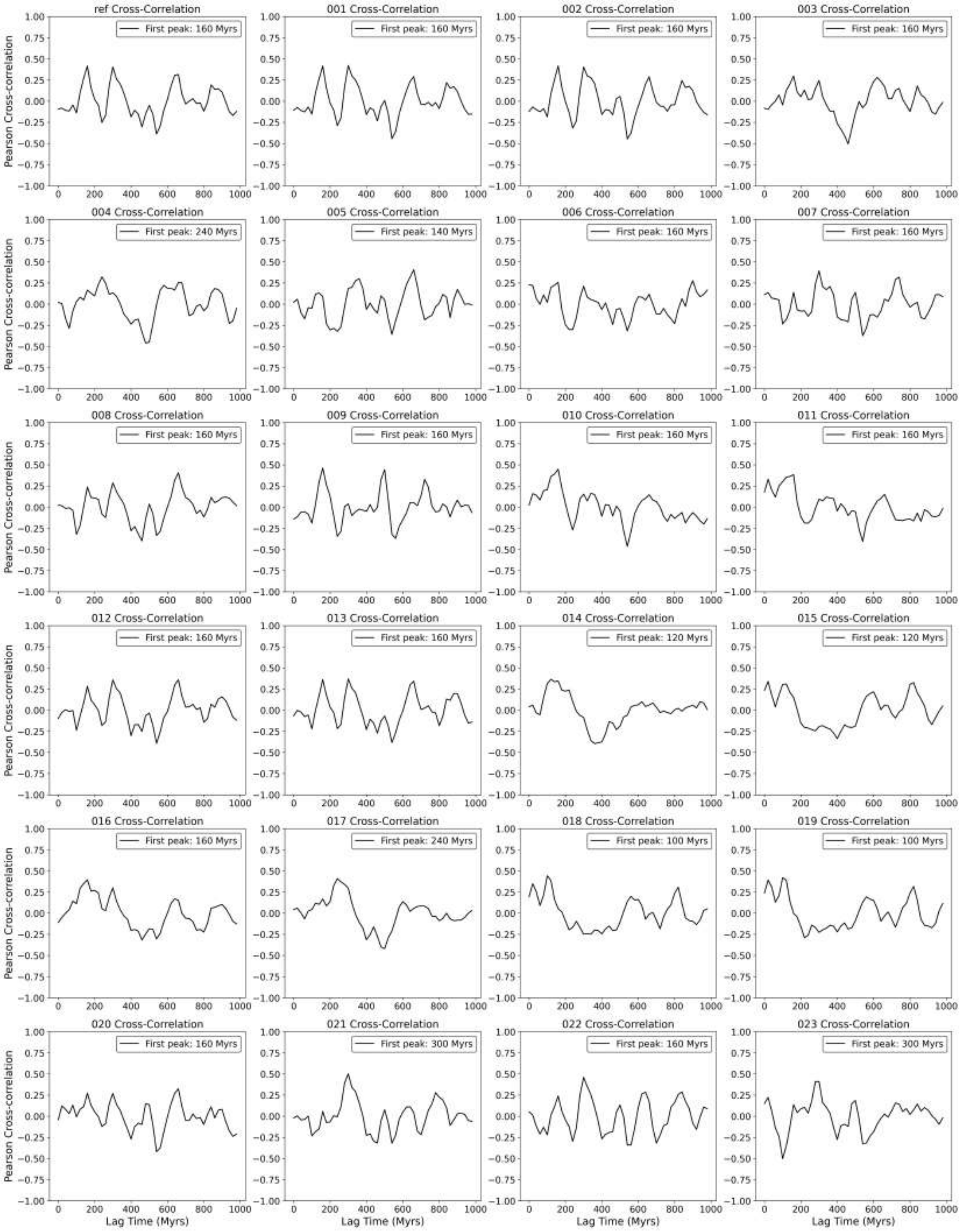

Figure 4.6 Results of cross correlation algorithm for each simulation showing cycling trend in positive correlations and lag time of the first significant peak in Pearson cross-correlation value. Cross-correlations for each model compare the relationship between the change in volume and the global length of subduction zones. Significant peaks are defined by positive Pearson correlation coefficients and a prominence threshold of 0.2.

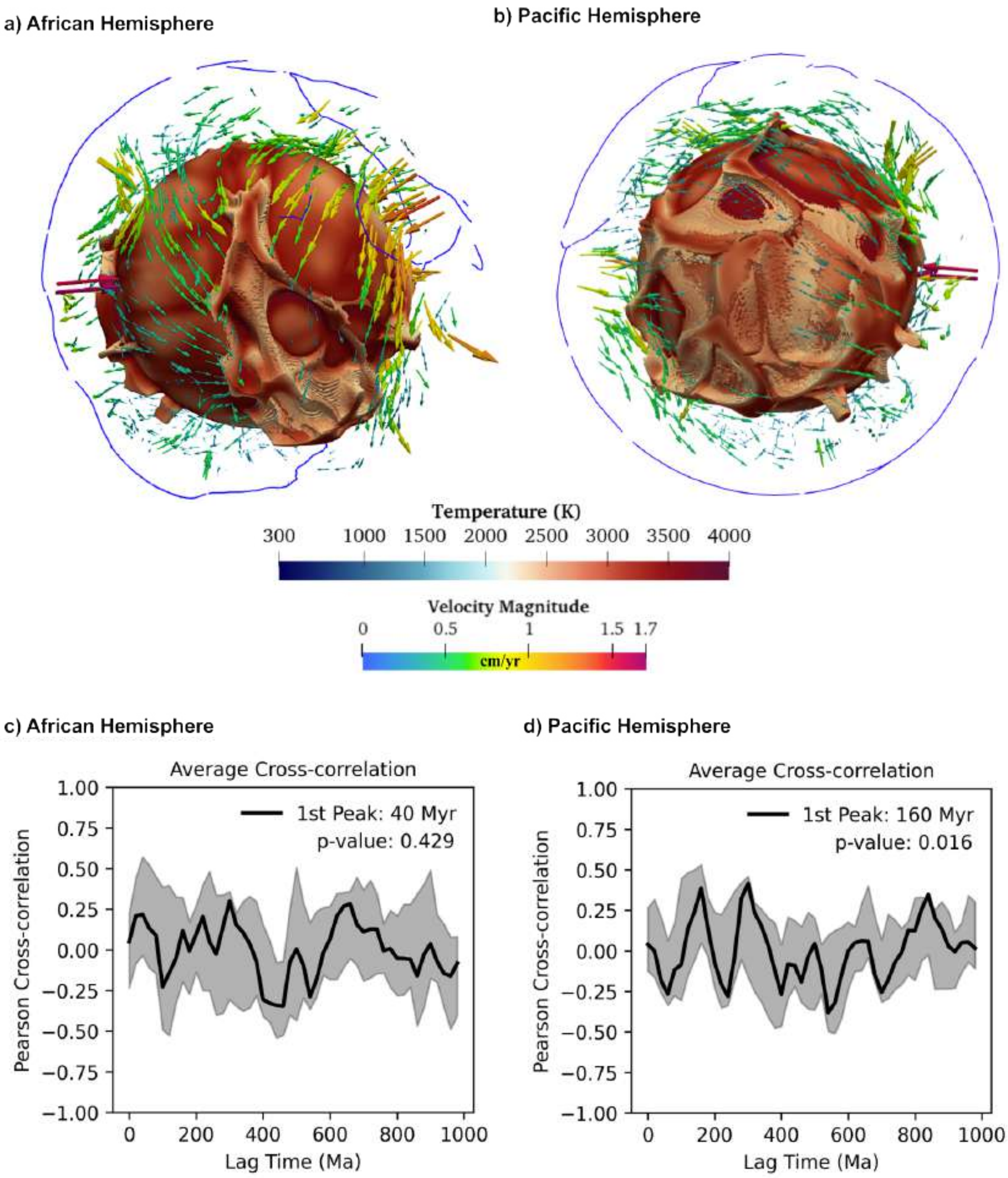

Figure 4.7 a) 3D visualisation of accumulation of BMS material in the African hemisphere for model 014 (chosen because of the pile-like morphologies associated with simulations with a primordial layer) at 0Ma, with the locations of subduction zones shown in blue. Arrows show the direction of flow within colder than average mantle material (representing flow associated with downwellings), scaled and coloured by the magnitude of the velocity. b) As with a) but for material accumulated in the Pacific hemisphere. c) Average cross-correlation between subduction zone lengths and BMS volume change beneath the African hemisphere. Grey space reflects the range in correlations across all of the simulations. d) As with c) but beneath the Pacific hemisphere.

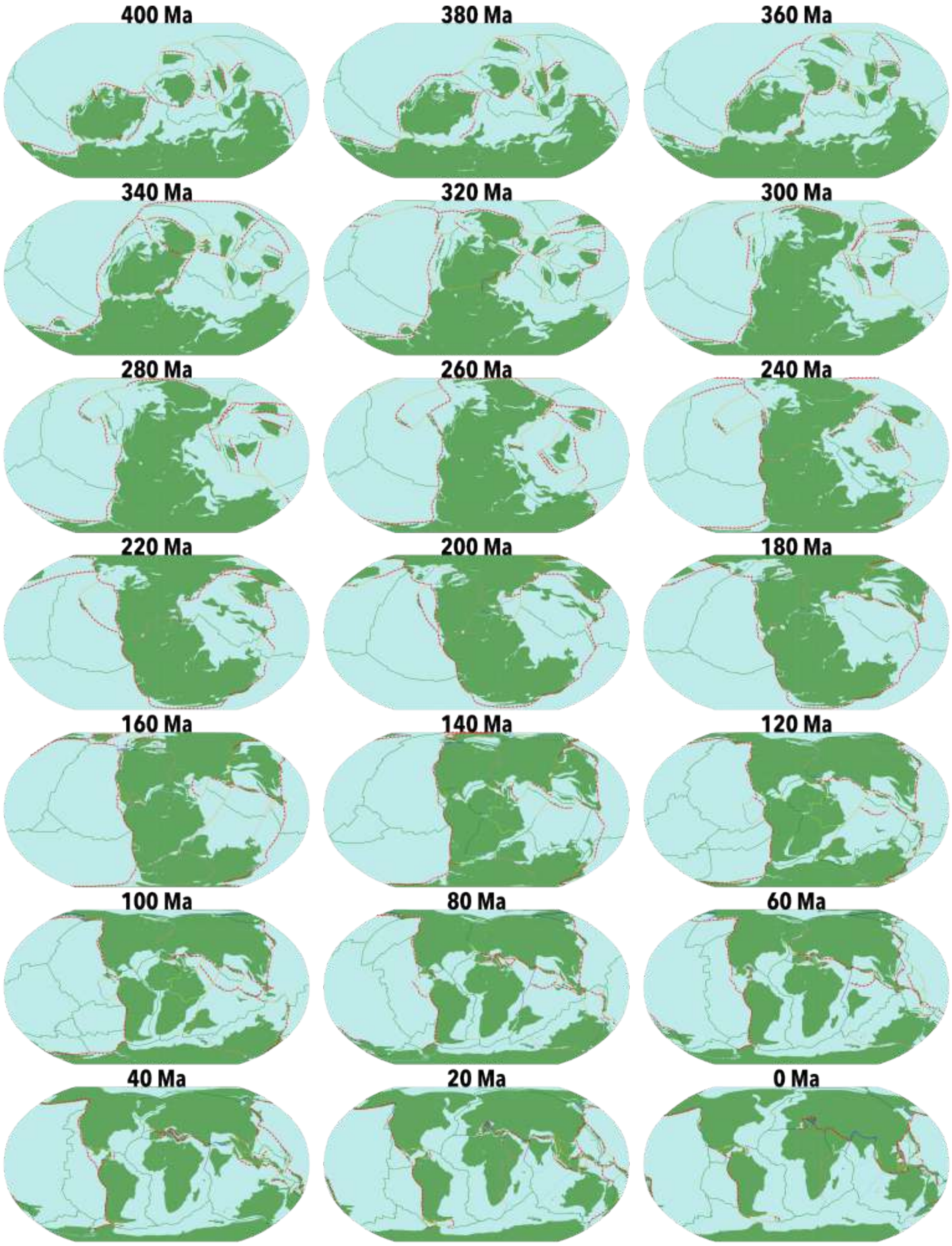

Figure 4.8 Global GPlates (Müller et al., 2018) reconstruction through time from the Müller et al. (2022) plate motion history showing the evolution of subduction zones, and their relative stability between ~ 320-100 Ma initially surrounding Pangaean supercontinent, and evolving into the Pacific Ring of Fire. Red - subduction zones, green - spreading ridges.

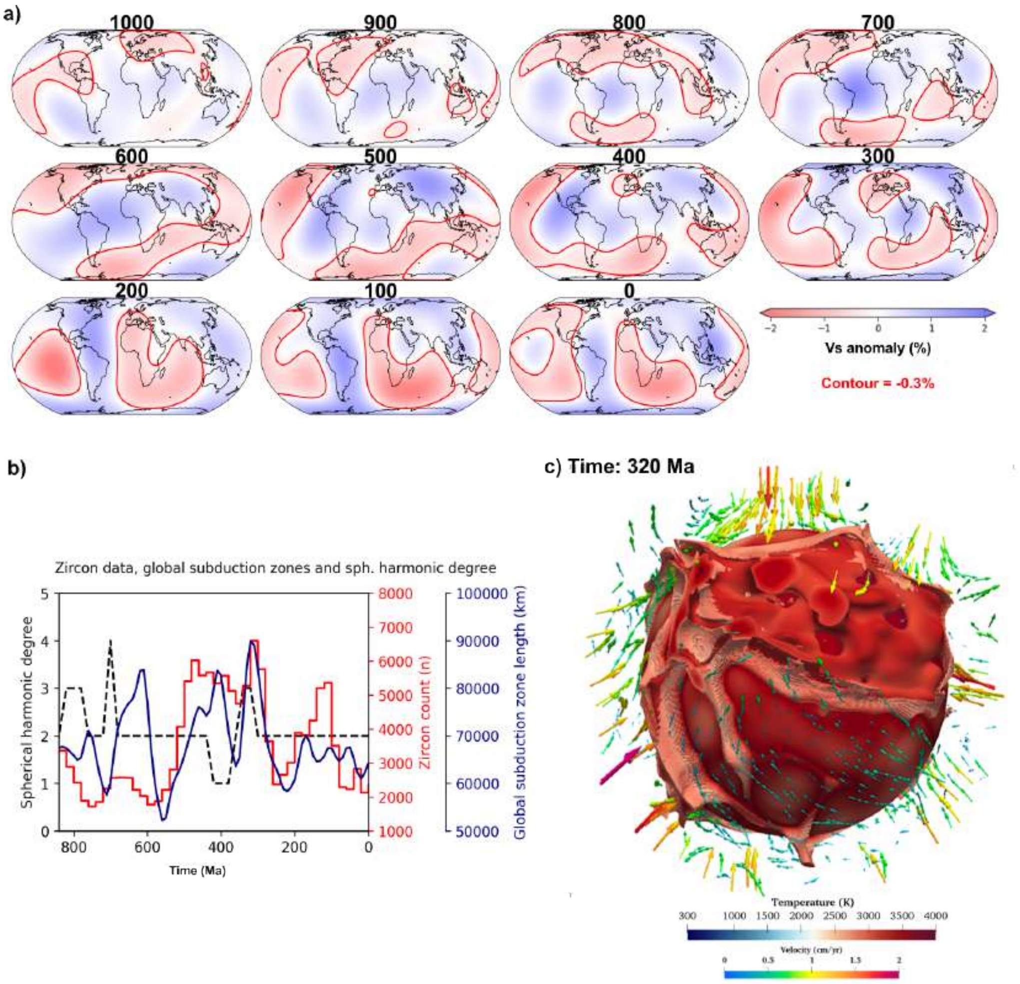

Figure 4.9 a) Morphology of the BMSs through time (Ma), contour represents -0.3 % Vs field for data with maximum spherical harmonic degree of 4, at 150 km above the CMB. b) Dominant spherical harmonic degree at 100 km above the CMB (reference model) compared to the global length of subduction zones in the Müller et al. (2022) plate motion history (blue) and Puetz et al. (2021) detrital zircon data (red), here shifted forwards by 200 Myr; c) 3D visualisation of BMS material for model 014 (chosen because of the pile-like morphology associated with models with primordial layer) at 320 Ma. Arrows show the direction of flow within colder than average mantle material (representing flow associated with downwellings), scaled and coloured by the magnitude of the velocity.

The present day antipodal structure beneath the Pacific and Africa only develops between 300-200 Ma, as material is swept by downwellings associated with the formation of Pangaea, during the period when BMS volume changes rapidly (figure 4.4). These simulations better represent the shape of the African LLSVP, compared to the shape of the Pacific (as is common across many geodynamic models Steinberger and Torsvik, 2012; Li and Zhong, 2017; Schuberth et al., 2009), though despite this potential mismatch between the shape of the Pacific LLSVP and the Pacific BMS in these simulations (which may be attributable to potentially distinct evolutions and origins of the two structures Panton et al., 2025; Doucet et al., 2020), the location of the structure is similar to that observed in the present-day, indicating that the processes involved in these simulations, namely subduction, exert a first-order control on the location of accumulated material in the deep Earth.

The dominant spherical harmonic degree near the CMB shows rapid changes $\sim$ 200 Myr after peaks in subduction zone length (figure 4.9b). These short-lived ($<$ 50 Myr) deviations from a dominant degree 2 structure in the deep Earth indicate a disturbance to the structures in the lowermost mantle, and point towards a similar subduction-related mechanism as discussed previously. Figure 4.9c shows three areas of downwelling flow (at the north pole, along the western margin of Pangaea, and along the north-eastern edge of Pangaea) in the deep mantle at 320 Ma, as the dominant spherical harmonic degree of the simulation changes from 3 to 2 (figure 4.9b). The relationship between subduction length and changes in dominant spherical harmonic degree is best reflected by an average 200 Myr forwards shift in the subduction zone lengths (figure 4.11), such that slabs have time to sink to the lowermost mantle and induce significant BMS migration to alter the dominant degree.

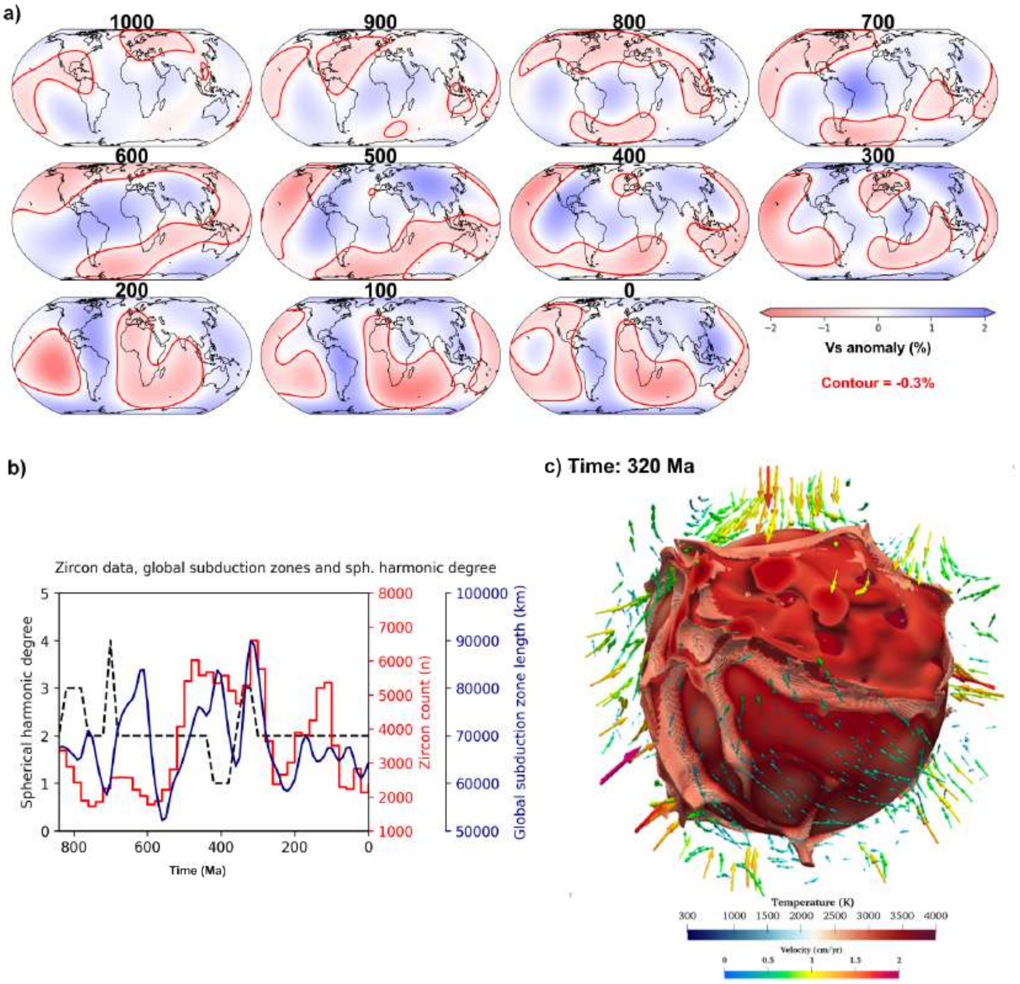

Figure 4.10 a) Dominant spherical harmonic degree at 100 km above the CMB (reference model) compared to the global length of subduction zones in the Müller et al. (2022) plate motion history (blue) and Puetz et al. (2021) detrital zircon data (red), here shifted by 200 Myr; b) 3D visualisation of BMS material for model 014 (chosen because of the pile-like morphology associated with models with primordial layer) at 320 Ma. Arrows show the direction of flow within colder than average mantle material (representing flow associated with downwellings), scaled and coloured by the magnitude of the velocity.

Our findings suggest that the formation of new subduction zones (and the reorganisation of older ones) disrupts the deep mantle structure, and the BMSs are swept around the CMB to a stable location (where flows converge). In these models, this reorganisation occurs over 10-40 Myrs (from when we observe

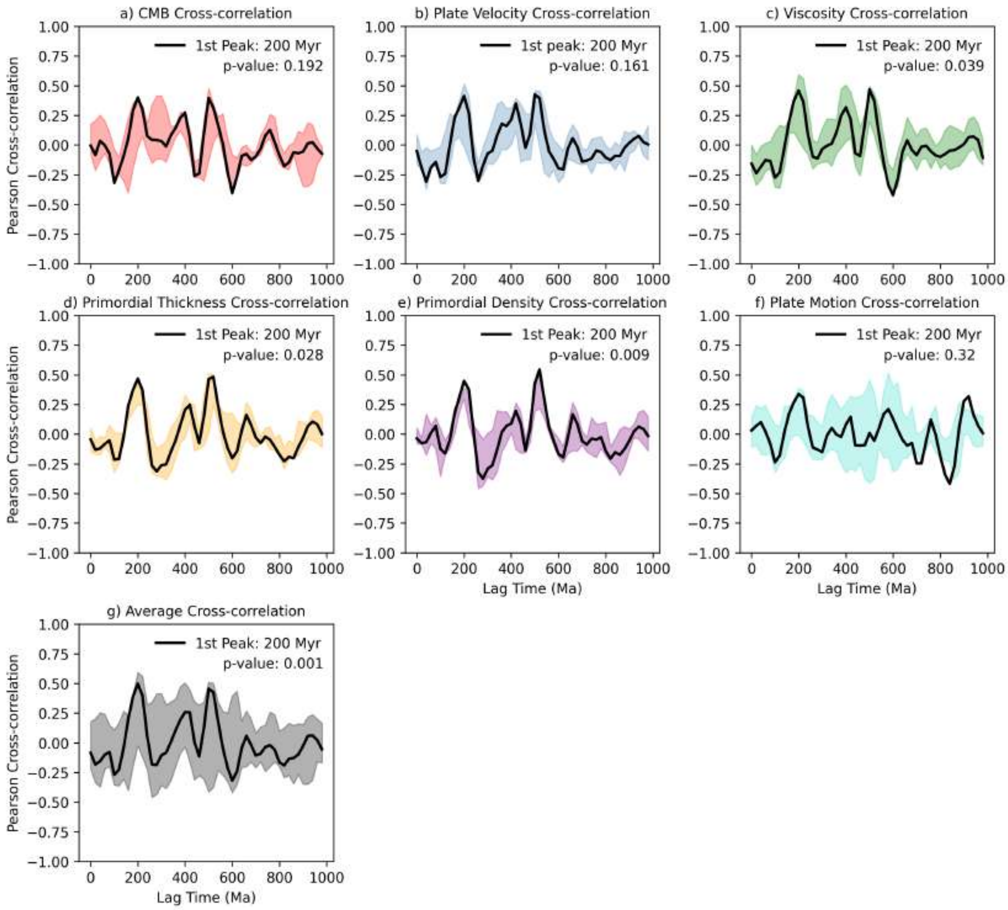

Figure 4.11 Results of cross-correlation algorithm showing the relationship between global length of subduction zones and the change in dominant spherical harmonic degree across basal mantle structures through time. (a-f) Black lines show the average cross-correlation for models with different CMB temperatures, plate velocities, viscosities, primordial layer thicknesses, primordial layer densities, and plate motion histories, respectively. Coloured space represents the range of values across each individual model. g) average across all of the models. P-values are calculated from Monte-Carlo simulation with 1000 iterations.

changes in shape and volume to the change in dominant spherical harmonic degree), which is hereafter referred to as ‘rearrangement events’. However, the timings of these events in the simulations (160-200 Myrs after the change in subduction patterns at the surface) are not necessarily representative of the

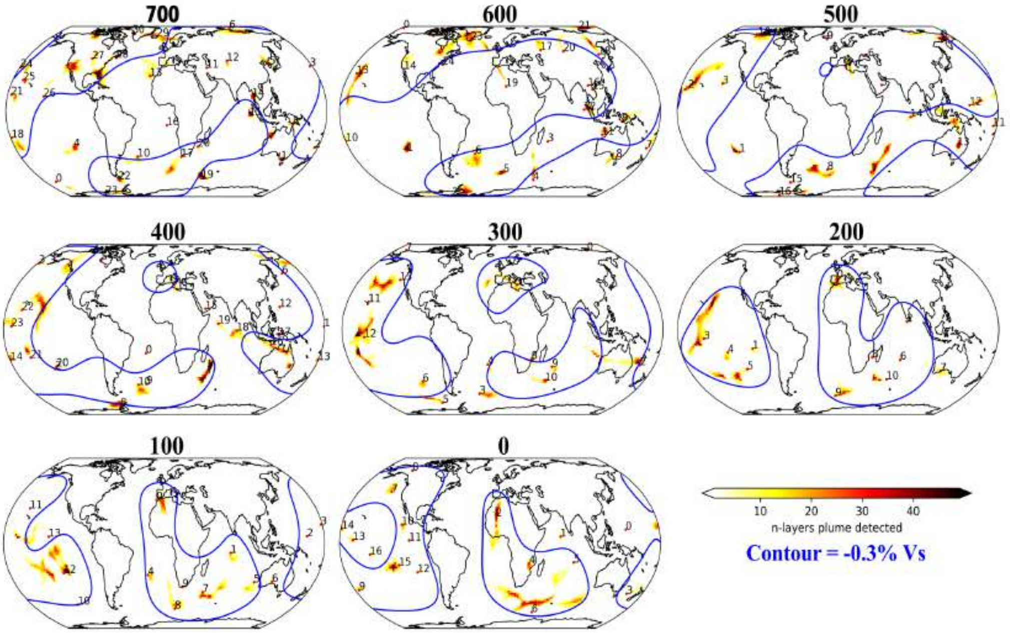

Figure 4.12 Location of plumes detected by K-means and density-based clustering between depths of 300-2500 km in reference model. Blue lines reflect the outline of BMSs as defined in figure 4.9a.

Earth, since the slab sinking rate is dependent on the viscosity structure of the mantle, which is currently poorly constrained.

4.3.3 Distribution of plumes through space and time

Peaks in plume production occur at $\sim$ 700 Ma and between 550-350 Ma across the simulations (figure 4.12), corresponding with the peaks in BMS rearrangement (volume change in inset; figure 4.4, changes in spherical harmon degree; figure 4.9b).

Many previous studies have suggested that plumes form from the convergence of flow in the deep mantle Davies et al., 2012; MacLeod et al., 2023; Hassan et al., 2015; Plimmer et al., 2024, which is supported by this study. The flow which controls the location of BMSs (figure 4.7a,b and figure 4.9c) is therefore intrinsically linked to the formation of plumes, and suggests that the two classes of structures are closely related. Most plumes ascend above BMSs in these simulations, and are not limited to the edges of the structures as has been suggested in some previous studies Burke et al., 2008b; Ganerød et al., 2010; Ganerød et al., 2011; Heron, 2019; McNamara, 2019; O'Connor et al., 2018. I highlight the 700-600 Ma and 500-400 Ma time intervals in figure 4.12, where a greater proportion of plumes lie outside of the BMS contours. This may reflect the complex flow in the deep mantle during the rearrangement events, as the BMSs begin to migrate and change morphology rapidly. As slabs induce rearrangement in the lower mantle, there is likely a period where the flow converges away from the location of BMSs, as they have not yet had significant time to stabilise in response to the changes in flow. When the behaviour of plumes is considered alongside the stability of BMSs, it is clear that the change in subduction locations have the capacity to impact the entire circulation cycle, and these findings are synthesised into a proposed 'superpile cycle'.

4.4 The Superpile Cycle

This superpile cycle describes the evolution of the deep mantle from the assembly of a supercontinent, through breakup and towards the assembly of the next supercontinent. The formation of a supercontinent such as Pangaea may be facilitated by the closure of an interior ocean and the formation of circum-continental subduction zones (figure 4.13, phase 1). At this stage the modelled BMSs, which can be related to real-world LLSVPs, are antipodal. As the supercontinent breaks apart, the circum-continental subduction zones spread, but retain a similar geometry to that during assembly, BMSs stabilise and remain beneath the disassembling supercontinent and its antipodal ocean (figure 4.13, phase 2).

During supercontinent dispersal, new subduction zones begin to develop (which we may be beginning to observe on Earth with the development of Atlantic subduction zones Schellart et al., 2023; Gutscher et al., 2012; Duarte et al., 2013; Duarte et al., 2018; Duarte et al., 2024). As these slabs descend into the mantle (figure 4.13, phase 3), the deep Earth undergoes a rearrangement event. Firstly, after $\sim$ 160 Myrs in these models, material is swept laterally near the CMB such that the structures change shape and volume. Rather than subduction promoting volume gain in the BMSs, it may be that the BMSs are hotter than average given the increase in cold slab material, which also shapes the structures. This interpretation does not require us to rule out a primordial layer as the origins for LLSVPs, where the maximum volume would be defined at the beginning of the simulations and constantly decreasing. As material is continually swept into piles, flow converges and plumes develop. During rearrangement events there are slabs in the mantle from both older and younger subduction zones, flow in the deep Earth is likely more complex, and plumes can form away from the tops of BMSs. Given that the dominant spherical harmonic degree changes across the suite of models after the change to BMS volume and shape, there is an additional time required after slabs reach near the CMB for the structures to split or merge, and migrate significantly to induce the change in dominant spherical harmonic degree. As newer subduction zones become established, the flow in the deep Earth settles back towards a degree 2 structure. BMSs are swept back into two antipodal structures, though perhaps in a different location to the previous, and a new supercontinent may assemble. Previous studies have discussed supercontinent-superplume coupling (Li and Zhong, 2009; Heron, 2019; Heron et al., 2025; Wang and Li, 2020; McNamara and Zhong, 2005; Condie, 1998) in which sinking oceanic lithosphere can stir mantle flow and drive whole mantle circulation. This study contributes to this work by linking slab sinking to the stability of LLSVP-like structures at the base of the mantle, and these structures need not resemble a superplume morphology but may instead be a cluster of upwellings which form in response to slab flow, with 'superpile' morphologies being the result of both limited seismic tomography and/or the interaction of multiple plume bases. Additionally, this study suggests that the dynamics of the deep mantle are inherently coupled through time, rather than the coupling between supercontinent cycles and deep mantle being expressed as distinct 'superplume events' Li and Zhong, 2009; Condie, 1998.

4.4.1 Limitations

Since there is much debate as to the properties of LLSVPs, it is difficult to know the optimum approach by which to define these structures in mantle models. This study defines them by a combination of a thermal and Vs anomaly, which results in structures which are similar to tomography data beneath Africa, but are less similar beneath the Pacific. At least some component of this mismatch beneath the Pacific may be attributable to the way in which LLSVP-like material is defined, and therefore future work should seek to continue reconciling seismic data with geodynamic models to better understand the evolution of these structures. Additionally, this study is limited by the 1 Gyr plate motion history which reflects the breakup of Rodinia, and the assembly and dispersal of Pangaea, so around 1.5 supercontinent cycles. Whilst this period is long enough to see some cyclical pattern, this could be better constrained with a longer plate motion history.

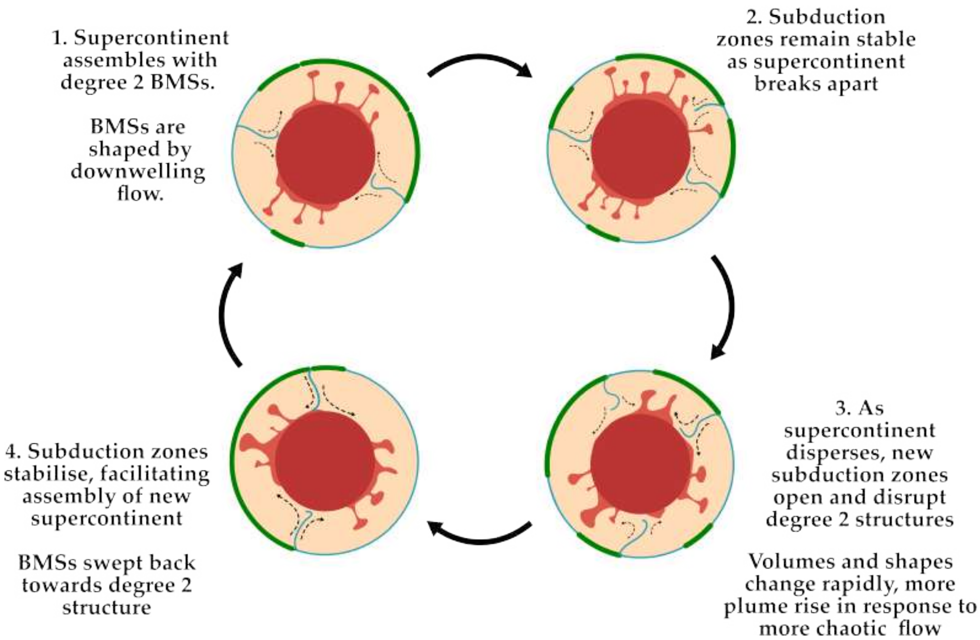

Figure 4.13 Schematic representation of the four stages of the proposed superpile cycle. Continental lithosphere is represented in green and oceanic lithosphere is represented in light blue. Dashed arrows reflects the flow associated with downwelling slabs. BMSs form piles above the CMB, with plumes ascending form their tops.

4.5 Conclusions

This study explored the stability of LLSVP-like structures in 3D mantle models in response to plate tectonics. This approach builds on previous studies to synthesise the evolution of basal mantle structures into a 'superpile cycle', comprising periods of relative stability interspersed with rapid 'rearrangement events' linked to changes in subduction dynamics at the surface. The cyclical nature of these changes in global-scale subduction dynamics are intrinsically linked to the supercontinent cycle, highlighting the coupling between the lithosphere and deep Earth on the greatest spatial and temporal scales. The size of basal mantle structures are dependent on the CMB temperature, and the potential presence of a primordial layer at the base of the mantle. Whilst CMB temperature and the presence of a primordial layer may affect the absolute stability and plume generating capacity of basal mantle structures, the timing of relative stability versus mobility is controlled from the top down.

Chapter 5

WHOLE MANTLE CIRCULATION:

The coupled evolution of mantle structures beneath an evolving supercontinent

Abstract

The relationship between the lithosphere and the mantle during the supercontinent cycle is complex and poorly constrained. The processes which drive dispersal are often simplified to two end members: slab pull and plume push. I aim to explore how lithosphere thickness and viscosity during supercontinent assembly may affect the interaction of deep mantle structures throughout the supercontinent cycle. Supercontinental lithosphere structure can be considered as one of many potential processes which may affect the evolution of upwellings and downwellings and therefore I systematically vary the properties of continental and cratonic lithosphere, respectively within these 3D spherical simulations.

The viscosity and thickness of the lithosphere alters the dip and trajectory of downwelling material beneath the supercontinent as it assembles. Focussing on Pangaea, I observe that plumes evolve and are swept beneath the centre of

the supercontinent by circum-continental subduction. The proximity of these upwelling and downwelling structures beneath the supercontinent interior varies with lithosphere thickness and viscosity. Where slabs impinge on the top of an evolving plume head (when continental and cratonic lithosphere are thick and viscous in our simulations), the cold slabs can reduce the magnitude of an evolving plume. Conversely, when the continental lithosphere is thin and weak in our simulations, slab dips shallow in the upper mantle and descend adjacent to the evolving plume, sweeping it laterally near the core-mantle boundary. These contrasting evolutions alter the magnitude of the thermal anomaly and the degree to which the plume can thin the lithosphere prior to breakup.

Declarations

Much of the work in this chapter has been published as a paper under the title "Investigating the effect of lithosphere thickness and viscosity on mantle dynamics throughout the supercontinent cycle.", Plimmer et al. (2024).

Author contributions and declarations: Abigail Plimmer is the main author of this work and undertook the numerical modelling, data processing, and analysis. Huw Davies and James Panton assisted with supervision of the manuscript and providing feedback.

5.1 Introduction

Supercontinent cycles represent one of the largest spatial and temporal processes on Earth, with each supercontinent breaking up and reassembling over hundreds of millions of years. This cycle has important implications on climatic and biological systems through time (Nance et al., 2014; Santosh, 2010) and represents the interaction of countless Earth processes. From plate tectonics to hot-spot volcanism, many of the geological features and processes that we observe today are the result of the interaction between the mantle and lithosphere through the supercontinent cycle. Despite this, the degree of feedback between these two domains remains poorly constrained, largely due to the complexity of Earth systems and the lack of accessible primary data from the mantle.

The processes which drive supercontinent breakup have long been discussed, with two end members often being the focus; subduction at the edges of the supercontinent (slab pull or slab suction; Conrad and Lithgow-Bertelloni, 2002; Conrad and Lithgow-Bertelloni, 2004) and plumes rising beneath the continental landmass to drive breakup from the interior (plume push; Zhang et al., 2018; Dang et al., 2024). The processes, and the evolution of our understanding regarding supercontinent cycles are summarized in reviews by Chen et al. (2020), Mitchell et al. (2021), and Nance et al. (2014). Previous studies have suggested a close relationship between the two end member processes (Anderson, 1982; Yoshida and Santosh, 2011; Santosh et al., 2009; Heron et al., 2015; Li and Zhong, 2009; Wolstencroft and Davies, 2017), though the degree to which upwellings and downwellings are coupled in the mantle is debated (Condie et al., 2015b; Heron and Lowman, 2011). Gurnis (1988) presented a 2D rectangle model in which a supercontinent dispersed in response to mantle flow and indicated a strong relationship between the supercontinent and long-wavelength thermal structures. Since then, numerous models have attempted to constrain the relationship between mantle structures and the lithosphere in both 2D and 3D geometries (e.g., Heron and Lowman, 2011; Heron et al., 2015; Yoshida and Santosh, 2011; Zhang et al., 2009; Phillips and Bunge, 2007; Zahirovic et al., 2015). The lithosphere is often simplified to a viscous homogeneous layer (Becker and O'Connell, 2001; Jian et al., 2022), where viscous continental 'caps' are implemented at the model surface (Phillips and Bunge, 2007; Coltice et al., 2009; Zhang et al., 2009), or models are initiated from a static, hypothetical supercontinent of uniform thickness (Yoshida, 2010; Yoshida, 2013). Zahirovic et al. (2015) showed that plate velocities are related to the proportion of continental and cratonic lithosphere, indicating the importance of such differentiation in understanding mantle driving forces. Dang et al. (2020) and Dang et al. (2024) distinguished cratonic, orogenic, and oceanic lithosphere, where each domain is assigned a thickness and yield stress within 3D spherical simulations, constrained by free-slip boundary conditions at the surface. I build upon this approach, differentiating between oceanic, continental, and cratonic lithospheres that are consistent with a published plate motion history, implemented as a boundary condition in these 3D spherical mantle circulation models.

I aim to evaluate the role of lithosphere heterogeneity throughout the supercontinent cycle. This can be broken down into four phases within the mantle; the effect of lithosphere thickness and viscosity on slab dip and sinking trajectory, proximity of slabs and plumes beneath a supercontinent interior in response to the varying slab dips, the effect of slab-plume proximity on the magnitude of upwellings beneath a supercontinent interior, and the ability of these upwellings to significantly thin the thermal lithosphere. Ultimately, I aim to investigate the way in which lithosphere structure (with varying lithosphere thicknesses and viscosities) can affect mantle dynamics throughout the supercontinent cycle from assembly towards breakup.

5.2 Methods

5.2.1 Modelling method

Modelling was once again carried out using the 3D mantle convection code, TERRA (Baumgardner, 1985; Bunge and Baumgardner, 1995; Bunge et al., 1997; Davies et al., 2013; Yang and Baumgardner, 2000). As with chapter 3, our simulations assume incompressibility (McKenzie et al., 1974) and apply the Boussinesq approximation to give the equations for conservation of mass (equation 2.6), energy (equation 2.7), and momentum (equation 2.8).

Simulations are calculated on the same grid as in previous chapters, a structured regular mesh based on an icosahedron (Baumgardner and Frederickson, 1985), with over 10 million grid points and an average radial spacing of 45 km, extending from the model Earth's surface to the core-mantle boundary (CMB) across 65 radial layers. Each simulation is analyzed from 460 Ma to present to allow for the assembly and dispersal of supercontinent Pangaea, following a conditioning period. Simulations are initiated from a randomly perturbed temperature field, with a two-layer (upper and lower mantle) viscosity structure, with no viscous lithosphere, and a free-slip boundary condition at the surface and CMB to allow this initial field to evolve and develop mantle upwellings and downwellings. At this stage, the mantle flow patterns are not spatially consistent with the plate motion reconstruction at the beginning of our investigation. Therefore we apply the plate motion reconstruction of Müller et al. (2022) as a surface boundary condition (section 2.4) , accompanied by a change to a 3-layer viscosity structure where the lithosphere is a factor of 100 more viscous than the reference viscosity (μ) down to 90 km depth, and then decreases to the reference value, before increasing to a value 30 times greater than the reference in the lower mantle. This phase of conditioning is run from 500-460 Ma, so that the mantle flow field is consistent with the plate motion history for the beginning of our circulation simulations. Given the numerical complexity of large lateral viscosity variations at the surface, I implement a greater reference viscosity than is Earth-like to maintain computational stability and so, convection is more sluggish than what we think of the present-day mantle (Rayleigh number of 10^7 in these simulations compared to $10^8 - 10^9$ for Earth). A scaling factor (section 2.4.2) is applied to the models according to the root mean square (RMS) velocity of the Earth surface at the present day and those calculated in convection simulations (equation 2.10). For these simulations $S_v = 5$.

The relevant model parameters for each of these simulations are listed in Table 5.1.

Table 5.1 Reference model parameters for suite of models investigating the affect of different lithosphere thicknesses and viscosities on mantle circulation.

Parameter	**Symbol**	**Value**	**Units**
Reference density	ρ	4500	kg m^{-3}
Gravitational acceleration	g	10	m s^{-2}
Thermal expansivity	α	2.5 x 10^{-5}	K^{-1}
Thermal diffusivity	k	9 x 10^{-6}	m^{2}s^{-1}
Specific heat capacity	C_p	1000	J K^{-1} kg^{-1}
Radiogenic heat production rate	H	4.0 x 10^{-12}	W kg^{-1}
Surface temperature	T_s	300	K
CMB temperature	T_{CMB}	3000	K
Reference viscosity	μ	1.0 x 10^{22}	Pa s
Rayleigh number	Ra	$\approx 10^7$	-

5.2.2 Identifying different lithospheric domains

GPlates software (Müller et al., 2018) is used to produce plate velocity files compatible with TERRA. Additionally, shapefiles store the geometries of continents and cratons at each time step, though oceans will be ascribed the default lithosphere parameters across each simulation, with a thickness of 90 km, approximating thermal oceanic lithospheres (Afonso et al., 2007; Doin and Fleitout, 1996; Walcott, 1970), and a viscosity which is two orders of magnitude greater than the upper mantle (Steinberger and Calderwood, 2006). Cratons and continents are considered as defined in the Müller et al. (2022) plate polygons and its constituent plate reconstruction model. A point-in-polygon algorithm is applied between the numerical grid points and the shapefiles. When a grid point falls within a continental or cratonic polygon, it is assigned a value of 1, or 2 respectively (figure 5.1). These values are appended to the GPlates velocity files which are subsequently read into TERRA to constrain the surface boundary layer in circulation models.

Viscosity is first calculated at each node within the simulation, according to the prescribed radial profile, then altered by a given factor for continental and cratonic regions. For cratons, these factors vary between 10 and 100 to reflect the highly viscous nature of stable cratonic roots (e.g., Lenardic and Moresi (1999), Pearson et al. (2021), Cooper and Conrad (2009), and Paul et al. (2019). For continents the values vary between 0.1 to 10 to reflect the debate surrounding the relative strengths of oceanic and continental lithosphere (Molnar, 1988; Pearson et al., 2021; Carlson et al., 2005). Such an implementation supports depth, temperature and/or compositionally dependent viscosity profiles.

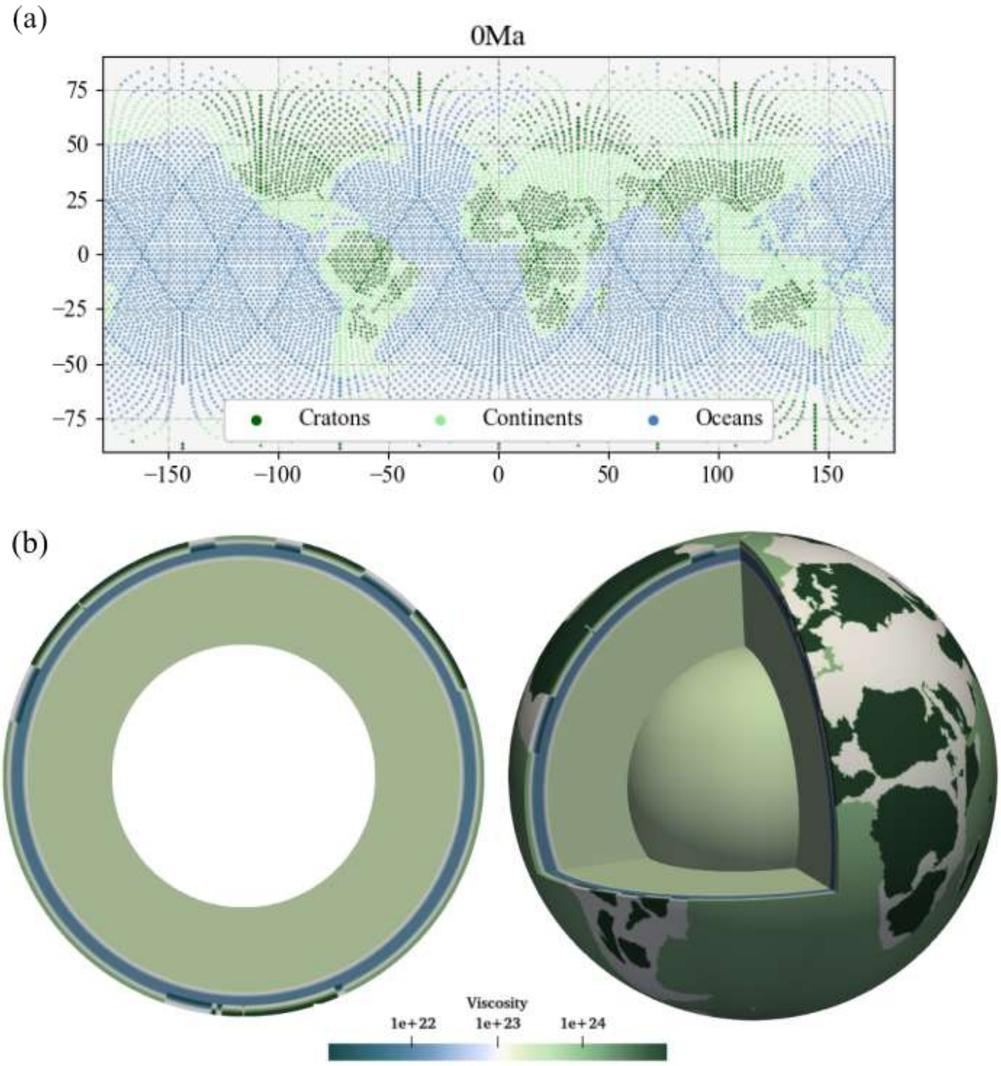

Figure 5.1 (a) Distribution of oceans, continents, and cratons when Time = 0 Ma expressed on the TERRA grid at a lower surface resolution of 240 km; (b) Example cross-section and 3D visualisation of viscosity field when oceans, continents, and cratons have thickness of 90 km, 180 km, and 270 km, respectively, and viscosity factors of 1, 0.1, and 10 times the reference, respectively at a radial resolution of 180 km.

5.2.3 Parameter space

To understand the role of different lithosphere properties, viscosity and depth of the different domains are varied from a reference case. Each simulation is initiated in line with the parameters outlined in Table 5.1. Additional parameters are systematically varied according to Table 5.2, such that each model can be compared to the reference simulation, with a homogeneous lithosphere (case000; viscosity = 1x10^{24} Pa s, thickness = 90 km).

Table 5.2 Parameter space for suite of models with varying continental and cratonic lithosphere thickness, and varying continental and cratonic lithosphere viscosity.

	Thickness (km)		**Viscosity (Pa s)**	
Model No.	Continent	Craton	Continent	Craton
000	90	90	1x10^{24}	1x10^{24}
001	90	90	1x10^{25}	1x10^{25}
002	90	90	1x10^{25}	1x10^{26}
003	90	90	1x10^{23}	1x10^{25}
004	180	180	1x10^{24}	1x10^{24}
005	180	180	1x10^{25}	1x10^{25}
006	180	180	1x10^{25}	1x10^{26}
007	180	180	1x10^{23}	1x10^{25}
008	180	270	1x10^{24}	1x10^{24}
009	180	270	1x10^{25}	1x10^{25}
010	180	270	1x10^{25}	1x10^{26}
011	180	270	1x10^{23}	1x10^{25}
000_td	90	90	2.5x10^{24}	2.5x10^{24}

In addition to the 12 simulations with depth-dependent viscosities, I also present case000_td, which is similar to the reference case except that it implements a temperature dependent viscosity according to the equation:

$$\mu = \mu_{ir} \cdot e^{(Va \cdot z' - Ea \cdot T')} \tag{5.1}$$

where μ_{ir} is the reference radial viscosity, Va is the non-dimensionalised constant for activation volume, z' is the non-dimensionalised depth (scaled by mantle depth), Ea is the non-dimensionalised constant for activation energy, and T' is the non-dimensionalised temperature (scaled by the temperature diffrence between the CMB and surface temperature). For case000_td, $Va = 1$ and $Ea = 1.5$, representing a mild temperature dependence.

To make the viscosity profile of this simulation comparable to the other simulations in the upper mantle, the reference viscosity of this simulation is increased from 1 x 10^{22}Pa s to 2.5 x 10^{22} Pa s (figure 5.2). As with model 000, the lithosphere in this simulation is 100 times more viscous than the reference viscosity.

This study focuses primarily on simulations with a depth-dependent viscosity for a number of reasons. A temperature and depth dependent viscosity structure is less numerically stable when large lateral viscosity contrasts are implemented for the lithosphere, and uses almost 6x the computational resource. I suggest that this additional time and resource would be justifiable if the results of the simulations were significantly different however, the large lateral viscosity variation implemented through the varying lithospheres have a larger impact on the dynamics of the interior than the comparatively smaller viscosity variations attributable to temperature dependence. Nonetheless case000_td, which includes the effects of mild temperature dependence of viscosity on the reference model, is also presented.

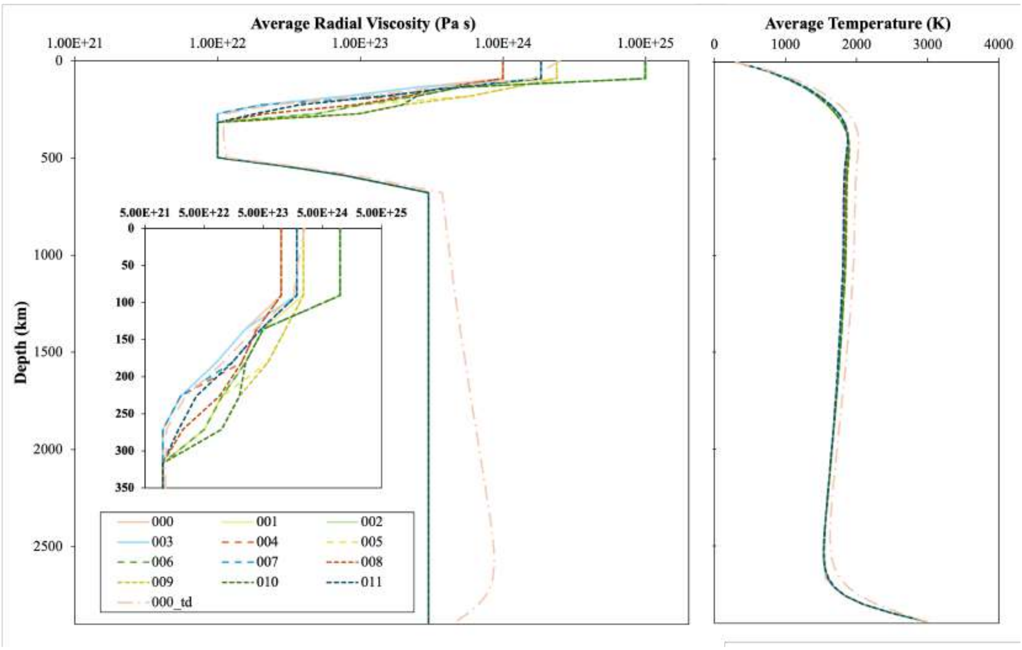

Figure 5.2 Average radial viscosity and temperature profiles at the end of each simulation. Inset: Average radial viscosity profiles, focusing on the uppermost 350 km.

5.3 Results

5.3.1 Effect of lithosphere structure on slab dip and trajectory in global 3D simulations

Pangaea formed by the collision of Laurasia and Gondwana, and the closure of the interior Rheic Ocean, therefore the results in this chapter focus on the features associated with this subduction zone (figure 5.3). Across the suite of simulations, oceanic lithosphere is dealt with in the same way, with a viscosity of 10^{24} Pa s, and a thickness of 90 km. Therefore, the differences across the models can be attributed to the thickness and viscosities of the continental and cratonic lithosphere as the supercontinent assembles.

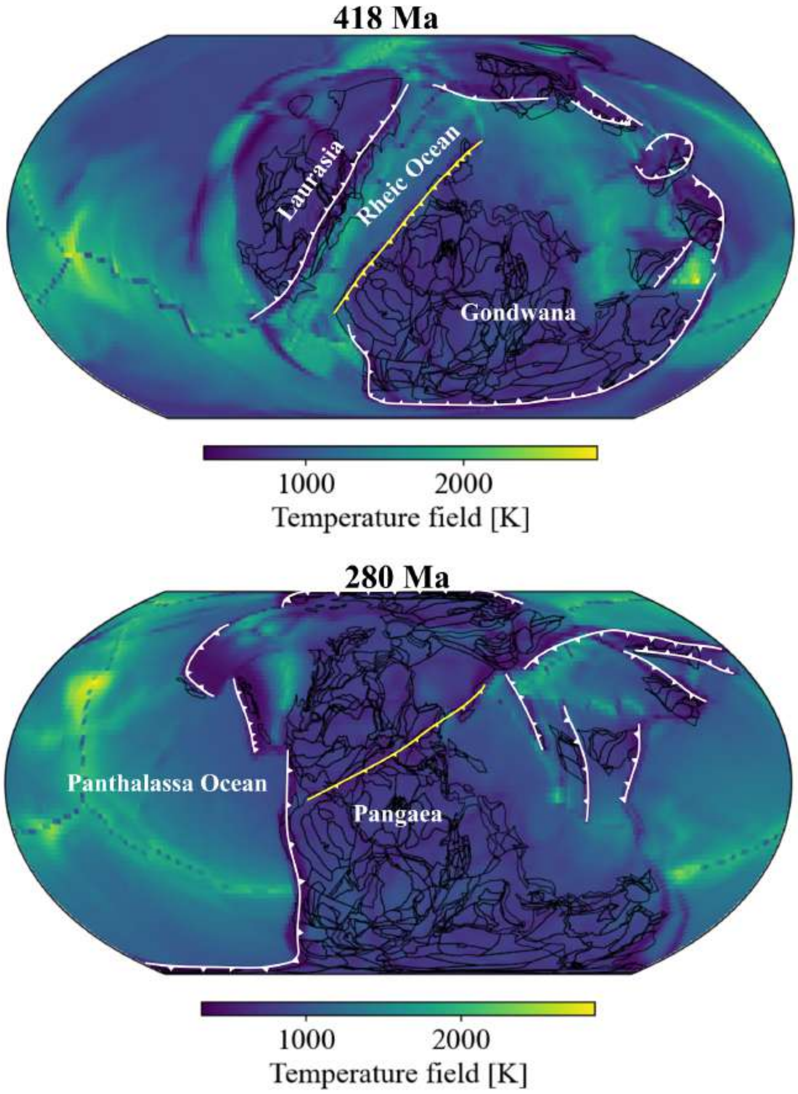

Figure 5.3 Temperature field of reference model at 415 Ma and 280 Ma, at 90 km depth. Subduction zones are shown by white lines. Subduction zone highlighted in yellow demarcates the focus of this study (Rheic suture). At 280 Ma, this subduction zone is no longer active but the associated cold temperature anomaly is visible beneath Pangaea.

In each simulation, the interior slab (which is subsequently referred to as slab A; defined by a -350 °K temperature anomaly) detaches from the lithosphere at the surface at 335 Ma. To understand the implications of lithosphere heterogeneity on slab behaviour, this study therefore focusses on the period of slab evolution prior to this time. The slabs can be grouped into 4 broad geometries, based on lateral extent at the surface, and subduction angle (figure 5.4), measured from a -500 °K temperature anomaly, to focus on the 'core' of the subducting slab and ignore the surrounding mantle cooled by the slab. Regimes α and β describe slabs with shallow, constant dips (though regime α has a shallower dip than regime β) whilst regimes γ and δ extend laterally at the surface before sinking with steeper dips (where regime δ is less coherent and extends deeper into the mantle). For cases with a lateral increase in viscosity (cases 001, 002, 005, 006, 009, 010) between the oceanic and supercontinental lithosphere (comprising continental and cratonic lithosphere) there is limited lateral trajectory of the slabs relative to cases 000, 003, 007, and 011, where there is a viscosity decrease from oceanic to continental lithosphere. Slab morphologies vary between the reference case (000) and a similar case which includes temperature dependent viscosity (000_td; figure 5.4), with the latter behaving more similarly to cases 005 and 009. This can be attributed to the similarity in average surface viscosity (figure 5.2) between these simulations, highlighting the importance of surface viscosity in determining slab dynamics in the upper mantle. This result may highlight the importance of slab rheology itself, which in reality is temperature and compositionally dependent and not considered within this suite of simulations.

The rigidity of the viscous supercontinent forces the subducting slab downwards without requiring significant lithospheric thicknesses as the velocities converge at the surface. When the supercontinent is less viscous, or as viscous as the

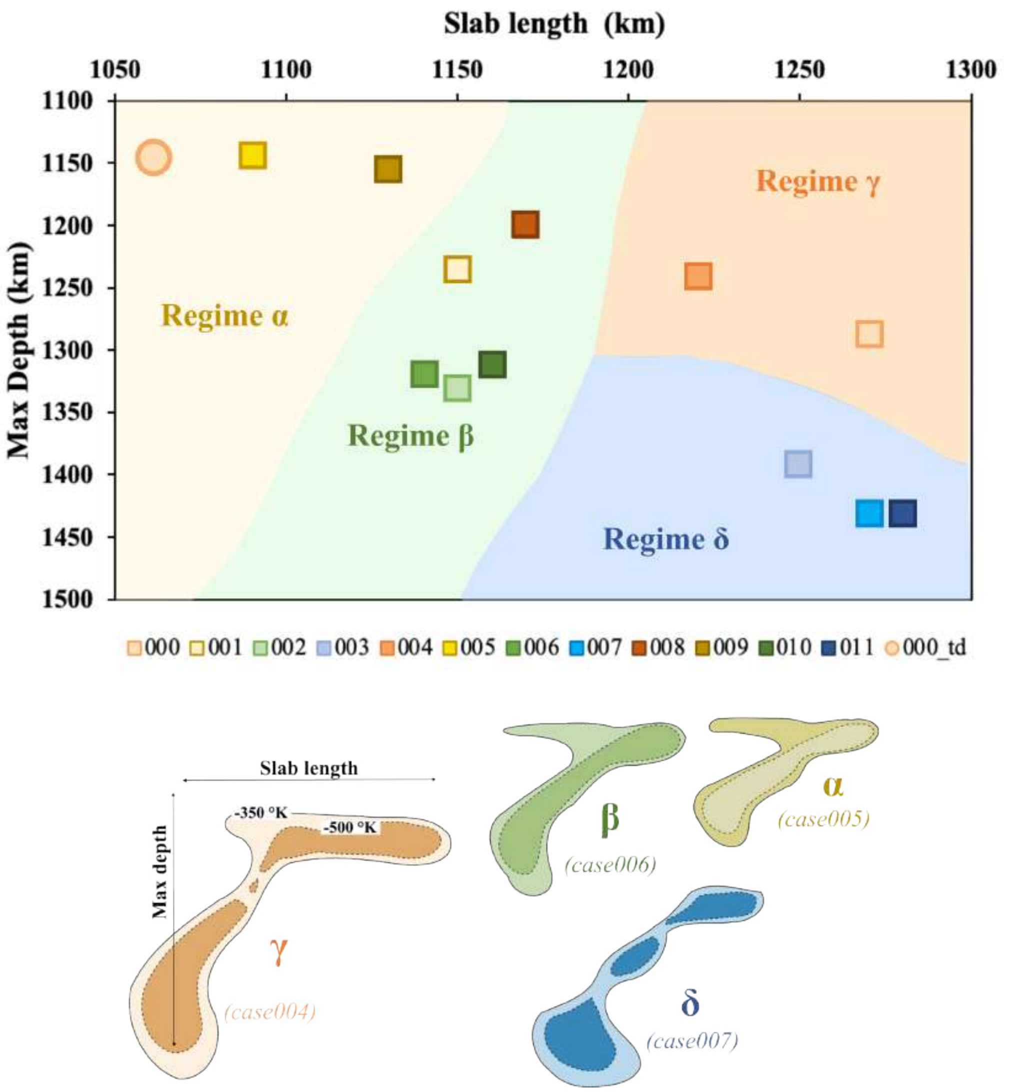

Figure 5.4 Comparison of slab length against depth for each simulation at 335 Ma, prior to slab break off, based on a temperature anomaly of -500 K. Models are grouped into 4 regimes based on slab geometry, labelled regime $\alpha, \beta, \gamma, \delta$. These correspond to slab geometries below. Solid black line marks the extent of the slab defined by a -350 K anomaly, while dashed line marks the extent defined by a -500 K anomaly as they appear in cross-section through the centre of the subduction zone.

oceanic lithosphere, the slab can instead migrate laterally until it becomes sufficiently negatively buoyant to sink further. This is especially true when the continental lithosphere is thin, in which case slab A subducts shallowly beneath the weak continent and then descends vertically as it approaches the discontinuity with the more viscous cratonic lithosphere (figure 5.5, models 000,008). When the continental and cratonic lithosphere are thicker than the oceanic lithosphere, the effect of the viscous continental lithosphere is more marked, causing the slabs to sink with a consistent, near vertical trajectory.

5.3.2 Proximity of slabs and plumes in response to varying lithosphere structure

At 280 Ma, around peak supercontinent assembly, we highlight four downwelling slabs which are similar across the simulations (figure 5.5). Each of these downwellings exhibit a different dynamic behaviour, where slab A is detached from the lithosphere at the surface, slab B extends from the surface to near the CMB, folding in the lower mantle. Slab C thickens significantly as it passes through the transition zone near 660 km depth and develops a cold plume head as it approaches cold material already residing in the lowermost mantle whilst slab D exhibits a similar cold plume head morphology without significant thickening through the transition zone, highlighting the range of dynamic behaviours. The upwellings (figure 5.5) beneath the supercontinent are labelled as i (developed beneath Laurasia), ii (developed beneath Gondwana), and iii (developed beneath Pangaea and not ubiquitous across the simulations).

Across the suite of models, there is a notable correlation between the lithosphere viscosity structure and the nature of the interaction between slab A and upwelling iii (figure 5.5). In each of the simulations, the largest continents are bound by subduction zones which sweep upwelling material towards their interior. As Pangaea formed by the collision of Laurasia and Gondwana, and the closure of the interior Rheic Ocean, slab A (attributed to the closure of the ocean) subducts directly above the evolving upwelling iii. In the viscous models (figure 5.5, models 001,002,005,006,009,010), where the cratonic and

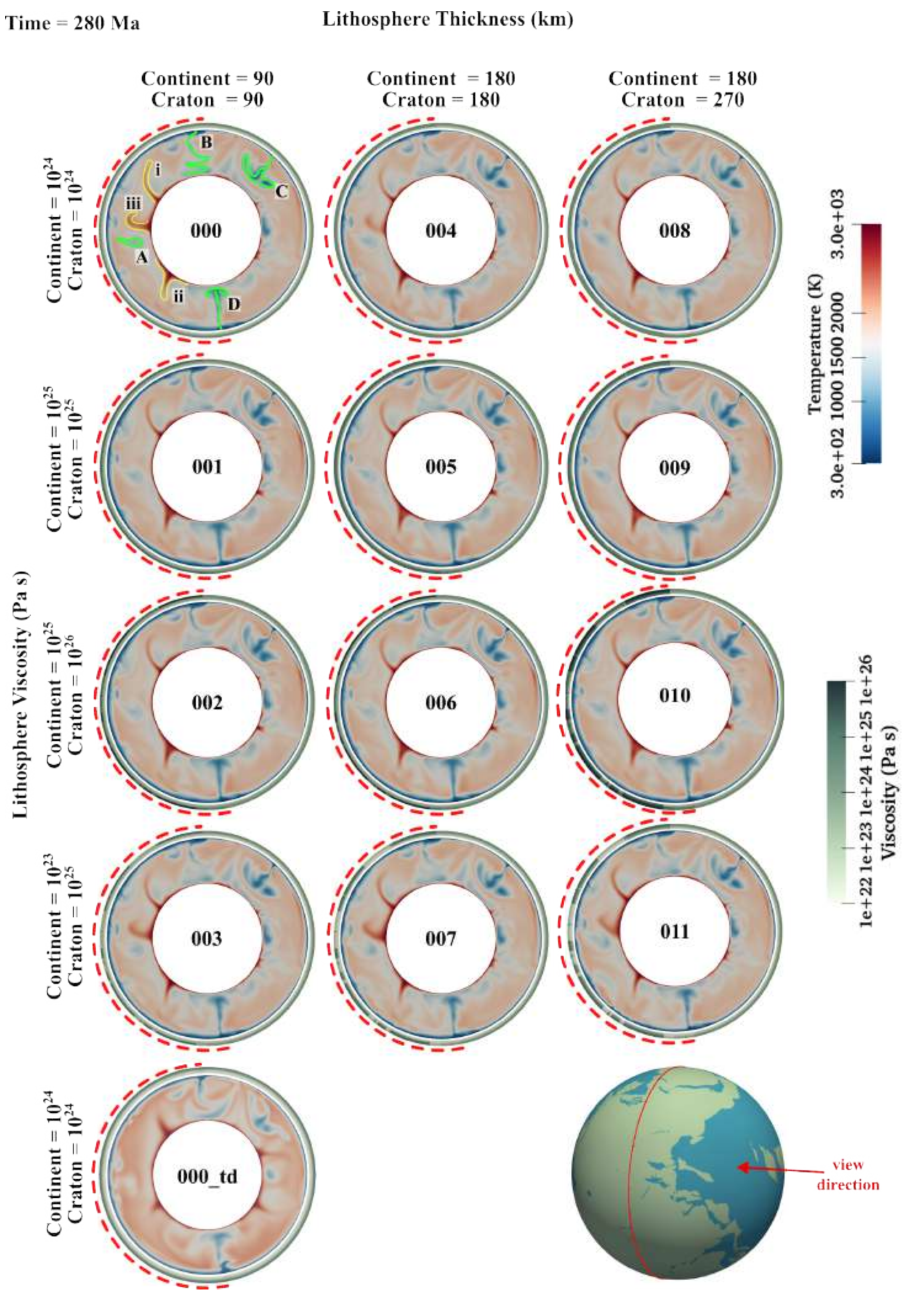

Figure 5.5 Slices through each simulation at 280 Ma showing the temperature field throughout the mantle and the viscosity structure from 0-300 km depth. Slices have been taken such that the left hemisphere comprises continental and cratonic lithosphere (dashed red line), forming the supercontinent Pangaea, and the right hemisphere represents the Tethys Ocean. For case000, green lines represent the geometry of different cold downwellings, labelled A-D. Yellow lines indicate the geometry of large upwellings (i-iii). Note upwelling iii is not present across all simulations. Below is location of cross section with viewing direction.

continental lithosphere are 1-2 orders of magnitude more viscous than the oceanic lithosphere, lateral slab migration is reduced compared to the the less viscous cases in the uppermost mantle (figure 5.4; regimes α-β), sinking directly on top of the developing upwelling, dampening out the thermal anomaly (see supplementary information for video file). Case000_td behaves similarly to other simulations classified by regime α (figure 5.4, case005, case009), given the similarity in average lithosphere viscosity (figure 5.2). Conversely, in the models with less viscous continents (figure 5.5, models 003,007,011), the slabs descend adjacent to the developing upwelling as the slab first migrates laterally in the upper mantle (figure 5.4; regimes γ-δ).

5.3.3 Evolution of upwellings in response to downwelling dynamics

Across this suite of models, large plumes develop beneath large continental landmasses. These simulations begin at 460 Ma, at which stage Laurasia and Gondwana were the two largest continents. After 40 Myr, two clusters of upwellings, interpreted as mantle plumes, which are consistent across each of the simulations. One plume cluster develops rapidly beneath Gondwana, with an antipodal cluster developing beneath the Panthalassic Ocean (figure 5.6). These plumes are mobile in the mantle, yet the clusters in the deepest mantle remain antipodal through time, such that at the present day, they reside beneath the African continent and Pacific Ocean. These clusters at present-day can be spatially correlated with the positions of Large Low Shear Velocity Provinces (LLSVPs) at the base of the mantle.

As cold downwellings descend from the surface, hot material is swept laterally near the CMB. In fact, the locations of plume development to be intrinsically linked to these downwellings. Initially, upwellings develop as broad hot regions at the CMB, but become narrow plume structures as downwelling material on

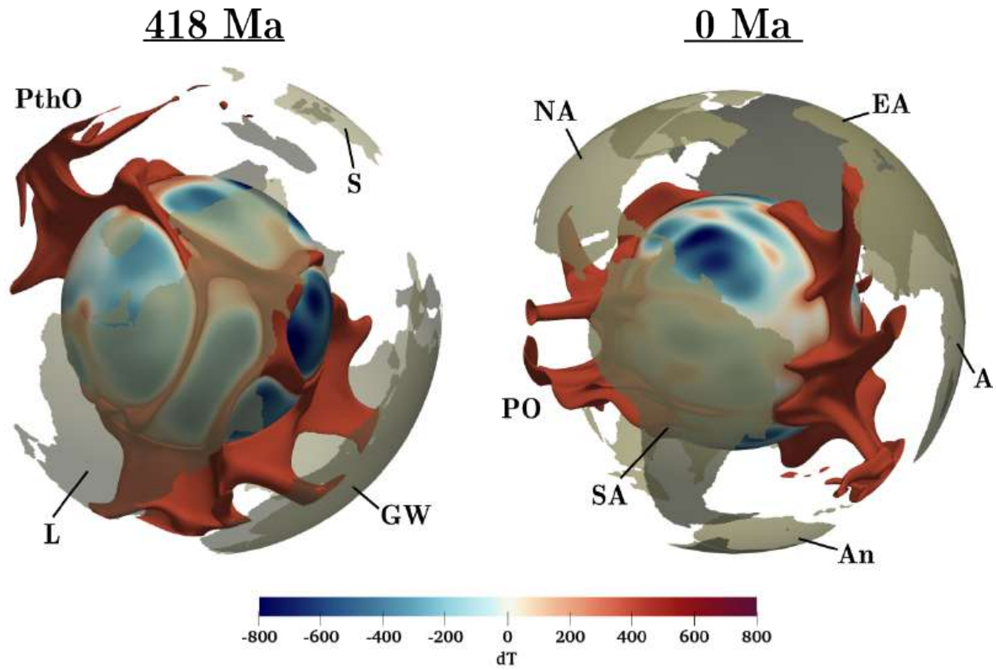

Figure 5.6 3D visualisation of reference case at 420 Ma, showing the clustering of plumes beneath Gondwana, and the antipodal Panthalassic Ocean. Same case at present day in these simulations, showing antipodal clusters beneath the Pacific Ocean and Africa. L - Laurasia; GW - Gondwana; PthO - Panthalassic Ocean; S - Siberia; NA - North America; SA - South America; EA - Eurasia; PO - Pacific Ocean; An - Antarctica; A - Africa. Paraview files available, see Open Research statement.

either side of the upwelling sweeps the hot material towards one locus (figure 5.7). Therefore, the positioning of plumes is largely determined by the clustering of hot material near the CMB induced by the return flow of slabs (also shown by Hassan et al. (2015), MacLeod et al. (2023), Davies et al. (2012)). As supercontinents form, downflow beneath circum-continental subduction zones sweeps upwellings beneath the landmass.

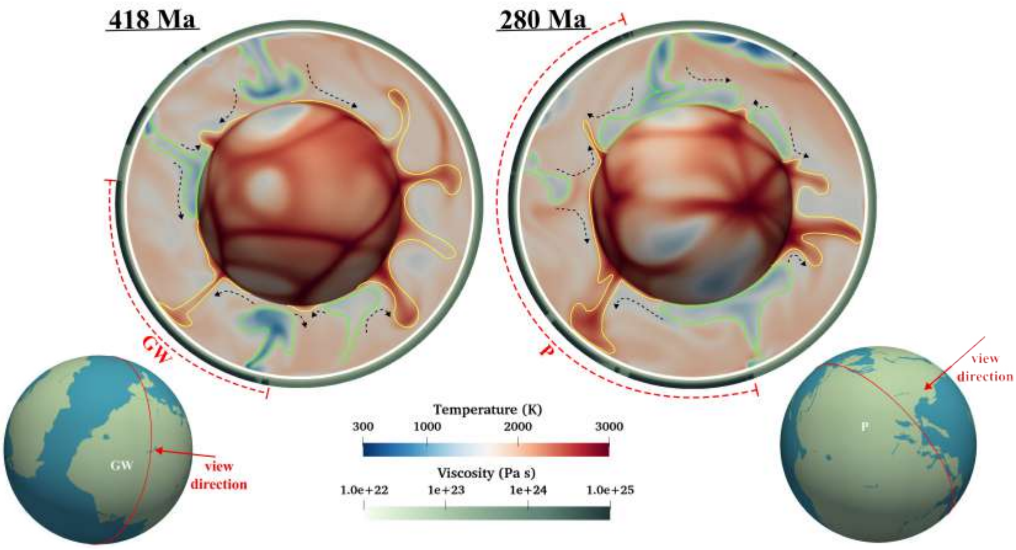

Figure 5.7 Slice through case005 at 418 Ma and 280 Ma showing the interaction between downwellings slabs and mantle upwellings. Yellow lines mark the edges of hot temperature anomalies which I interpret as plumes and green lines mark the edges of cold temperature anomalies which I interpret as slabs. Black arrows indicate the flow direction induced by the downwellings, which ultimately sweeps upwelling material together into narrow plume structures. GW - Gondwana, P - Pangaea. Globes indicate the corresponding cross section location and view direction.

These simulations show that when the plumes and downwellings develop adjacent to one another beneath the supercontinent, the upwelling material is swept towards upwelling i, which is continually swept beneath the supercontinent by slab B. These upwellings merge into a strong 'superplume' structure before 177 Ma, coeval with the breakup of the supercontinent Pangaea (figure 5.8). When the downwelling encroaches on top of the plume and reduces the magnitude of upwelling iii, upwelling i still develops into a large plume as it migrates but the magnitude is significantly smaller than in the former case. The larger superplume is sufficient to reach shallow depths and thin the thermal lithosphere whilst the extent of the smaller plume is limited and the degree of lithosphere thinning is reduced (figure 5.8). These results more broadly suggest the closely coupled nature of upwelling and downwelling processes across the supercontinent cycle and the importance of lithosphere heterogeneity in sub-continental dynamics.

5.4 Discussion

5.4.1 Following the effects of lithosphere heterogeneity throughout the supercontinent cycle

Lithosphere thickness and viscosity are two factors which can alter slab dip, and trajectory through the mantle and therefore alter the proximity of subcontinental plumes and interior slabs. The interplay between these two structures have implications for the evolution of the thermal lithosphere. Where slabs (planar structures) and plumes (cylindrical structures) interact directly, the magnitude of sub-continental upwellings are limited, whilst when slabs and plumes evolve adjacent to one another, upwellings are swept towards each other, forming larger plume structures. It can be expected that large plumes are capable of significantly thinning and weakening the lithosphere whilst smaller plumes have little effect on the thermal lithosphere. In these models, breakup will occur as

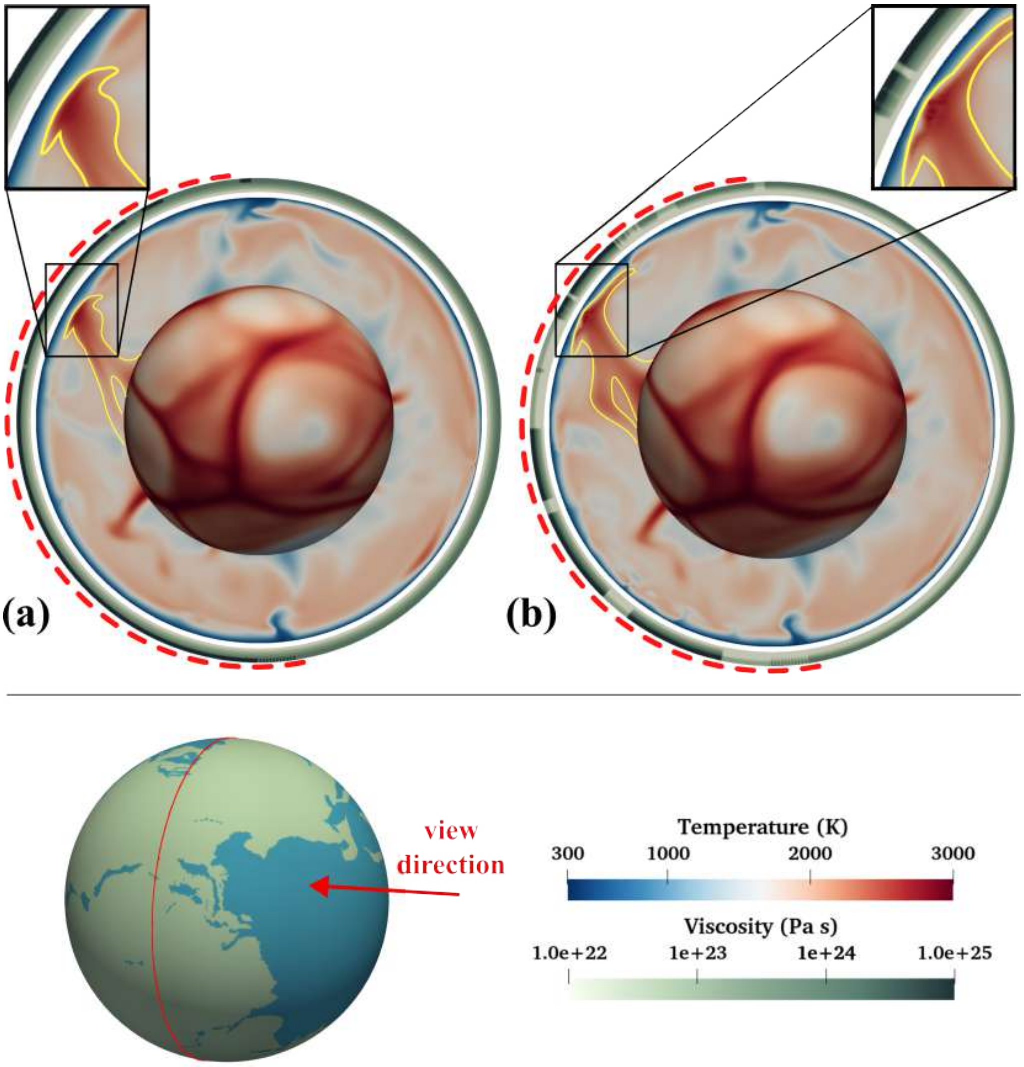

Figure 5.8 Evolution of the 'superplume' at 177 Ma for (a) case 001, where the slab descends on top of the upwelling iii and (b) case 011, where the slab descends adjacent to the upwelling and instead sweeps the material towards upwelling i. Yellow line encompasses the edge of the superplume and highlights the contrasting morphologies and extent of spreading beneath the lithosphere across the simulations. Insets highlight the thinning of the thermal lithosphere. Red dashed line reflects the location of the supercontinent. Below, globe view shows position of cross section with view direction.

dictated by the plate motion history, though increased lithosphere thinning may relate to an increased role for plume push in breaking supercontinents.

These models have demonstrated the close relationship between slabs in the mantle and plume evolution. Previous studies have shown that plumes develop beneath supercontinents (e.g. Anderson, 1982; Yoshida and Santosh, 2011; Santosh et al., 2009; Heron and Lowman, 2011; Heron et al., 2015; Li and Zhong, 2009), though Condie et al. (2015b) suggests that plume generation occurs independently of the supercontinent cycle, in response to lower mantle thermochemical dynamics. This work is consistent with that of Heron and Lowman (2011), who showed using 3D models that subcontinental plumes develop in response to subduction patterns. Any large continental landmass which is bound by subduction zones, develops subcontinental plumes as hot material is swept by descending slabs. These patterns are consistent across my models, regardless of lithosphere structure, in response to the plate motion history at the surface and the associated location of subduction zones.

Across this suite of models, young plume (upwelling iii) evolves beneath the centre of Pangaea, but the lifespan of this plume varies significantly depending on its proximity to a descending slab. Since Pangaea formed through the closure of the interior Rheic Ocean, and therefore had an interior subduction zone as Gondwana and Laurasia collided, the developing plume and subducting slab evolved contemporaneously. Therefore, plume development beneath a supercontinent may be intrinsically tied to subduction patterns (Heyn et al., 2020; Heron and Lowman, 2011; Heron et al., 2015), both in terms of plumes evolving in response to return flow from sinking slabs and, in the case of supercontinent introversion (where continents collide as an interior ocean closes; Martin et al., 2024; Santosh, 2010), possible plume dampening as the slabs and plumes come into direct contact. Since the internal dynamics of the Earth and surface rheology are not well understood, this study does not aim to determine which of these simulations is most Earth-like. Similarly, there is little geological or geophysical evidence for the deep mantle dynamics during the lifespan of Pangaea. However, many studies have shown slab-plumes interactions at various mantle depths in the present day using seismic tomography (Obrebski et al., 2010; Tan et al., 2002; Li et al., 2019a). In figure 5.6, the cluster of plumes beneath Pangaea is similar to that currently beneath Africa. Chang et al. (2020) used seismic data and geodynamic experiments to show that the present-day Afar plume may be detached from the CMB by interaction with the Tethyan slab in the deep mantle. Therefore, whilst these models cannot be used to predict the dynamics beneath Pangaea, the range of dynamics observed across these simulations have been observed in the present day.

Therefore, I propose that the structure of the lithosphere has the capacity to feed back into a mantle circulation cycle which ultimately determines the relative contribution of plume push forces in the breakup of a supercontinent. The viscosity structure of the supercontinent under which a slab subducts may alter the trajectory of the slab in the upper mantle and therefore alter the proximity of the slab and an evolving upwelling near the CMB. Furthermore, the viscosity of the surface is more important for the behaviour of slabs as they descend than the degree of temperature-dependence in mantle viscosities. Case000_td is most similar in its dynamics to cases001,005, and 009 despite the differing viscosities in the lower mantle. It is the similarity in the viscosities at the surface which determine the slab trajectory. The interaction between the interior slab and upwelling iii are also similar between these simulations (figure 5.5), highlighting that the large variations in surface viscosity are more important for the dynamics of these simulations than the smaller variations in viscosity attributable to temperature-dependence. Across these models, slabs either dampen the upwelling or sweep it towards a larger developing plume. It is then the magnitude of this large plume, and its ability to thin the lithosphere which determines the role of plume push in supercontinent breakup.

The interaction between subcontinental plumes and interior slabs will be important for any supercontinent which formed through the closure of an interior ocean (introversion). Martin et al. (2024) indicate that all previous supercontinents, except for Neoproterozoic supercontinent Rodinia, formed through introversion and therefore, the implications of slab-plume interactions on the development of a subcontinental superplume which may contribute to supercontinent breakup, are likely applicable to almost all previous supercontinents.

5.4.2 Limitations

This study is limited by the complexity of the lithosphere, and the difficulty in representing this within the models. Whilst I aim to introduce more complexity than some previous mantle circulation models, the simulations still represent an oversimplification of Earth's lithosphere, given the implementation of homogeneous continents, oceans and cratons. To simplify the computational complexity of these simulations, I consider mostly depth-dependent mantle viscosity structures, where lateral variations are applied only in the lithosphere. It is worth noting that the temperature-dependent simulation has a mild temperature dependence, and that the dynamics of the downwellings and upwellings may be different if a greater temperature dependence was applied. Whilst a temperature dependent viscosity has been shown to alter the dynamics of the reference case, the behaviour is still within the range of behaviours presented within this study, and is consistent with models with similar average lithosphere viscosities. Whilst implementing a temperature dependent viscosity may change the dynamics of an individual simulation, the results are consistent with the findings across other similar models in this study. With greater temperature dependence it may be expected that the details of these results to vary more significantly, but that is not to discount these findings as a range of possible behaviours. For this study, it is the proximity of slabs and plumes which affect the dynamics beneath the supercontinent. Therefore, whilst the dynamics of the simulations may differ under different viscosity conditions, the range of slab behaviours, and the potential for these slabs to interact with evolving plumes, remain consistent.

Additionally, when we consider the behaviour of slabs and upwellings across the whole mantle depth, the behaviour of structures across the transition zone at 660 km must also be considered. This region is solely defined as a viscosity jump in this suite of models, without considering any phase changes that exist within the mantle. Therefore, it is possible that both upwellings and downwellings may experience more significant changes in their velocities than these models demonstrate as they pass through phase changes. This may impact the details of the simulations, for example the exact timing of the interactions between upwellings and downwellings. However, mantle structures are often long-lived, on the order of 10-100s millions of years, therefore it is proximity between slabs and plumes that is likely more important for the conclusions of this study. The recent findings of Li et al. (2024) show that segmented slabs can migrate more than 1000 km along the transition zone and indicates the future simulations in this field will benefit from implementing more complex mantle rheologies than the current configuration. However, these results are not attempting to be reflective of the real Earth dynamics, but rather present a range of possible behaviours and therefore still provide insight into the possible effects of lithosphere viscosity and thickness on mantle dynamics.

5.5 Conclusions

The aim of this study was to consider the role of lithosphere heterogeneity across each phase of mantle circulation during a supercontinent cycle. This holistic approach builds on previous studies to isolate the role of lithosphere viscosity and thickness on mantle dynamics from supercontinent assembly through to breakup. Lateral viscosity and thickness variations in continental lithosphere have the ability to alter the trajectory of slabs which subduct beneath them, where viscous and thicker continental lithospheres promote steeper slab dips. This study, like others (e.g. Heron and Lowman, 2011; Heron et al., 2015; Li et al., 2003) have found that plumes develop preferentially beneath developing supercontinents as material is swept towards the interior by slabs at the edges of continents. Slabs are a significant force in shaping the morphology of upwellings structures in the lower mantle, and by extension the morphology of structures as they ascend through the mantle (figure 5.9).

The proximity between slabs and plumes have the ability to substantially alter the dynamics at the surface. Subducting slabs may dampen out the signature of evolving plumes if sinking directly above the plume head, such that the contribution of plume push to supercontinent breakup is limited. Conversely, slabs may sweep plumes towards each other where they merge and reach the base of the lithosphere with a magnitude sufficient to promote lithosphere thinning. Varying degrees of lithosphere thinning develop across these models as plumes develop heterogeneously in response to varying slab morphologies, induced by differing lithosphere properties. In this suite of simulations, thin, weak continental lithosphere descend adjacent to upwellings, sweeping them towards a larger evolving plume which in turn thin the lithosphere. This suggests that the structure of the lithosphere during supercontinent formation is one of many processes which may play a role in determining the contribution of plume push forces during the late-stage of supercontinent life.

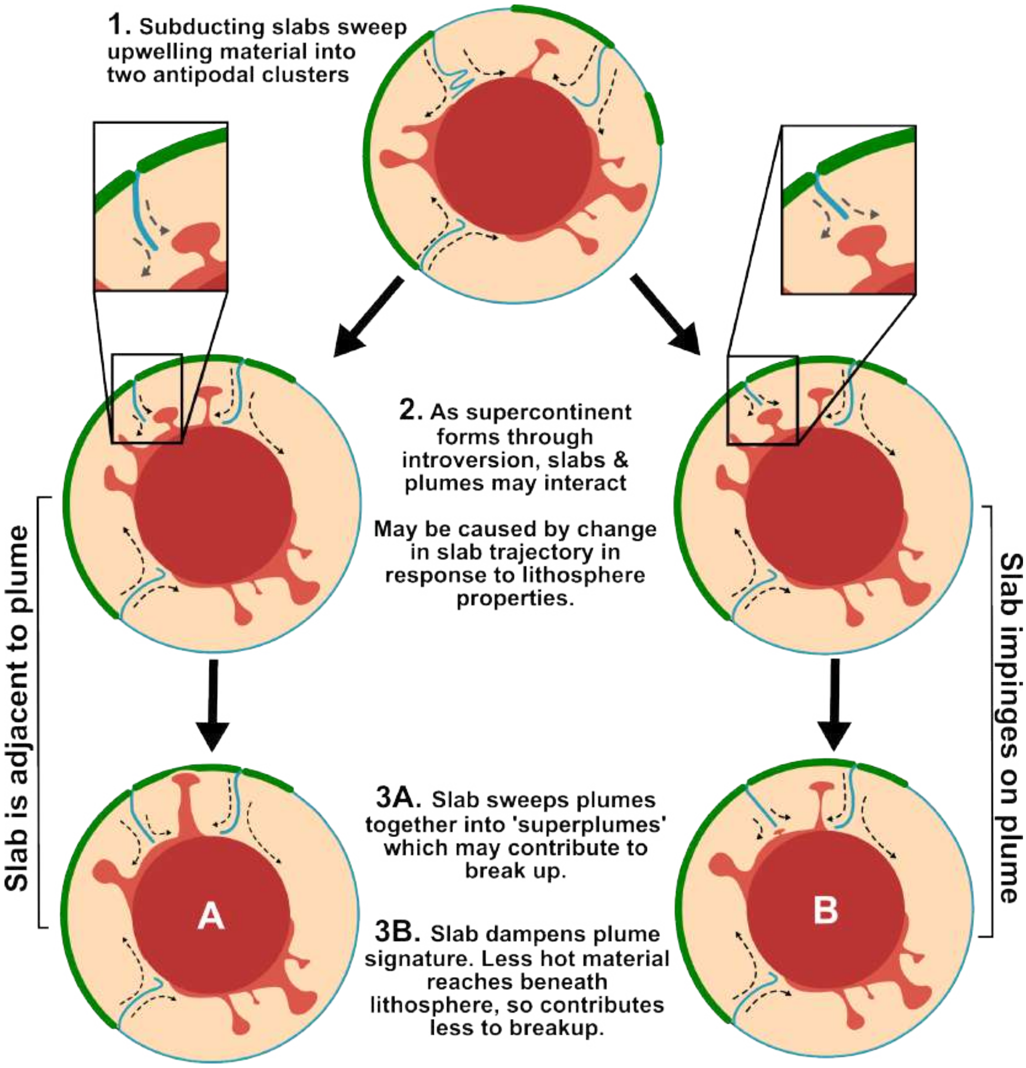

Figure 5.9 Schematic representation of the interactions of slabs and plumes during supercontinent assembly. Green lines represent continental lithosphere, blue lines represent oceanic lithosphere (and therefore also reflects slabs in the mantle), black arrows indicate the direction of flow around a slab. Across the suite of simulations, slabs are adjacent to plumes when the viscosity of continental lithosphere is as viscous, or less viscous than the oceanic lithosphere. Conversely, greater continental viscosities and lithosphere thicknesses promote vertical slabs, which impinge on plumes in these simulations.

Chapter 6

DISCUSSION

6.1 Introduction

This thesis has sought to constrain the relationship between mantle circulation and supercontinent cycles by considering the feedback between plate tectonics and downwellings, upwellings and LLSVPs in the mantle. Specifically, I sought to explore the extent to which the behaviour and velocities of slabs sinking through the mantle is dependent on plate properties, and then how these downwelling dynamics feed into the dynamics of the lowermost mantle to promote upwellings which contribute towards supercontinent breakup. These questions have been addressed using TERRA, the 3D finite element code for mantle circulation, driven by plate motion reconstructions at the surface to simulate the evolution of the Earth's interior. This discussion chapter will synthesise the findings of each research chapter to show that supercontinent cycles are, in many ways, self driven, where plate tectonics exert a first-order control on each stage of the mantle circulation cycle, which in turn feeds back towards sustaining plate motion.

6.2 Synthesis

The introduction to this thesis (chapter 1) presented a hypothetical mantle circulation cycle, which considered downwellings, deep Earth structures, and upwellings as the fundamental components of Earth's internal dynamics (figure 1.2). The subsequent research chapters in this thesis originally aimed to explore each of these processes in turn, though there is much to be learnt about each phase by integrating the work across this thesis. This synthesis summarises the findings across this body of work, to highlight the constraints on the relationship between each phase of mantle circulation and the supercontinent cycle.

6.2.1 Downwelling dynamics

Downwelling dynamics can be considered as the mantle expression of subduction, so it is no surprise that this process is closely linked to plate tectonics. Chapter 3 has shown that slab sinking is mainly controlled by the viscosity of the mantle, which is poorly understood across the literature (e.g., McKenzie, 1967; King, 1995; Hirth and Kohlstedf, 2003; Van der Meer et al., 2018; Peltier et al., 1981; Weertman and Weertman, 1975). Despite this, I have shown that slab velocities cannot be accurately predicted by Stokes' Law alone because they are driven from the surface, and highlighted plate trench length and plate velocity as two potential variables which affect slab sinking. Additionally, chapter 5 showed that the viscosity and thicknesses of continents and cratons can alter the slab dip in the upper mantle. Therefore, the evolution of downwellings are sensitive to plate tectonics through space and time. The time taken for the slabs to reach the lower mantle, and the location of the slabs as they descend are therefore closely related to the structure and dynamics of the surface, even when then slabs are simplified to cuboids (as they are in chapter 3) or distinct areas of oceanic, continental, or cratonic lithosphere (as in chapter 5). Both of these chapters have also alluded to a potential difference in the relative role of plate processes acting on the upper and lower mantle. In the upper mantle, the variations in plate trench length and plate velocity induce a greater divergence from the natural settling velocity as calculated by Stokes' Law. Similarly, weaker continental lithospheres result in shallower slab dips in the uppermost mantle, whilst in the lower mantle velocities are closer to the natural settling velocity and slabs sink more vertically. The relationship between the upper and lower mantle is therefore potentially very important to the spatial and temporal evolution of the Earth, especially as slabs have often be suggested to stagnate at, or near to, the 660 km transition zone (e.g., Fukao et al., 2001; Fukao et al., 2009; Faccenda, 2014; Li et al., 2019b; Lay, 1994; Mao and Zhong, 2018; Goes et al., 2017; Van der Meer et al., 2018; King et al., 2015; Fukao et al., 1992; Fukao and Obayashi, 2013). Whilst many of the models presented in this thesis implement a negative Clapeyron slope and an increase in viscosity at 660 km depth, few of these models show any evidence of slab stagnation. If slabs do stagnate, the residence times at the transition zone is small enough to impart little effect on the simulations, though this may be consistent with some of the proposed residence times presented in the literature of $<$ 60 Myrs (Van der Meer et al., 2018; Burkett and Gurnis, 2013; Mao and Zhong, 2018). Whilst having a more marked transition zone in these models may produce more Earth-like behaviour, in which some slabs do stagnate for significant periods, it likely does not detract from the findings of the studies in this thesis. Whilst the specific location of slabs in the deep mantle, and the time it takes for them the to reach these depths are strongly dependent on the model set up, there is still so much to learn about the coupled dynamics of plate tectonics and downwellings. Ultimately, whilst mantle viscosities are likely the dominant control on the radial velocities of slabs, especially in the lower mantle, the dynamics of the plate at the surface have the capacity to significantly alter the behaviour of the slab through the mantle and can shape the major circulation patterns in the deep Earth. The location of slabs has been consistently shown to be fundamental to shaping the structure of the lower mantle in this thesis, especially regarding the stability of LLSVP-like structures, and mantle plumes. Therefore, we explore the evolution of these structures next.

6.2.2 Basal mantle structures

Chapter 4 and chapter 5 have shown that basal mantle structures are shaped by slabs as they descend through the mantle. The location of slabs is primarily determined by the location of subduction zones at the surface, though we have shown that the mantle viscosity and the properties of the plates at the surface can affect the lateral migration of slabs through the mantle. The Earth science community has produced a significant body of work regarding the origins of LLSVPs which has also lead to more questions surrounding their stability and dynamics. Whilst this thesis has not sought to determine the origins of LLSVPs, there are some results which may contribute to the discussion. In chapter 4, I have shown that basal mantle structures do not require chemical heterogeneity or an intrinsic density difference to resemble LLSVPs in the present day, as they appear in seimsology. Therefore, I propose that LLSVPs are likely predominantly thermal since they form across all models in chapters 4 and 5, purely in response to mantle flow. These findings are consistent with many other studies (Davies et al., 2012; Davies et al., 2015; Ritsema et al., 2007; Schuberth et al., 2009), which find that LLSVP observations can be largely reconciled by thermal structures. However, we do find that these structures are larger and more pile-like with the implementation of a primordial layer at the base of the mantle (chapter 4). This is also consistent with other studies (Kreielkamp et al., 2022; Jackson et al., 2021; Ballmer et al., 2016; Zhang et al., 2016) which propose that geochemical constraints of the mantle and geochemical anomalies in ocean island basalts are best reconciled with a primitive reservoir in the deep Earth. Recently, studies have discussed the density anomaly associated with LLSVPs, with some indicating that they must be significantly denser than the ambient mantle to remain stable over long time periods (Garnero et al., 2016; Zhang et al., 2010; McNamara and Zhong, 2005; Jellinek and Manga, 2004; Lau et al., 2017; Richards et al., 2023) whilst others indicate that they are less dense (Yuan and Li, 2022; Koelemeijer et al., 2017). Our parameter space in chapter 4 did not implement a basal mantle layer which was less dense than the ambient mantle, but the model with the most dense basal layer (10% denser than the ambient mantle) forms piles which are not stable over a supercontinent cycle. Therefore whilst this thesis does not attempt to constrain the actual density of LLSVPs in the Earth, I propose that the perceived stability of LLSVPs does not necessitate a dense layer.

This thesis shows that LLSVP-like structures are not stable over supercontinent cycles, and are instead relatively stable for the duration of stable subduction girdles. Since a single supercontinent cycle is usually considered from the breakup of a supercontinent to the formation of the next, the location of major subduction girdles in the Earth are unlikely to remain stable over the course of the cycle. In chapter 4, I proposed the concept of a 'Superpile Cycle' which is closely related to the supercontinent cycle but describes the stability of LLSVP-like basal mantle structures. I showed that there is a delay between changes to subduction patterns and the migration and change in morphology of LLSVP-like structures. I discussed in that chapter that the proposed timing of that delay is dependent on the mantle structure and found, as in chapter 5, that the delay reflects the time take for slabs to reach certain depths in the mantle, where the morphology of the LLSVP-like structures react to slabs before they migrate significantly to alter the dominant spherical harmonic degree. Across the three research chapters in this thesis, we consistently show that the structure of the deep Earth is strongly dependent on the depths of slabs in the mantle, which I propose control the dominant circulation flow pattern. As such, rapid changes to the location of subduction girdles at the surface can induce a more complex field in the mantle. As new subduction zones form, and slabs descend through the mantle, there will still be slabs associated with the previous major subduction zones for a time, given that they often take between 100-300 Myrs to reach the CMB (Van der Meer et al., 2018; Butterworth et al., 2014; van der Wiel et al., 2024; Peng and Liu, 2022; Hounslow et al., 2018; Domeier et al., 2016). During these periods of more complex flow, the degree 2 structure of the deep Earth is disrupted as LLSVP-like structures are shaped by the flow from slabs across the mantle. We have referred to these periods as 'rearrangement events', which are relative short-lived. In the wider context of the supercontinent cycle, it becomes increasingly clear that the structure of the deep Earth evolves in response to downwelling dynamics. The controls on the location and timing of new subduction zones are difficult to constrain (Stern and Gerya, 2018; Stern, 2004; Yang, 2022; Lallemand and Arcay, 2021). Studies have suggested that plate motions can be partly driven by geoid perturbations, plume push forces and slab pull forces (Anderson, 1982; Phillips et al., 2009; Evans, 2003; Zhang et al., 2018; Alvarez, 1982; Chen et al., 2020; Conrad and Lithgow-Bertelloni, 2004; Forsyth and Uyeda, 1975). Geoid perturbations and plumes have both been associated with LLSVPs (Liu and Zhong, 2016; Liu and Zhong, 2015; Richards et al., 2023; Richards et al., 1988; Courtney and White, 1986), such that better understanding the stability and morphology of these structures may be a fundamental step in constraining the relationship between mantle circulation and supercontinent cycles. It may be that slabs sweep piles and promote upwellings, and the locations of the these structures then alter the plate motion directions and velocities, inducing rifting and promoting the formation of new subduction zones which then repeat the cycle.

6.2.3 Upwellings

The work in this thesis has consistently shown that plumes are a key player in mantle circulation and are sensitive to the the surrounding mantle flow, as are the LLSVP-like structures. Chapters 4 and 5 both show that broad upwellings are localised by the convergence of flows from downwelling slabs, at which point they form narrow, columnar structures and rise through the mantle. Previous studies have suggested that LLSVPs represent plume clusters or some distinct material from which plumes rise (e.g., Thompson and Tackley, 1998; Schubert et al., 2004; Davies et al., 2012; Schuberth et al., 2009; Burke et al., 2008a; Davaille and Romanowicz, 2020). This thesis hopes to contribute to this discussion by proposing that plumes and LLSVPs are formed in response to the same process, the convergence of flow associated with downwellings. Therefore, I consider that whatever the chemistry of LLSVPs, they may currently reflect a cluster of upwellings. This is further supported by the work presented in chapter 4, where I showed that during 'rearrangement events' plumes can develop away from the basal mantle structures as the flow from downwellings is more complex than a simple degree 2 structure.

As they rise through the mantle, the dynamics of plumes remain closely tied to downwelling processes. Chapter 5 showed the consequences of downwellings and upwellings which evolve in close proximity to one another. Our work is consistent with other studies (Obrebski et al., 2010; Tan et al., 2002; Li et al., 2019a) which showed slabs interacting with plumes. Most previous studies have focussed on this concept in the upper mantle, whilst this work discusses the interactions between the processes at depth. As discussed previously, the structure of the lithosphere can alter the trajectory of slabs through the mantle and therefore some of our models (chapter 5) showed a range of behaviours beneath Pangaea as it formed. I proposed supercontinents which form by introversion will originally develop upwellings beneath the major continental landmasses as circum-continental subduction girdles sweep warmer material beneath the centre of the developing supercontinent and it's antipodal ocean. As the interior ocean closes and the slab descends from beneath the centre of the assembled supercontinent, it can interact with the developing plumes. We showed that the nature of the lithosphere is one major control which may determine whether or not slabs and plumes interact, as they likely have a significant effect on the trajectory of the slab. If the slab descends directly above an evolving plume, then the plume signature is dampened out, and the magnitude of the thermal anomaly is decreased. Conversely, when slabs and plumes are very close but adjacent to one another, the plume is rapidly swept by the downwelling flow. The simulations in this thesis (chapter 5) show that when plumes are swept rapidly, they can combine with other plumes to form much larger upwellings. Larger, hotter plumes have a greater capacity to thin the lithosphere (Saunders et al., 1992; Davies, 1994; Shi et al., 2021; Moore et al., 1999; Koptev et al., 2018; Leitch et al., 1998; Issachar et al., 2024) and potentially influence the location of rifting more than smaller, narrower plumes. The models in this thesis test varying degrees of mild to moderate temperature-dependent rheologies within the mantle, and observe similar top-down influences on plume development. However, a strong temperature dependence may influence these results, and potentially result in a greater decoupling between plumes and slabs. Whilst most studies agree that plume push forces are secondary to slab pull forces in breaking apart a supercontinent and sustaining plate tectonics, it is interesting to consider how the contribution of plume push forces my vary. If plume push forces are significant to thin the lithosphere and promote rifting, then the axis of spreading may also influence the direction in which the plates move (Issachar et al., 2024; Morgan, 1972; Chen et al., 2020; Burke and Cannon, 2014; Ratcliff et al., 1998; Stotz et al., 2023). When considered alongside the potential for a geoid perturbation associated with LLSVPs (Liu and Zhong, 2016; Liu and Zhong, 2015; Richards et al., 2023; Richards et al., 1988; Courtney and White, 1986), it may be that they two forces have a greater impact on the evolution of global tectonics. Rather than slab pull and plume push being considered as end member driving mechanisms of plate tectonics, they are instead closely related, where plume dynamics are highly dependent on slab dynamics. Therefore slabs are the most fundamental process driving tectonics. Directly, downwellings slabs pull the plate towards the trench and maintain the motion whilst the passive return flow associated with the slabs forms a circulation cell which drives the plates. Indirectly, slab forces determine the location, morphology and potentially magnitude of upwellings which accelerate plate motion and potentially influence the direction of motion. Furthermore, the change in direction and velocity of plates may determine the location of future plate collisions which result in the formation of new subduction zones (Liu et al., 2022; Chertova et al., 2014; Cloetingh et al., 1989). It is at this stage that it becomes clear that the relationship between mantle circulation and supercontinent cycles are intrinsically interconnected, and are predominantly dependent on the subduction history across the previous supercontinent cycle. This concept of 'mantle memory' is not new, there have been multiple studies which have shown that the lithosphere preferentially breaks apart along areas of inherited lithospheric weakness (e.g., orogens or back-arc basins; Vauchez et al., 1997; Petersen and Schiffer, 2016; Will and Frimmel, 2018; Buiter and Torsvik, 2014), and that mantle structures can exist across supercontinent cycles. This thesis contributes to this concept by highlighting the temporal lag between the formation of new subduction zones, and significant rearrangement in the deep mantle (chapter 4), which may contribute to significant changes in plate motion which determine the assembly of the next supercontinent.

6.3 Future directions

6.3.1 An interdisciplinary approach to geodynamic problems

Whilst this thesis contributes to a large body of research surrounding mantle circulation and supercontinent coupling, it also highlights how far we have to go before we can make any claim to truly understand the dynamics of the Earth's interior. This area of research is incredibly interdisciplinary, having referred to seismological, geochemical, dynamic topography and mineral physics studies, across this thesis. Being able to reconcile these vast bodies of research and work collaboratively to better integrate geological observations, geophysical data, and geodynamic models will enable the Earth Science community to better constrain the innumerable processes acting on Earth. Specifically, geodynamic models in the future will be able to integrate dynamics of different scales, since we know that geodynamic processes range from atomic scale creep mechanisms to global scale circulation.

Better imaging of the deep Earth may go hand in hand with better constraints on the density, chemistry, and mineral physics, which in turn may facilitate a better understanding of deformation mechanisms at a range of scales. Crucially, we have shown that the viscosity of the mantle is likely the primary control on the timing of mantle circulation and the interaction of structures within the Earth's interior, yet this remains poorly constrained. The MC^2 project, which this project has been completed worked alongside, has made great strides in providing an approach by which disparate observations can be considered holistically to learn more about the dynamics of Earth. Future work should consider this approach, and build upon it, to integrate a wider range of data and work collaboratively towards advancing our knowledge.

6.3.2 Advances in numerical modelling

Some of biggest challenges presented by geodynamic modelling studies are determining the optimum modelling parameters and the trade off between numerical complexity and computing resource. For a given TERRA model, an increase in resolution of x2 may require up to four times the computational resource, and takes significantly longer to run. As such, each simulation in this thesis has been ran at a resolution of $mt = 128$, corresponding to an average resolution of 45 km, and a lateral spacing of $\sim$ 60 km at the surface. Implementing additional lithosphere complexity, (such as implementing narrow zones of deformation to represent previous orogens) would require better surface resolution, and there would be a significant trade off between the time and resource needed and the additional information we could gain from the simulation. As computers continue to advance over the coming decades, this issue is likely to become less significant, as the efficiency of the calculations improves. However, given the increased computational resource, they may still be a trade off between the resolution of scientific results and the environmental cost of running such large simulations. This is an issue that will become increasingly prevalent going forwards, and will also take significant scientific collaboration to mitigate these effects.

6.3.3 Applications to previous tectonic regimes and other planets

In the introduction to this thesis, I outlined previous supercontinents (before Pangaea) and previous tectonic regimes. Thus far, my research has primarily focussed on processes acting during the most recent supercontinent cycle, largely because of the 1 billion year plate motion reconstructions which are applied to the surface in our simulations. However, there are previous supercontinents which have existed in a pre-Wilson cycle tectonic regime. Future work should look at the evolution of mantle dynamics through time to better understand how supercontinents formed and dispersed, especially prior to subduction on Earth. Studies which seek to better understand the fundamental dynamics of our planet can also be applied to other planets. In this age of space exploration, especially given the development of missions to Venus, studies which seek to demystify the coupling between the lithosphere and mantle are due to become increasingly exciting.

Chapter 7

CONCLUSIONS

This thesis aimed to constrain the relationship between mantle circulation and supercontinent cycles by considering the interactions between the lithosphere, downwelling slabs, deep mantle structures, and upwelling plumes. The main conclusions are:

- Downwelling is likely the most fundamental process driving mantle circulation, controlling the morphology and potentially the dynamics of other structures within the mantle. As slabs sink from the surface, they sweep warmer material to form piles which then rises to form plumes where the flows converge. Whilst the dynamics of the slab may be dependent on many things, the mantle viscosity and structure of the plates at the surface are crucial to the evolutions of downwellings both in space and time. Therefore, whilst slabs are likely the primary driving force in circulation, they cannot be considered in isolation, as they are dependent on the tectonic history at the surface.

- LLSVP-like basal mantle structures and plumes are mobile in response to changing subduction girdles at the Earth's surface. As new subduction zones form and slabs begin to sink in new locations, the stability of basal mantle structures is disturbed and they rapidly rearrange, swept by the more chaotic mantle flow. During supercontinent assembly, circum-continental subduction zones sweep basal mantle structures beneath the supercontinent and the antipodal ocean. At some stage during breakup, when new subduction zones form, this degree 2 structure is disrupted until the subduction girdles restabilise and the cycle repeats.

- The interactions between slabs and plumes in the deep Earth can affect the size of the upwelling plume and the magnitude of the thermal anomaly. When plumes are larger and hotter, they have a greater ability to thin the lithosphere, which can contribute to rifting, alter plate velocities, and ultimately effect the timing and location of new subduction zones.

Considering each of these points together, I propose that mantle circulation and the supercontinent cycle are intrinsically coupled. Downwellings drive the dynamics of the deep Earth, producing upwellings which, in turn, can change the plate motion at the surface and determine where new subduction zones form. In this respect, supercontinent cycles are not just closely related to mantle circulation cycles, but are a fundamental component, relating upwellings and downwellings whilst both driving, and being driven by mantle processes.

References

Afonso, J., Ranalli, G., and Fernandez, M. (2007). Density structure and buoyancy of the oceanic lithosphere revisited. *Geophysical Research Letters* **34**.

Alvarez, W. (1982). Geological evidence for the geographical pattern of mantle return flow and the driving mechanism of plate tectonics. *Journal of Geophysical Research: Solid Earth* **87**, 6697–6710.

Anderson, D. L. (1982). Hotspots, polar wander, Mesozoic convection and the geoid. *Nature* **297**, 391–393.

Armstrong, R. L. (1981). Radiogenic isotopes: the case for crustal recycling on a near-steady-state no-continental-growth Earth. *Philosophical Transactions of the Royal Society of London. Series A, Mathematical and Physical Sciences* **301**, 443–472.

Arnould, M., Coltice, N., Flament, N., and Mallard, C. (2020). Plate tectonics and mantle controls on plume dynamics. *Earth and Planetary Science Letters* **547**, 116439.

Artemieva, I. (2011). The Lithosphere: An Interdisciplinary Approach. eng. 1st ed. Cambridge: Cambridge University Press.

Baker, M. B. and Beckett, J. R. (1999). The origin of abyssal peridotites: a reinterpretation of constraints based on primary bulk compositions. *Earth and Planetary Science Letters* **171**, 49–61.

Ballmer, M. D., Schumacher, L., Lekic, V., Thomas, C., and Ito, G. (2016). Compositional layering within the large low shear-wave velocity provinces in the lower mantle. *Geochemistry, Geophysics, Geosystems* **17**, 5056–5077.

Ballmer, M., Lekic, V., and Ito, G. (2014). "Simultaneous generation of Superpiles and Superplumes in the lower mantle". In: *AGU Fall Meeting Abstracts*. Vol. 2014, DI33B–08.

Baumgardner, J. R. (1985). Three-dimensional treatment of convective flow in the Earth's mantle. *Journal of Statistical Physics* **39**, 501–511.

Baumgardner, J. R. and Frederickson, P. O. (1985). Icosahedral discretization of the two-sphere. *SIAM Journal on Numerical Analysis* **22**, 1107–1115.

Becker, T. W., Faccenna, C., O'Connell, R. J., and Giardini, D. (1999). The development of slabs in the upper mantle: Insights from numerical and laboratory experiments. *Journal of Geophysical Research: Solid Earth* **104**, 15207–15226.

Becker, T. W. and O'Connell, R. J. (2001). Predicting plate velocities with mantle circulation models. *Geochemistry, Geophysics, Geosystems* **2**.

Bédard, J. H. (2018). Stagnant lids and mantle overturns: Implications for Archaean tectonics, magmagenesis, crustal growth, mantle evolution, and the start of plate tectonics. *Geoscience Frontiers* **9**, 19–49.

Bocher, M., Coltice, N., Fournier, A., and Tackley, P. J. (2016). A sequential data assimilation approach for the joint reconstruction of mantle convection and surface tectonics. *Geophysical Journal International* **204**, 200–214.

Boschi, L. and Dziewonski, A. M. (2000). Whole Earth tomography from delay times of P, PcP, and PKP phases: Lateral heterogeneities in the outer core or radial anisotropy in the mantle? *Journal of Geophysical Research: Solid Earth* **105**, 13675–13696.

Bottke, W. F. and Norman, M. D. (2017). The late heavy bombardment. *Annual Review of Earth and Planetary Sciences* **45**, 619–647.

Bower, D. J., Gurnis, M., and Seton, M. (2013). Lower mantle structure from paleogeographically constrained dynamic Earth models. *Geochemistry, Geophysics, Geosystems* **14**, 44–63.

Bradley, D. C. (2011). Secular trends in the geologic record and the supercontinent cycle. *Earth-Science Reviews* **108**, 16–33.

Buiter, S. J. and Torsvik, T. H. (2014). A review of Wilson Cycle plate margins: A role for mantle plumes in continental break-up along sutures? *Gondwana Research* **26**, 627–653.

Bull, A., McNamara, A., and Ritsema, J. (2009). Synthetic tomography of plume clusters and thermochemical piles. *Earth and Planetary Science Letters* **278**, 152–162.

Bunge, H.-P., Richards, M. A., Lithgow-Bertelloni, C., Baumgardner, J. R., Grand, S. P., and Romanowicz, B. A. (1998). Time scales and heterogeneous structure in geodynamic Earth models. *Science* **280**, 91–95.

Bunge, H.-P. and Baumgardner, J. R. (1995). Mantle convection modeling on parallel virtual machines. *Computers in physics* **9**, 207–215.

Bunge, H.-P., Richards, M. A., and Baumgardner, J. R. (1997). A sensitivity study of three-dimensional spherical mantle convection at 108 Rayleigh number: Effects of depth-dependent viscosity, heating mode, and an endothermic phase change. *Journal of Geophysical Research: Solid Earth* **102**, 11991–12007.

Burke, K. (2011). Plate Tectonics, the Wilson Cycle, and Mantle Plumes: Geodynamics from the Top. *Annual Review of Earth and Planetary Sciences* **39**, 1–29.

Burke, K. and Cannon, J. M. (2014). Plume–plate interaction. *Canadian Journal of Earth Sciences* **51**, 208–221.

Burke, K., Steinberger, B., Torsvik, T. H., and Smethurst, M. A. (2008a). Plume generation zones at the margins of large low shear velocity provinces on the core-mantle boundary. *Earth and Planetary Science Letters* **265**, 49–60.

– (2008b). Plume Generation Zones at the margins of Large Low Shear Velocity Provinces on the core–mantle boundary. *Earth and Planetary Science Letters* **265**, 49–60.

Burkett, E. and Gurnis, M. (2013). Stalled slab dynamics. *Lithosphere* **5**, 92–97.

Butterworth, N., Talsma, A., Müller, R., Seton, M., Bunge, H.-P., Schuberth, B., Shephard, G., and Heine, C. (2014). Geological, tomographic, kinematic and geodynamic constraints on the dynamics of sinking slabs. *Journal of Geodynamics* **73**, 1–13.

Campbell, I. and Hill, R. (1988). A two-stage model for the formation of the granite-greenstone terrains of the Kalgoorlie-Norseman area, Western Australia. *Earth and Planetary Science Letters* **90**, 11–25.

Cao, X., Flament, N., Bodur, Ö. F., and Müller, R. D. (2021a). The evolution of basal mantle structure in response to supercontinent aggregation and dispersal. *Scientific Reports* **11**, 22967.

Cao, X., Flament, N., and Müller, R. D. (2021b). Coupled Evolution of Plate Tectonics and Basal Mantle Structure. *Geochemistry, Geophysics, Geosystems* **22**, e2020GC009244.

Carlson, R. W., Pearson, D. G., and James, D. E. (2005). Physical, chemical, and chronological characteristics of continental mantle. *Reviews of Geophysics* **43**.

Chang, S.-J., Kendall, E., Davaille, A., and Ferreira, A. M. (2020). The evolution of mantle plumes in East Africa. *Journal of Geophysical Research: Solid Earth* **125**, e2020JB019929.

Chen, L., Wang, X., Liang, X., Wan, B., and Liu, L. (2020). Subduction tectonics vs. Plume tectonics—Discussion on driving forces for plate motion. *Science China Earth Sciences* **63**, 315–328.

Chertova, M., Spakman, W., Van den Berg, A., and Van Hinsbergen, D. (2014). Absolute plate motions and regional subduction evolution. *Geochemistry, Geophysics, Geosystems* **15**, 3780–3792.

Cloetingh, S., Wortel, R., and Vlaar, N. J. (1989). "On the Initiation of Subduction Zones". In: *Subduction Zones Part II.* Ed. by L. J. Ruff and H. Kanamori. Basel: Birkhäuser Basel, 7–25.

Collins, W. (2003). Slab pull, mantle convection, and Pangaean assembly and dispersal. *Earth and Planetary Science Letters* **205**, 225–237.

Coltice, N., Bertrand, H., Rey, P., Jourdan, F., Phillips, B. R., and Ricard, Y. (2009). Global warming of the mantle beneath continents back to the Archaean. *Gondwana Research* **15**, 254–266.

Coltice, N. and Shephard, G. E. (2018). Tectonic predictions with mantle convection models. *Geophysical Journal International* **213**, 16–29.

Condie, K., Pisarevsky, S. A., Korenaga, J., and Gardoll, S. (2015a). Is the rate of supercontinent assembly changing with time? *Precambrian Research* **259**, 278–289.

Condie, K. C. (1998). Episodic continental growth and supercontinents: a mantle avalanche connection? *Earth and Planetary Science Letters* **163**, 97–108.

Condie, K. C. (2002). The supercontinent cycle: are there two patterns of cyclicity? *Journal of African Earth Sciences* **35**, 179–183.
Condie, K. C. and Aster, R. C. (2010). Episodic zircon age spectra of orogenic granitoids: the supercontinent connection and continental growth. *Precambrian Research* **180**, 227–236.
Condie, K. C., Davaille, A., Aster, R. C., and Arndt, N. (2015b). Upstairs-downstairs: supercontinents and large igneous provinces, are they related? *International Geology Review* **57**, 1341–1348.
Connolly, J. A. D. (2009). The geodynamic equation of state: What and how. *Geochemistry, Geophysics, Geosystems* **10**.
Conrad, C. P. and Lithgow-Bertelloni, C. (2002). How mantle slabs drive plate tectonics. *Science* **298**, 207–209.
– (2004). The temporal evolution of plate driving forces: Importance of "slab suction" versus "slab pull" during the Cenozoic. *Journal of Geophysical Research: Solid Earth* **109**.
Conrad, C. P., Steinberger, B., and Torsvik, T. H. (2013). Stability of active mantle upwelling revealed by net characteristics of plate tectonics. *Nature* **498**, 479–482.
Cooper, C. and Conrad, C. P. (2009). Does the mantle control the maximum thickness of cratons? *Lithosphere* **1**, 67–72.
Courtney, R. C. and White, R. S. (1986). Anomalous heat flow and geoid across the Cape Verde Rise: evidence for dynamic support from a thermal plume in the mantle. *Geophysical Journal International* **87**, 815–867.
Creager, K. C. and Jordan, T. H. (1986). Aspherical structure of the core-mantle boundary from PKP travel times. *Geophysical Research Letters* **13**, 1497–1500.
Dal Zilio, L., Faccenda, M., and Capitanio, F. (2018). The role of deep subduction in supercontinent breakup. *Tectonophysics* **746**, 312–324.
Dang, Z., Zhang, N., Li, Z.-X., Huang, C., Spencer, and Liu, Y. (Nov. 2020). Weak orogenic lithosphere guides the pattern of plume-triggered supercontinent break-up. *Communications Earth & Environment*.
Dang, Z., Zhang, N., Li, Z.-X., and Yan, P. (2024). Pangea's breakup: The roles of mantle plumes, orogens, and subduction retreat. *Geological Society, London, Special Publications* **542**, SP542–2022.
Davaille, A. and Romanowicz, B. (2020). Deflating the LLSVPs: Bundles of Mantle Thermochemical Plumes Rather Than Thick Stagnant "Piles". *Tectonics* **39**, e2020TC006265.
Davies, D. R., Goes, S., and Lau, H. C. P. (2015). Thermally Dominated Deep Mantle LLSVPs: A Review. In: *The Earth's Heterogeneous Mantle: A Geophysical, Geodynamical, and Geochemical Perspective*. Ed. by A. Khan and F. Deschamps. Springer International Publishing, 441–477.
Davies, D. R., Goes, S., Davies, J., Schuberth, B., Bunge, H.-P., and Ritsema, J. (2012). Reconciling dynamic and seismic models of Earth's lower mantle: The dominant role of thermal heterogeneity. *Earth and Planetary Science Letters* **353-354**, 253–269.

Davies, D. R., Davies, J. H., Bollada, P. C., Hassan, O., Morgan, K., and Nithiarasu, P. (2013). A hierarchical mesh refinement technique for global 3-D spherical mantle convection modelling. *Geoscientific Model Development* **6**, 1095–1107.

Davies, G. F. (1977). Whole-mantle convection and plate tectonics. *Geophysical Journal International* **49**, 459–486.

– (1994). Thermomechanical erosion of the lithosphere by mantle plumes. *Journal of Geophysical Research: Solid Earth* **99**, 15709–15722.

– (2022). "Perspective; Imperfect but Better Than Shouting". In: *Stories from the Deep Earth: How Scientists Figured Out What Drives Tectonic Plates and Mountain Building.* Cham: Springer International Publishing, 193–200.

Dhuime, B., Hawkesworth, C. J., Cawood, P. A., and Storey, C. D. (2012). A change in the geodynamics of continental growth 3 billion years ago. *Science* **335**, 1334–1336.

Dhuime, B., Hawkesworth, C. J., Delavault, H., and Cawood, P. A. (2017). Continental growth seen through the sedimentary record. *Sedimentary Geology* **357**, 16–32.

Doin, M. and Fleitout, L. (1996). Thermal evolution of the oceanic lithosphere: an alternative view. *Earth and Planetary Science Letters* **142**, 121–136.

Domeier, M., Doubrovine, P. V., Torsvik, T. H., Spakman, W., and Bull, A. L. (2016). Global correlation of lower mantle structure and past subduction. *Geophysical Research Letters* **43**, 4945–4953.

Doucet, L. S., Li, Z.-X., Ernst, R. E., Kirscher, U., El Dien, H. G., and Mitchell, R. N. (2020). Coupled supercontinent–mantle plume events evidenced by oceanic plume record. *Geology* **48**, 159–163.

Duarte, J. C., Schellart, W. P., and Rosas, F. M. (2018). The future of Earth's oceans: consequences of subduction initiation in the Atlantic and implications for supercontinent formation. *Geological Magazine* **155**, 45–58.

Duarte, J. C., Riel, N., Rosas, F. M., Popov, A., Schuler, C., and Kaus, B. J. (2024). Gibraltar subduction zone is invading the Atlantic. *Geology* **52**, 331–335.

Duarte, J. C., Rosas, F. M., Terrinha, P., Schellart, W. P., Boutelier, D., Gutscher, M.-A., and Ribeiro, A. (2013). Are subduction zones invading the Atlantic? Evidence from the southwest Iberia margin. *Geology* **41**, 839–842.

Dziewonski, A. M., Hager, B. H., and O'Connell, R. J. (1977). Large-scale heterogeneities in the lower mantle. *Journal of Geophysical Research (1896-1977)* **82**, 239–255.

Elkins-Tanton, L. (2008). Linked magma ocean solidification and atmospheric growth for Earth and Mars. *Earth and Planetary Science Letters* **271**, 181–191.

Elming, S.-Å., Salminen, J., and Pesonen, L. J. (2021). Chapter 16 - Paleo-Mesoproterozoic Nuna supercycle. eng. In: *Ancient Supercontinents and the Paleogeography of Earth.* Elsevier Inc, 499–548.

Ernst, W. (2009). Archean plate tectonics, rise of Proterozoic supercontinentality and onset of regional, episodic stagnant-lid behavior. *Gondwana Research* **15**, 243–253.

– (2017). Earth's thermal evolution, mantle convection, and Hadean onset of plate tectonics. *Journal of Asian Earth Sciences* **145**, 334–348.

Evans, D. A. (2003). True polar wander and supercontinents. *Tectonophysics* **362**, 303–320.

– (2013). Reconstructing pre-Pangean supercontinents. *Bulletin* **125**, 1735–1751.

Evans, D. A. and Mitchell, R. N. (2011). Assembly and breakup of the core of Paleoproterozoic–Mesoproterozoic supercontinent Nuna. *Geology* **39**, 443–446.

Evans, M. E. and Muxworthy, A. R. (2019). Vaalbara palaeomagnetism. *Canadian Journal of Earth Sciences* **56**, 912–916.

Faccenda, M. (2014). Water in the slab: A trilogy. *Tectonophysics* **614**, 1–30.

Flament, N., Bodur, Ö. F., Williams, S. E., and Merdith, A. S. (2022). Assembly of the basal mantle structure beneath Africa. *Nature* **603**, 846–851.

Forsyth, D. and Uyeda, S. (1975). On the relative importance of the driving forces of plate motion. *Geophysical Journal International* **43**, 163–200.

Fossen, H., Khani, H. F., Faleide, J. I., Ksienzyk, A. K., and Dunlap, W. J. (2017). Post-Caledonian extension in the West Norway–northern North Sea region: the role of structural inheritance. *Geological Society, London, Special Publications* **439**, 465–486.

Fukao, Y. and Obayashi, M. (2013). Subducted slabs stagnant above, penetrating through, and trapped below the 660 km discontinuity. *Journal of Geophysical Research: Solid Earth* **118**, 5920–5938.

Fukao, Y., Obayashi, M., Inoue, H., and Nenbai, M. (1992). Subducting slabs stagnant in the mantle transition zone. *Journal of Geophysical Research: Solid Earth* **97**, 4809–4822.

Fukao, Y., Obayashi, M., Nakakuki, T., and Deep Slab Project Group, the (2009). Stagnant Slab: A Review. *Annual Review of Earth and Planetary Sciences* **37**, 19–46.

Fukao, Y., Widiyantoro, S., and Obayashi, M. (2001). Stagnant slabs in the upper and lower mantle transition region. *Reviews of Geophysics* **39**, 291–323.

Gamal El Dien, H., Doucet, L. S., Li, Z.-X., Cox, G., and Mitchell, R. (2019). Global geochemical fingerprinting of plume intensity suggests coupling with the supercontinent cycle. *Nature Communications* **10**, 5270.

Ganerød, M., Smethurst, M., Torsvik, T., Prestvik, T., Rousse, S., McKenna, C., Van Hinsbergen, D., and Hendriks, B. (2010). The North Atlantic Igneous Province reconstructed and its relation to the plume generation zone: the Antrim Lava Group revisited. *Geophysical Journal International* **182**, 183–202.

Ganerød, M., Torsvik, T. H., Van Hinsbergen, D., Gaina, C., Corfu, F., Werner, S., Owen-Smith, T., Ashwal, L., Webb, S., and Hendriks, B. (2011). Palaeoposition of the Seychelles microcontinent in relation to the Deccan Traps and the

Plume Generation Zone in Late Cretaceous-Early Palaeogene time. *Geological Society, London, Special Publications* **357**, 229–252.

Gardiner, N., Mulder, J., Kirkland, C., Johnson, T., and Nebel, O. (2021). Palaeoarchaean TTGs of the Pilbara and Kaapvaal cratons compared; an early Vaalbara supercraton evaluated. *South African Journal of Geology 2021* **124**, 37–52.

Garnero, E. J. and McNamara, A. K. (2008). Structure and dynamics of Earth's lower mantle. *science* **320**, 626–628.

Garnero, E. J., McNamara, A. K., and Shim, S.-H. (2016). Continent-sized anomalous zones with low seismic velocity at the base of Earth's mantle. *Nature Geoscience* **9**, 481–489.

Gassmöller, R., Dannberg, J., Bangerth, W., Heister, T., and Myhill, R. (2020). On formulations of compressible mantle convection. *Geophysical Journal International* **221**, 1264–1280.

Goes, S., Agrusta, R., Hunen, J. van, and Garel, F. (2017). Subduction-transition zone interaction: A review. *Geosphere* **13**, 644–664.

Goes, S., Cammarano, F., and Hansen, U. (2004). Synthetic seismic signature of thermal mantle plumes. *Earth and Planetary Science Letters* **218**, 403–419.

Goodwin, A. M. (1996). Principles of Precambrian geology. eng. London ; Academic Press.

Griffiths, R. and Turner, J. (1988). Viscous entrainment by sinking plumes. *Earth and planetary science letters* **90**, 467–477.

Gurnis, M. (1988). Large-scale mantle convection and the aggregation and dispersal of supercontinents. *Nature* **332**, 695–699.

Gutscher, M.-A., Dominguez, S., Westbrook, G. K., Le Roy, P., Rosas, F., Duarte, J. C., Terrinha, P., Miranda, J., Graindorge, D., Gailler, A., et al. (2012). The Gibraltar subduction: A decade of new geophysical data. *Tectonophysics* **574**, 72–91.

Hager, B. H., Clayton, R. W., Richards, M. A., Comer, R. P., and Dziewonski, A. M. (1985). Lower mantle heterogeneity, dynamic topography and the geoid. *Nature* **313**, 541–545.

Hamano, K., Abe, Y., and Genda, H. (2013). Emergence of two types of terrestrial planet on solidification of magma ocean. *Nature* **497**, 607–610.

Hassan, R., Flament, N., Gurnis, M., Bower, D. J., and Müller, D. (2015). Provenance of plumes in global convection models. *Geochemistry, Geophysics, Geosystems* **16**, 1465–1489.

Hawkesworth, C., Cawood, P. A., and Dhuime, B. (2019). Rates of generation and growth of the continental crust. *Geoscience Frontiers* **10**, 165–173.

Helffrich, G. (2000). Topography of the transition zone seismic discontinuities. *Reviews of Geophysics* **38**, 141–158.

Heron, P. J. (2019). Mantle plumes and mantle dynamics in the Wilson cycle. *Geological Society, London, Special Publications* **470**, 87–103.

Heron, P. J. and Lowman, J. P. (2011). The effects of supercontinent size and thermal insulation on the formation of mantle plumes. *Tectonophysics* **510**, 28–38.

Heron, P. J., Lowman, J. P., and Stein, C. (2015). Influences on the positioning of mantle plumes following supercontinent formation. *Journal of Geophysical Research: Solid Earth* **120**, 3628–3648.

Heron, P. J., Dannberg, J., Gassmöller, R., Shephard, G. E., van Hunen, J., and Pysklywec, R. N. (2025). The impact of Pangean subducted oceans on mantle dynamics: Passive piles and the positioning of deep mantle plumes. *Gondwana Research* **138**, 168–185.

Heyn, B. H., Conrad, C. P., and Trønnes, R. G. (2020). How thermochemical piles can (periodically) generate plumes at their edges. *Journal of Geophysical Research: Solid Earth* **125**, e2019JB018726.

Hirth, G. and Kohlstedf, D. (2003). Rheology of the upper mantle and the mantle wedge: A view from the experimentalists. *Geophysical monograph-american geophysical union* **138**, 83–106.

Hoffman, P. F. (1991). Did the breakout of Laurentia turn Gondwanaland inside-out? *Science* **252**, 1409–1412.

Hounslow, M. W., Domeier, M., and Biggin, A. J. (2018). Subduction flux modulates the geomagnetic polarity reversal rate. *Tectonophysics* **742**, 34–49.

Huang, C., Leng, W., and Wu, Z. (2015). Iron-spin transition controls structure and stability of LLSVPs in the lower mantle. *Earth and Planetary Science Letters* **423**, 173–181.

– (2020). The Continually Stable Subduction, Iron-Spin Transition, and the Formation of LLSVPs From Subducted Oceanic Crust. *Journal of Geophysical Research: Solid Earth* **125**, e2019JB018262.

Issachar, R., Haas, P., Augustin, N., and Ebbing, J. (2024). Rift and plume: a discussion on active and passive rifting mechanisms in the Afro-Arabian rift based on synthesis of geophysical data. *Solid Earth* **15**, 807–826.

Iwamori, H. and Nakamura, H. (2015). Isotopic heterogeneity of oceanic, arc and continental basalts and its implications for mantle dynamics. *Gondwana Research* **27**, 1131–1152.

Jackson, M. G., Becker, T. W., and Steinberger, B. (2021). Spatial Characteristics of Recycled and Primordial Reservoirs in the Deep Mantle. *Geochemistry, Geophysics, Geosystems* **22**, e2020GC009525.

Jadamec, M. A. and Billen, M. I. (2010). Reconciling surface plate motions with rapid three-dimensional mantle flow around a slab edge. *Nature* **465**, 338–341.

Jellinek, A. M. and Manga, M. (2004). Links between long-lived hot spots, mantle plumes, D", and plate tectonics. *Reviews of Geophysics* **42**.

Jian, D., Williams, S. E., Yu, S., and Zhao, G. (2022). Quantifying the Link Between the Detrital Zircon Record and Tectonic Settings. *Journal of Geophysical Research: Solid Earth* **127**, e2022JB024606.

Kameyama, M. and Harada, A. (2017). Supercontinent cycle and thermochemical structure in the mantle: inference from two-dimensional numerical simulations of mantle convection. *Geosciences* **7**, 126.

Kankanamge, D. G. and Moore, W. B. (2016). Heat transport in the Hadean mantle: From heat pipes to plates. *Geophysical Research Letters* **43**, 3208–3214.

King, S. D. (1995). The viscosity structure of the mantle. *Reviews of Geophysics* **33**, 11–17.

King, S. D., Frost, D. J., and Rubie, D. C. (2015). Why cold slabs stagnate in the transition zone. *Geology* **43**, 231–234.

Koelemeijer, P. J., Deuss, A., and Trampert, J. (July 2012). Normal mode sensitivity to Earth's D" layer and topography on the core-mantle boundary: what we can and cannot see. *Geophysical Journal International* **190**, 553–568.

Koelemeijer, P., Deuss, A., and Ritsema, J. (2017). Density structure of Earth's lowermost mantle from Stoneley mode splitting observations. *Nature Communications* **8**, 15241.

Koptev, A., Burov, E., Gerya, T., Le Pourhiet, L., Leroy, S., Calais, E., and Jolivet, L. (2018). Plume-induced continental rifting and break-up in ultra-slow extension context: Insights from 3D numerical modeling. *Tectonophysics* **746**, 121–137.

Kreielkamp, P., Stein, C., and Hansen, U. (2022). LLSVPs of primordial origin: Implications for the evolution of plate tectonics. *Earth and Planetary Science Letters* **579**, 117357.

Kröner, A. (1981). Precambrian plate tectonics. In: *Developments in Precambrian geology.* Vol. 4. Elsevier, 57–90.

Kumar, A., Parashuramulu, V., Shankar, R., and Besse, J. (2017). Evidence for a Neoarchean LIP in the Singhbhum craton, eastern India: Implications to Vaalbara supercontinent. *Precambrian Research* **292**, 163–174.

Lallemand, S. and Arcay, D. (2021). Subduction initiation from the earliest stages to self-sustained subduction: Insights from the analysis of 70 Cenozoic sites. *Earth-Science Reviews* **221**, 103779.

Landau, L. D. (D. and Lifshits, E. M. (M. (1987). Fluid mechanics. eng. 2nd edition. Course of theoretical physics ; Volume 6. Oxford: Pergamon Press.

Lassak, T. M., McNamara, A. K., Garnero, E. J., and Zhong, S. (2010). Core–mantle boundary topography as a possible constraint on lower mantle chemistry and dynamics. *Earth and Planetary Science Letters* **289**, 232–241.

Lassak, T. M., McNamara, A. K., and Zhong, S. (2007). Influence of thermochemical piles on topography at Earth's core–mantle boundary. *Earth and Planetary Science Letters* **261**, 443–455.

Lau, H. C., Mitrovica, J. X., Davis, J. L., Tromp, J., Yang, H.-Y., and Al-Attar, D. (2017). Tidal tomography constrains Earth's deep-mantle buoyancy. *Nature* **551**, 321–326.

Lay, T. (1994). The fate of descending slabs. *Annual Review of Earth and Planetary Sciences* **22**, 33–61.

Lay, T., Hernlund, J., and Buffett, B. A. (2008). Core–mantle boundary heat flow. *Nature geoscience* **1**, 25–32.

Le Bars, M. and Davaille, A. (2004). Whole layer convection in a heterogeneous planetary mantle. *Journal of Geophysical Research: Solid Earth* **109**.

Lebrun, T., Massol, H., Chassefière, E., Davaille, A., Marcq, E., Sarda, P., Leblanc, F., and Brandeis, G. (2013). Thermal evolution of an early magma ocean in interaction with the atmosphere. *Journal of Geophysical Research: Planets* **118**, 1155–1176.

Lee, C.-T. A., Luffi, P., Höink, T., Li, J., Dasgupta, R., and Hernlund, J. (2010). Upside-down differentiation and generation of a 'primordial'lower mantle. *Nature* **463**, 930–933.

Leitch, A., Davies, G., and Wells, M. (1998). A plume head melting under a rifting margin. *Earth and Planetary Science Letters* **161**, 161–177.

Leith, D. (1987). Drag on nonspherical objects. *Aerosol science and technology* **6**, 153–161.

Lenardic, A. and Moresi, L.-N. (1999). Some thoughts on the stability of cratonic lithosphere: Effects of buoyancy and viscosity. *Journal of Geophysical Research: Solid Earth* **104**, 12747–12758.

Li, K., Hu, J., Li, Y., Zhou, H., and Zhang, H. (2024). Slab Segmentation and Stacking in Mantle Transition Zone Controls Disparate Surface and Lower Mantle Subducting Rates and Complex Slab Morphology. *Geophysical Research Letters* **51**, e2024GL110202.

Li, L., Chen, Y.-W., Zheng, Y., Hu, H., and Wu, J. (2019a). Seismic evidence for plume-slab interaction by high-resolution imaging of the 410-km discontinuity under Tonga. *Geophysical Research Letters* **46**, 13687–13694.

Li, M. and Zhong, S. (2017). The source location of mantle plumes from 3D spherical models of mantle convection. *Earth and Planetary Science Letters* **478**, 47–57.

Li, Z.-X., Bogdanova, S., Collins, A., Davidson, A., De Waele, B., Ernst, R., Fitzsimons, I., Fuck, R., Gladkochub, D., Jacobs, J., et al. (2008). Assembly, configuration, and break-up history of Rodinia: a synthesis. *Precambrian research* **160**, 179–210.

Li, Z.-X., Li, X., Kinny, P., Wang, J., Zhang, S., and Zhou, H. (2003). Geochronology of Neoproterozoic syn-rift magmatism in the Yangtze Craton, South China and correlations with other continents: evidence for a mantle superplume that broke up Rodinia. *Precambrian Research* **122**, 85–109.

Li, Z.-X., Liu, Y., and Ernst, R. (2023). A dynamic 2000—540 Ma Earth history: From cratonic amalgamation to the age of supercontinent cycle. *Earth-Science Reviews* **238**, 104336.

Li, Z.-X. and Zhong, S. (2009). Supercontinent-superplume coupling, true polar wander and plume mobility: Plate dominance in whole-mantle tectonics. *Physics of the Earth and Planetary interiors* **176**, 143–156.

Li, Z.-H., Gerya, T., and Connolly, J. A. (2019b). Variability of subducting slab morphologies in the mantle transition zone: Insight from petrological-thermomechanical modeling. *Earth-Science Reviews* **196**, 102874.

Liu, M., Yang, D., and Huangfu, P. (2022). Effects of Plate Velocity Slowdown on Altering Continental Collision Patterns and Crustal-Lithospheric Deformation During the Collision Process. *Frontiers in Earth Science* **10**, 814710.

Liu, X. and Zhong, S. (2015). The long-wavelength geoid from three-dimensional spherical models of thermal and thermochemical mantle convection. *Journal of Geophysical Research: Solid Earth* **120**, 4572–4596.

– (2016). Constraining mantle viscosity structure for a thermochemical mantle using the geoid observation. *Geochemistry, Geophysics, Geosystems* **17**, 895–913.

Lourenço, D. L., Rozel, A. B., Ballmer, M. D., and Tackley, P. J. (2020). Plutonic-squishy lid: A new global tectonic regime generated by intrusive magmatism on Earth-like planets. *Geochemistry, Geophysics, Geosystems* **21**, e2019GC008756.

MacLeod, S. J., Müller, R. D., Hassan, R., and Williams, S. E. (2023). Chapter 18 - Evolution of Mantle Plumes and Lower Mantle Structure in Numerical Models Using Tectonic Reconstructions as Boundary Conditions. In: *Dynamics of Plate Tectonics and Mantle Convection.* Ed. by J. C. Duarte. Elsevier, 427–458.

Maguire, R., Ritsema, J., van Keken, P. E., Fichtner, A., and Goes, S. (May 2016). P- and S-wave delays caused by thermal plumes. *Geophysical Journal International* **206**, 1169–1178.

Mao, W. and Zhong, S. (2018). Slab stagnation due to a reduced viscosity layer beneath the mantle transition zone. *Nature Geoscience* **11**, 876–881.

Marquardt, H. and Miyagi, L. (2015). Slab stagnation in the shallow lower mantle linked to an increase in mantle viscosity. *Nature Geoscience* **8**, 311–314.

Martin, E. L., Cawood, P. A., Murphy, J. B., Nance, R. D., and Heron, P. J. (2024). The tectonics of introversion and extroversion: redefining interior and exterior oceans in the supercontinent cycle. *Geological Society, London, Special Publications* **542**, 15–29.

Maruyama, S., Santosh, M., and Zhao, D. (2007). Superplume, supercontinent, and post-perovskite: mantle dynamics and anti-plate tectonics on the core–mantle boundary. *Gondwana Research* **11**, 7–37.

Matas, J. and Bukowinski, M. S. (2007). On the anelastic contribution to the temperature dependence of lower mantle seismic velocities. *Earth and Planetary Science Letters* **259**, 51–65.

Matsui, T. and Abe, Y. (1986). Evolution of an impact-induced atmosphere and magma ocean on the accreting Earth. *Nature* **319**, 303–305.

Maurice, M., Tosi, N., Samuel, H., Plesa, A.-C., Hüttig, C., and Breuer, D. (2017). Onset of solid-state mantle convection and mixing during magma ocean solidification. *Journal of Geophysical Research: Planets* **122**, 577–598.

McKenzie, D. P., Roberts, J. M., and Weiss, N. O. (1974). Convection in the Earth's mantle: towards a numerical simulation. *Journal of fluid mechanics* **62**, 465–538.

McKenzie, D. (1967). The viscosity of the mantle. *Geophysical Journal International* **14**, 297–305.

McLennan, S. M. and Taylor, S. R. (1983). Continental freeboard, sedimentation rates and growth of continental crust. *Nature* **306**, 169–172.

McNamara, A. K. and Zhong, S. (2005). Thermochemical structures beneath Africa and the Pacific Ocean. *Nature* **437**, 1136–1139.

McNamara, A. K. (2019). A review of large low shear velocity provinces and ultra low velocity zones. *Tectonophysics* **760**, 199–220.

Merdith, A. S., Williams, S. E., Collins, A. S., Tetley, M. G., Mulder, J. A., Blades, M. L., Young, A., Armistead, S. E., Cannon, J., and Zahirovic, S. (2021). Extending full-plate tectonic models into deep time: Linking the Neoproterozoic and the Phanerozoic. *Earth-Science Reviews* **214**, 103477.

Mitchell, R. N., Zhang, N., Salminen, J., Liu, Y., Spencer, C. J., Steinberger, B., Murphy, J. B., and Li, Z.-X. (2021). The supercontinent cycle. *Nature Reviews Earth & Environment* **2**, 358–374.

Molnar, P. (1988). Continental tectonics in the aftermath of plate tectonics. *Nature* **335**, 131–137.

Moore, W. B. and Webb, A. A. G. (2013). Heat-pipe earth. *Nature* **501**, 501–505.

Moore, W. B., Schubert, G., and Tackley, P. J. (1999). The role of rheology in lithospheric thinning by mantle plumes. *Geophysical Research Letters* **26**, 1073–1076.

Morelli, A. and Dziewonski, A. M. (1987). Topography of the core–mantle boundary and lateral homogeneity of the liquid core. *Nature* **325**, 678–683.

Moresi, L.-N. and Solomatov, V. (1995). Numerical investigation of 2D convection with extremely large viscosity variations. *Physics of Fluids* **7**, 2154–2162.

Morgan, W. J. (1972). Deep mantle convection plumes and plate motions. *AAPG bulletin* **56**, 203–213.

Müller, R. D., Cannon, J., Qin, X., Watson, R. J., Gurnis, M., Williams, S., Pfaffelmoser, T., Seton, M., Russell, S. H., and Zahirovic, S. (2018). GPlates: building a virtual Earth through deep time. *Geochemistry, Geophysics, Geosystems* **19**, 2243–2261.

Müller, R. D., Flament, N., Cannon, J., Tetley, M. G., Williams, S. E., Cao, X., Bodur, Ö. F., Zahirovic, S., and Merdith, A. (2022). A tectonic-rules-based mantle reference frame since 1 billion years ago–implications for supercontinent cycles and plate–mantle system evolution. *Solid Earth* **13**, 1127–1159.

Mulyukova, E., Steinberger, B., Dabrowski, M., and Sobolev, S. V. (2015). Survival of LLSVPs for billions of years in a vigorously convecting mantle: Replenishment and destruction of chemical anomaly. *Journal of Geophysical Research: Solid Earth* **120**, 3824–3847.

Murakami, M., Khan, A., Sossi, P. A., Ballmer, M. D., and Saha, P. (2024). The Composition of Earth's Lower Mantle. *Annual Review of Earth and Planetary Sciences* **52**, 605–638.

Murphy, J. B. and Nance, R. D. (2003). Do supercontinents introvert or extrovert?: Sm-Nd isotope evidence. *Geology* **31**, 873–876.

– (2013). Speculations on the mechanisms for the formation and breakup of supercontinents. *Geoscience Frontiers* **4**, 185–194.

Nakajima, M. and Stevenson, D. J. (2014). Investigation of the initial state of the Moon-forming disk: Bridging SPH simulations and hydrostatic models. *Icarus* **233**, 259–267.

Nance, R. D., Evans, D. A., and Murphy, J. B. (2022). Pannotia: To be or not to be? *Earth-Science Reviews* **232**, 104128.

Nance, R. D., Murphy, J. B., and Santosh, M. (2014). The supercontinent cycle: a retrospective essay. *Gondwana Research* **25**, 4–29.

Niu, Y. (2018). Origin of the LLSVPs at the base of the mantle is a consequence of plate tectonics–a petrological and geochemical perspective. *Geoscience Frontiers* **9**, 1265–1278.

Nowacki, A., Panton, J., Ward, J., Myhill, B., Walker, A., Wookey, J., and Davies, J. H. (2024). "terratools: A Python package to analyse TERRA mantle convection simulations." Journal Article.

O'Connor, J., Jokat, W., Wijbrans, J., and Colli, L. (2018). Hotspot tracks in the South Atlantic located above bands of fast flowing asthenosphere driven by waning pulsations from the African LLSVP. *Gondwana Research* **53**, 197–208.

O'nions, R. and Tolstikhin, I. (1996). Limits on the mass flux between lower and upper mantle and stability of layering. *Earth and Planetary Science Letters* **139**, 213–222.

Obayashi, M. and Fukao, Y. (1997). P and PcP travel time tomography for the core-mantle boundary. *Journal of Geophysical Research: Solid Earth* **102**, 17825–17841.

Obrebski, M., Allen, R. M., Xue, M., and Hung, S.-H. (2010). Slab-plume interaction beneath the Pacific Northwest. *Geophysical Research Letters* **37**.

Olson, P. and Amit, H. (2015). Mantle superplumes induce geomagnetic superchrons. *Frontiers in Earth Science* **3**, 38.

Panton, J., Davies, J. H., Koelemeijer, P., Myhill, R., and Ritsema, J. (2025). Unique composition and evolutionary histories of large low velocity provinces. *Scientific Reports* **15**, 4466.

Panton, J., Davies, J. H., and Myhill, R. (2023). The Stability of Dense Oceanic Crust Near the Core-Mantle Boundary. *Journal of Geophysical Research: Solid Earth* **128**, e2022JB025610.

Paul, J., Ghosh, A., and Conrad, C. P. (2019). Traction and strain-rate at the base of the lithosphere: an insight into cratonic survival. *Geophysical Journal International* **217**, 1024–1033.

Pearson, D. G., Scott, J. M., Liu, J., Schaeffer, A., Wang, L. H., van Hunen, J., Szilas, K., Chacko, T., and Kelemen, P. B. (2021). Deep continental roots and cratons. *Nature* **596**, 199–210.

Peltier, W. R., Wu, P., and Yuen, D. A. (1981). "The Viscosities of the Earth's Mantle". In: *Anelasticity in the Earth*. American Geophysical Union (AGU), 59–77.

Peng, D. and Liu, L. (2022). Quantifying slab sinking rates using global geodynamic models with data-assimilation. *Earth-Science Reviews* **230**, 104039.

Peron-Pinvidic, G., Fourel, L., and Buiter, S. (2022). The influence of orogenic collision inheritance on rifted margin architecture: Insights from comparing numerical experiments to the Mid-Norwegian margin. *Tectonophysics* **828**, 229273.

Petersen, K. D. and Schiffer, C. (2016). Wilson cycle passive margins: Control of orogenic inheritance on continental breakup. *Gondwana Research* **39**, 131–144.

Phillips, B. R. and Bunge, H.-P. (2007). Supercontinent cycles disrupted by strong mantle plumes. *Geology* **35**, 847–850.

Phillips, B. R., Bunge, H.-P., and Schaber, K. (2009). True polar wander in mantle convection models with multiple, mobile continents. *Gondwana Research* **15**, 288–296.

Plimmer, A., Davies, J. H., and Panton, J. (2024). Investigating the Effect of Lithosphere Thickness and Viscosity on Mantle Dynamics Throughout the Supercontinent Cycle. *Geochemistry, Geophysics, Geosystems* **25**, e2024GC011688.

Price, M. G., Davies, J. H., and Panton, J. (2019). Controls on the Deep-Water Cycle Within Three-Dimensional Mantle Convection Models. *Geochemistry, Geophysics, Geosystems* **20**, 2199–2213.

Puetz, S. J., Ganade, C. E., Zimmermann, U., and Borchardt, G. (2018). Statistical analyses of global U-Pb database 2017. *Geoscience Frontiers* **9**, 121–145.

Puetz, S. J., Spencer, C. J., and Ganade, C. E. (2021). Analyses from a validated global UPb detrital zircon database: Enhanced methods for filtering discordant UPb zircon analyses and optimizing crystallization age estimates. *Earth-Science Reviews* **220**, 103745.

Pujol, M., Marty, B., Burgess, R., Turner, G., and Philippot, P. (2013). Argon isotopic composition of Archaean atmosphere probes early Earth geodynamics. *Nature* **498**, 87–90.

Ratcliff, J. T., Bercovici, D., Schubert, G., and Kroenke, L. W. (1998). Mantle plume heads and the initiation of plate tectonic reorganizations. *Earth and Planetary Science Letters* **156**, 195–207.

Richards, F. D., Hoggard, M. J., Ghelichkhan, S., Koelemeijer, P., and Lau, H. C. (2023). Geodynamic, geodetic, and seismic constraints favour deflated and dense-cored LLVPs. *Earth and Planetary Science Letters* **602**, 117964.

Richards, M. A., Hager, B. H., and Sleep, N. H. (1988). Dynamically supported geoid highs over hotspots: Observation and theory. *Journal of Geophysical Research: Solid Earth* **93**, 7690–7708.

Ringwood, A. E. (1968). Phase transformations in the mantle. *Earth and Planetary Science Letters* **5**, 401–412.

Ritsema, J., McNamara, A. K., and Bull, A. L. (2007). Tomographic filtering of geodynamic models: Implications for model interpretation and large-scale mantle structure. *Journal of Geophysical Research: Solid Earth* **112**.

Roberts, N. M. (2013). The boring billion?–Lid tectonics, continental growth and environmental change associated with the Columbia supercontinent. *Geoscience Frontiers* **4**, 681–691.

Rogers, J. J. and Santosh, M. (2003). Supercontinents in Earth history. *Gondwana Research* **6**, 357–368.

Royden, L. H. and Husson, L. (2006). Trench motion, slab geometry and viscous stresses in subduction systems. *Geophysical Journal International* **167**, 881–905.

Santosh, M. (2010). Supercontinent tectonics and biogeochemical cycle: a matter of 'life and death'. *Geoscience Frontiers* **1**, 21–30.

Santosh, M., Maruyama, S., and Yamamoto, S. (2009). The making and breaking of supercontinents: some speculations based on superplumes, super downwelling and the role of tectosphere. *Gondwana Research* **15**, 324–341.

Saunders, A. D., Storey, M., Kent, R., and Norry, M. (1992). Consequences of plume-lithosphere interactions. *Geological Society, London, Special Publications* **68**, 41–60.

Schellart, W. P. (2024). Subduction dynamics and overriding plate deformation. *Earth-Science Reviews*, 104755.

Schellart, W. P., Freeman, J., Stegman, D. R., Moresi, L., and May, D. (2007). Evolution and diversity of subduction zones controlled by slab width. *Nature* **446**, 308–311.

Schellart, W. P. and Moresi, L. (2013). A new driving mechanism for backarc extension and backarc shortening through slab sinking induced toroidal and poloidal mantle flow: Results from dynamic subduction models with an overriding plate. *Journal of Geophysical Research: Solid Earth* **118**, 3221–3248.

Schellart, W. P., Stegman, D. R., and Freeman, J. (2008). Global trench migration velocities and slab migration induced upper mantle volume fluxes: Constraints to find an Earth reference frame based on minimizing viscous dissipation. *Earth-Science Reviews* **88**, 118–144.

Schellart, W., Strak, V., Beniest, A., Duarte, J., and Rosas, F. (2023). Subduction invasion polarity switch from the Pacific to the Atlantic Ocean: A new geodynamic model of subduction initiation based on the Scotia Sea region. *Earth-Science Reviews* **236**, 104277.

Schubert, G. and Reymer, A. (1985). Continental volume and freeboard through geological time. *Nature* **316**, 336–339.

Schubert, G., Masters, G., Olson, P., and Tackley, P. (2004). Superplumes or plume clusters? *Physics of the Earth and Planetary Interiors* **146**, 147–162.

Schuberth, B. S. A., Bunge, H.-P., and Ritsema, J. (2009). Tomographic filtering of high-resolution mantle circulation models: Can seismic heterogeneity be explained by temperature alone? *Geochemistry, Geophysics, Geosystems* **10**.

Sengör, A. C. and Burke, K. (1978). Relative timing of rifting and volcanism on Earth and its tectonic implications. *Geophysical Research Letters* **5**, 419–421.

Senshu, H., Maruyama, S., Rino, S., and Santosh, M. (2009). Role of tonalite-trodhjemite-granite (TTG) crust subduction on the mechanism of supercontinent breakup. *Gondwana Research* **15**, 433–442.

Shi, Y.-N., Li, Z.-H., Chen, L., and Morgan, J. P. (2021). Connection Between a Subcontinental Plume and the Mid-Lithospheric Discontinuity Leads to Fast and Intense Craton Lithospheric Thinning. *Tectonics* **40**, e2021TC006711.

Shi, Z., Mitchell, R. N., Li, Y., Wan, B., Chen, L., Peng, P., Zhao, L., Liu, L., and Zhu, R. (2024). Sluggish thermochemical basal mantle structures support their long-lived stability. *Nature Communications* **15**, 10000.

Silver, P. G., Carlson, R. W., and Olson, P. (Jan. 1988). Deep Slabs, Geochemical Heterogeneity, and the Large-Scale Structure of Mantle Convection: Investigation of an Enduring Paradox. *Annual Review of Earth and Planetary Sciences* **16**, 477.

Sizova, E., Gerya, T., Stüwe, K., and Brown, M. (2015). Generation of felsic crust in the Archean: a geodynamic modeling perspective. *Precambrian Research* **271**, 198–224.

Sobolev, S. V. and Brown, M. (2019). Surface erosion events controlled the evolution of plate tectonics on Earth. *Nature* **570**, 52–57.

Solomatov, V. (2007). Magma oceans and primordial mantle differentiation. *Evolution of the Earth* **9**, 91–119.

Spencer, C., Roberts, N., and Santosh, M. (2017). Growth, destruction, and preservation of Earth's continental crust. *Earth-Science Reviews* **172**, 87–106.

Stähler, S. C., Sigloch, K., and Nissen-Meyer, T. (2012). Triplicated P-wave measurements for waveform tomography of the mantle transition zone. *Solid Earth* **3**, 339–354.

Stegman, D. R., Richards, M. A., and Baumgardner, J. R. (2002). Effects of depth-dependent viscosity and plate motions on maintaining a relatively uniform mid-ocean ridge basalt reservoir in whole mantle flow. *Journal of Geophysical Research: Solid Earth* **107**, ETG 5-1-ETG 5–8.

Stegman, D. R., Freeman, J., Schellart, W. P., Moresi, L., and May, D. (2006). Influence of trench width on subduction hinge retreat rates in 3-D models of slab rollback. *Geochemistry, Geophysics, Geosystems* **7**.

Stegman, D. R., Schellart, W., and Freeman, J. (2010). Competing influences of plate width and far-field boundary conditions on trench migration and morphology of subducted slabs in the upper mantle. *Tectonophysics* **483**, 46–57.

Stein, M. and Hofmann, A. (1994). Mantle plumes and episodic crustal growth. *Nature* **372**, 63–68.

Steinberger, B. and Calderwood, A. R. (2006). Models of large-scale viscous flow in the Earth's mantle with constraints from mineral physics and surface observations. *Geophysical Journal International* **167**, 1461–1481.

Steinberger, B. and Torsvik, T. H. (2012). A geodynamic model of plumes from the margins of Large Low Shear Velocity Provinces. *Geochemistry, Geophysics, Geosystems* **13**.

Stern, R. J. (2004). Subduction initiation: spontaneous and induced. *Earth and Planetary Science Letters* **226**, 275–292.
– (2018). The evolution of plate tectonics. eng. *Philosophical transactions of the Royal Society of London. Series A: Mathematical, physical, and engineering sciences* **376**, 20170406–.
Stern, R. J. and Gerya, T. (2018). Subduction initiation in nature and models: A review. *Tectonophysics* **746**, 173–198.
Stixrude, L. and Lithgow-Bertelloni, C. (Sept. 2021). Thermal expansivity, heat capacity and bulk modulus of the mantle. *Geophysical Journal International* **228**, 1119–1149.
Stokes, G. G. (Jan. 1851). On the Effect of the Internal Friction of Fluids on the Motion of Pendulums. *Transactions of the Cambridge Philosophical Society* **9**, 8.
Storey, B. C. (1995). The role of mantle plumes in continental breakup: case histories from Gondwanaland. *Nature* **377**, 301–308.
Stotz, I. L., Vilacís, B., Hayek, J. N., Carena, S., and Bunge, H.-P. (2023). Plume driven plate motion changes: New insights from the South Atlantic realm. *Journal of South American Earth Sciences* **124**, 104257.
Sze, E. K. and Hilst, R. D. van der (2003). Core mantle boundary topography from short period PcP, PKP, and PKKP data. *Physics of the Earth and Planetary Interiors* **135**, 27–46.
Tackley, P. J. (2012). Dynamics and evolution of the deep mantle resulting from thermal, chemical, phase and melting effects. *Earth-Science Reviews* **110**, 1–25.
Tajima, F. and Grand, S. P. (1995). Evidence of high velocity anomalies in the transition zone associated with Southern Kurile Subduction Zone. *Geophysical Research Letters* **22**, 3139–3142.
Tajima, F., Katayama, I., and Nakagawa, T. (2009). Variable seismic structure near the 660 km discontinuity associated with stagnant slabs and geochemical implications. *Physics of the Earth and Planetary Interiors* **172**, 183–198.
Tan, E., Gurnis, M., and Han, L. (2002). Slabs in the lower mantle and their modulation of plume formation. *Geochemistry, Geophysics, Geosystems* **3**, 1–24.
Tanaka, S. (2010). Constraints on the core-mantle boundary topography from P4KP-PcP differential travel times. *Journal of Geophysical Research: Solid Earth* **115**.
Tetley, M. G., Williams, S. E., Gurnis, M., Flament, N., and Müller, R. D. (2019). Constraining absolute plate motions since the Triassic. *Journal of Geophysical Research: Solid Earth* **124**, 7231–7258.
Thompson, P. F. and Tackley, P. J. (1998). Generation of mega-plumes from the core-mantle boundary in a compressible mantle with temperature-dependent viscosity. *Geophysical Research Letters* **25**, 1999–2002.
Timmerman, S., Stachel, T., Koornneef, J. M., Smit, K. V., Harlou, R., Nowell, G. M., Thomson, A. R., Kohn, S. C., Davies, J. H., Davies, G. R., et al.

(2023). Sublithospheric diamond ages and the supercontinent cycle. *Nature* **623**, 752–756.

Tonks, W. B. and Melosh, H. J. (1993). Magma ocean formation due to giant impacts. *Journal of Geophysical Research: Planets* **98**, 5319–5333.

Torsvik, T. H., Burke, K., Steinberger, B., Webb, S. J., and Ashwal, L. D. (2010). Diamonds sampled by plumes from the core–mantle boundary. *Nature* **466**, 352–355.

Torsvik, T. H., Smethurst, M. A., Burke, K., and Steinberger, B. (2008). Long term stability in deep mantle structure: Evidence from the 300 Ma Skagerrak-Centered Large Igneous Province (the SCLIP). *Earth and Planetary Science Letters* **267**, 444–452.

Valley, J. W., Cavosie, A. J., Ushikubo, T., Reinhard, D. A., Lawrence, D. F., Larson, D. J., Clifton, P. H., Kelly, T. F., Wilde, S. A., Moser, D. E., et al. (2014). Hadean age for a post-magma-ocean zircon confirmed by atom-probe tomography. *Nature Geoscience* **7**, 219–223.

Van der Meer, D. G., van Hinsbergen, D. J., and Spakman, W. (2018). Atlas of the underworld: Slab remnants in the mantle, their sinking history, and a new outlook on lower mantle viscosity. *Tectonophysics* **723**, 309–448.

van der Wiel, E., van Hinsbergen, D. J., Thieulot, C., and Spakman, W. (2024). Linking rates of slab sinking to long-term lower mantle flow and mixing. *Earth and Planetary Science Letters* **625**, 118471.

Van Heck, H. J., Davies, J. H., Elliott, T., and Porcelli, D. (2016). Global-scale modelling of melting and isotopic evolution of Earth's mantle: melting modules for TERRA. *Geoscientific Model Development* **9**, 1399–1411.

Van Hunen, J., Van Keken, P. E., Hynes, A., Davies, G. F., Condie, K., and Pease, V. (2008). Tectonics of early Earth: Some geodynamic considerations. *When did plate tectonics begin on planet Earth*, 157–171.

Van Keken, P. E. and Ballentine, C. J. (1998). Whole-mantle versus layered mantle convection and the role of a high-viscosity lower mantle in terrestrial volatile evolution. *Earth and Planetary Science Letters* **156**, 19–32.

Vauchez, A., Barruol, G., and Tommasi, A. (1997). Why do continents break-up parallel to ancient orogenic belts? *Terra Nova* **9**, 62–66.

Vezinet, A., Chugunov, A. V., Sobolev, A. V., Jain, C., Sobolev, S. V., Batanova, V. G., Asafov, E. V., Koshlyakova, A. N., Arndt, N. T., Danyushevsky, L. V., et al. (2025). Growth of continental crust and lithosphere subduction in the Hadean revealed by geochemistry and geodynamics. *Nature Communications* **16**, 3850.

Voice, P. J., Kowalewski, M., and Eriksson, K. A. (2011). Quantifying the timing and rate of crustal evolution: global compilation of radiometrically dated detrital zircon grains. *The Journal of Geology* **119**, 109–126.

Walcott, R. (1970). Flexural rigidity, thickness, and viscosity of the lithosphere. *Journal of Geophysical Research* **75**, 3941–3954.

Walter, M. (2003). 2.08 - Melt Extraction and Compositional Variability in Mantle Lithosphere. In: *Treatise on Geochemistry*. Ed. by H. D. Holland and K. K. Turekian. Oxford: Pergamon, 363–394.

Wang, S., Liu, H., Zheng, Y., Chen, Y., Ai, S., Zeng, S., Qin, L., Guo, R., Yuan, X., and Xu, Y.-G. (2024). Translithospheric magma plumbing system fossilized in the Emeishan large igneous province. *Communications Earth & Environment* **5**, 458.

Wang, Y. and Li, M. (2020). Constraining mantle viscosity structure from a statistical analysis of slab stagnation events. *Geochemistry, Geophysics, Geosystems* **21**, e2020GC009286.

Weertman, J. and Weertman, J. R. (1975). High Temperature Creep of Rock and Mantle Viscosity. *Annual Review of Earth and Planetary Sciences* **3**, 293–315.

Wegener, A. (1966). The origin of continents and oceans. Courier Corporation.

Wetherill, G. (1975). "Late heavy bombardment of the moon and terrestrial planets". In: *In: Lunar Science Conference, 6th, Houston, Tex., March 17-21, 1975, Proceedings. Volume 2.(A78-46668 21-91) New York, Pergamon Press, Inc., 1975, p. 1539-1561.* Vol. 6, 1539–1561.

White, R. and McKenzie, D. (1989). Magmatism at rift zones: the generation of volcanic continental margins and flood basalts. *Journal of Geophysical Research: Solid Earth* **94**, 7685–7729.

White, W. and Klein, E. (2014). 4.13 - Composition of the Oceanic Crust. In: *Treatise on Geochemistry (Second Edition)*. Ed. by H. D. Holland and K. K. Turekian. Second Edition. Oxford: Elsevier, 457–496.

Will, T. M. and Frimmel, H. E. (2018). Where does a continent prefer to break up? Some lessons from the South Atlantic margins. *Gondwana Research* **53**, 9–19.

Wilson, J. T. (1966). Did the Atlantic Close and then Re-Open? *Nature* **211**, 676–681.

Wilson, R. W., Houseman, G. A., Buiter, S., McCaffrey, K. J., and Doré, A. G. (2019). Fifty years of the Wilson Cycle concept in plate tectonics: an overview. *Geological Society, London, Special Publications* **470**, 1–17.

Wolf, J. and Evans, D. A. (2022). Reconciling supercontinent cycle models with ancient subduction zones. *Earth and Planetary Science Letters* **578**, 117293.

Wolstencroft, M., Davies, J. H., and Davies, D. R. (2009). Nusselt–Rayleigh number scaling for spherical shell Earth mantle simulation up to a Rayleigh number of 109. *Physics of the Earth and Planetary Interiors* **176**, 132–141.

Wolstencroft, M. and Davies, J. H. (2017). Breaking supercontinents; no need to choose between passive or active. *Solid Earth* **8**, 817–825.

Yang, G. (2022). Subduction initiation triggered by collision: A review based on examples and models. *Earth-Science Reviews* **232**, 104129.

Yang, W.-S. (1997). Variable viscosity thermal convection at infinite Prandtl number in a thick spherical shell. University of Illinois at Urbana-Champaign.

Yang, W.-S. and Baumgardner, J. R. (2000). A matrix-dependent transfer multigrid method for strongly variable viscosity infinite Prandtl number thermal convection. *Geophysical & Astrophysical Fluid Dynamics* **92**, 151–195.

Yoshida, M. (2010). Preliminary three-dimensional model of mantle convection with deformable, mobile continental lithosphere. *Earth and Planetary Science Letters* **295**, 205–218.

– (2013). Mantle temperature under drifting deformable continents during the supercontinent cycle. *Geophysical Research Letters* **40**, 681–686.

Yoshida, M. and Santosh, M. (2011). Supercontinents, mantle dynamics and plate tectonics: A perspective based on conceptual vs. numerical models. *Earth-Science Reviews* **105**, 1–24.

Young, A., Flament, N., Maloney, K., Williams, S., Matthews, K., Zahirovic, S., and Müller, R. D. (2019). Global kinematics of tectonic plates and subduction zones since the late Paleozoic Era. *Geoscience Frontiers* **10**, 989–1013.

Young, A., Flament, N., Williams, S. E., Merdith, A., Cao, X., and Müller, R. D. (2022). Long-term Phanerozoic sea level change from solid Earth processes. *Earth and Planetary Science Letters* **584**, 117451.

Yuan, Q. and Li, M. (Apr. 2022). Instability of the African large low-shear-wave-velocity province due to its low intrinsic density. *Nature Geoscience* **15**.

Zahirovic, S., Müller, R. D., Seton, M., and Flament, N. (2015). Tectonic speed limits from plate kinematic reconstructions. *Earth and Planetary Science Letters* **418**, 40–52.

Zhang, N., Dang, Z., Huang, C., and Li, Z.-X. (2018). The dominant driving force for supercontinent breakup: Plume push or subduction retreat? *Geoscience Frontiers* **9**, 997–1007.

Zhang, N., Zhong, S., Leng, W., and Li, Z.-X. (2010). A model for the evolution of the Earth's mantle structure since the Early Paleozoic. *Journal of Geophysical Research: Solid Earth* **115**.

Zhang, N., Zhong, S., and McNarmara, A. K. (2009). Supercontinent formation from stochastic collision and mantle convection models. *Gondwana Research* **15**, 267–275.

Zhang, Z., Dorfman, S. M., Labidi, J., Zhang, S., Li, M., Manga, M., Stixrude, L., McDonough, W. F., and Williams, Q. (2016). Primordial metallic melt in the deep mantle. *Geophysical Research Letters* **43**, 3693–3699.

Zhao, D. (2004). Global tomographic images of mantle plumes and subducting slabs: insight into deep Earth dynamics. *Physics of the Earth and Planetary Interiors* **146**, 3–34.

Zhao, G., Sun, M., Wilde, S. A., and Li, S. (2004). A Paleo-Mesoproterozoic supercontinent: assembly, growth and breakup. *Earth-Science Reviews* **67**, 91–123.

Zhong, S. and Rudolph, M. L. (2015). On the temporal evolution of long-wavelength mantle structure of the Earth since the early Paleozoic. *Geochemistry, Geophysics, Geosystems* **16**, 1599–1615.

Zhong, S., Zhang, N., Li, Z.-X., and Roberts, J. H. (2007). Supercontinent cycles, true polar wander, and very long-wavelength mantle convection. *Earth and Planetary Science Letters* **261**, 551–564.